DETECTION STRATEGIES FOR A MULTI-INTERFEROMETER TRIGGERED SEARCH

Wm. Robert Johnston*
University of Texas at Brownsville
thesis for M.S. in Physics from the University of Texas at El Paso
(Dated: 19 April 2004 (rev. 7 May 2004))

Interferometric detectors such as LIGO are now being used in searches for astrophysical gravitational waves. One search seeks to test for possible gravitational wave bursts correlated with external astrophysical triggers (e.g. gamma ray bursts). Statistical tests are necessarily used since these searches involve detector correlations with signal amplitude comparable to or less than the noise RMS. This study compares various statistical tests for signal detection in an externally triggered burst search and identifies optimal detection strategies. Tests initially compared include the likelihood ratio test and various components of the likelihood ratio statistic for two co-located co-aligned detectors. Performances were found from analytic derivations for ideal noise (stationary Gaussian) and Monte Carlo simulations were used for both ideal noise and a realistic noise model. The noise model used was mixed Gaussian, in which samples are drawn from a mixture of two Gaussian distributions, an individual sample having a small probability of being drawn from the larger variance distribution ("noisy" samples). In the case of realistic noise, the cross-correlation test significantly outperformed the likelihood ratio test for low signal-to-noise ratios even if "noisy" samples comprised less than one percent of the signal time series. Optimized likelihood ratio tests were then obtained analytically for generalized cases including two detectors and multiple detectors, of varying locations and orientations, with the aim of extracting the cross-correlation part. This identified issues with the likelihood ratio approach in which, absent additional constraints, the test does not converge to cross-correlation for a pair of mis-aligned detectors. Cross-correlation terms are present, however, in the optimized test for detector networks of three or more. An expression is obtained for term coefficients in a general detector network. This was used in a computer code written to compare the magnitudes of individual cross-correlation terms in a multi-interferometer network of real detectors (including LIGO, VIRGO, GEO, and TAMA). The output shows in particular which pair-wise cross-correlation term contributes the most as a function of source direction. For such networks, relative contributions of individual cross-correlation terms are compared for various combinations of existing interferometer detectors. Directions for further development are discussed.

Contents

I. Introduction 2

II. Gravitational waves 2
- A. Relativity 2
- B. Gravitational waves 3
- C. Gravitational wave sources 4
- D. Gamma ray bursts 5

III. Detection of gravitational waves 6
- A. Introduction 6
- B. Bar detectors 6
- C. Interferometric detectors 7
- D. Orientation and antenna patterns 8
- E. Noise 10
- F. Data analysis 12
- G. Triggered burst analysis 12
- H. Hypotheses testing 13

IV. Likelihood ratio test for burst signal detection 14
- A. Introduction 14
- B. Analytical derivation 14
- C. Simulation, Gaussian noise 16
- D. Simulation, realistic noise 16

V. General networks of detectors 18
- A. Introduction 18
- B. Likelihood ratio statistic for two detectors 19
- C. Likelihood ratio statistic for multiple detectors 19
- D. Dependence on polarization angle 20
- E. Mapping weightings 21
- F. Comparison to other works on optimized detection 22

VI. Conclusions and directions for further development 22

VII. acknowledgments 23

References 23

A. List of abbreviations 25

B. List of gravitational wave detectors 25

*Electronic address: johnston@phys.utb.edu

C. Likelihood ratio statistic for two co-located co-aligned detectors 26

D. Derivation of means and variances for sample tests 26
1. Cross-correlation test 26
2. Likelihood ratio test 27
3. Variance sum test 29

E. Likelihood ratio optimum statistic for a pair of detectors 30
1. General assumptions 30
2. Deriving the likelihood ratio statistic for the generalized two detector case 30

F. Derivation of optimum statistic for three or more detectors 32
1. General assumptions 32
2. Deriving the likelihood ratio statistic for the generalized three detector case 32
3. Deriving the likelihood ratio statistic for n detectors 35

G. LR statistic derivation for unknown polarization angle 36

H. Sky maps 38

I. Code for Monte Carlo simulations 41

J. Code for LR coefficients in detector correlations 43

I. INTRODUCTION

This project is concerned with developing optimal detection strategies for a triggered burst search for gravitational waves. Such a search seeks to identify a short burst of gravitational waves potentially associated with an independently observed trigger.

Background for this research will begin with an introduction to general relativity and the theory of gravitational waves. This is followed by a review of potential astrophysical sources of gravitational waves (including the potential amplitude of resulting signals) and the relationship to gamma ray bursts. Then we review types of gravitational wave detectors, beginning briefly with resonant bar detectors followed by interferometer detectors. We consider issues with direction-dependent sensitivity of interferometer detectors followed by the nature of noise in such detectors and the statistical methods for extracting signals from noise.

The research began by comparing several statistical tests for a pair of identical, co-located and co-aligned detectors. The first objective was to compare the performance of the likelihood ratio test and the cross-correlation test under different noise conditions (a test based on the sum of the individual variances was also used). Analytic results and a Monte Carlo simulation code were used in the case of ideal Gaussian noise, affirming that the likelihood ratio test performs best. Having validated the performance of the Monte Carlo code, it was used to compare the tests in the presence of more realistic noise, modeled as a mixture of two Gaussian distributions. This demonstrated that for low signal-to-noise signals, the cross-correlation test is superior for such non-Gaussian noise.

The next objective was to develop a cross-correlation-based test for optimally combining the detector outputs within a generalized network. This was accomplished by computing the likelihood ratio test for a general network, then extracting the cross-correlation part. In the case of a two-detector network, the likelihood ratio statistic obtained was merely the sum of the auto-correlation terms with no cross-correlation component. Reasons for this result are discussed. For networks of three or more misaligned detectors, cross-correlation terms were obtained and expressions are given for such generalized networks. Some simplifying assumptions are identified, including ignoring the effect of unknown polarization angle and assuming that the detector noise is white. A computer code was written to compare the magnitudes of the contributions of individual cross-correlation terms for real networks. Using this code and idealized comparisons of the LIGO, VIRGO, TAMA, and GEO detectors, the relative weights of cross-correlation terms are computed for networks comprising various combinations of these detectors. Several directions for further work are identified, including incorporating physically appropriate constraints to address the breakdown in the two detector case, and developing the analytic results to incorporate unknown polarization angle and differing noise power spectral density among detectors.

II. GRAVITATIONAL WAVES

A. Relativity

Einstein's special relativity invokes two postulates: all inertial frames are equally valid (in terms of say, physical observations), and the speed of light is constant for all observers. From these postulates it can be shown that time should be considered a dimension on comparable footing with the three spatial dimensions, and that these space-time dimensions are "mixed" for different observers. More specifically, when translating between a pair of inertial frames moving relative to each other, spatial coordinates in one frame will be a function of both spatial and time coordinates in the other frame.

Space-time in special relativity is then a four-dimensional manifold referred to as Minkowski space.

The Minkowski metric applies to this space and is

$$\eta_{\mu\nu} = \begin{bmatrix} -1 & 0 & 0 & 0 \\ 0 & 1 & 0 & 0 \\ 0 & 0 & 1 & 0 \\ 0 & 0 & 0 & 1 \end{bmatrix}. \quad (1)$$

As an application, consider the norm of a vector V^μ in Minkowski space:

$$V \cdot V = \eta_{\mu\nu} V^\mu V^\nu = -V^0 V^0 + V^1 V^1 + V^2 V^2 + V^3 V^3 \quad (2)$$

where V^0 is the time dimension of V and V^1, V^2, and V^3 are the spatial dimensions of V. V is called timelike if this norm is negative, spacelike if the norm is positive, and null if the norm is zero. From this description comes the conclusion that the speed of light is a physical limit on communication of any form between locations in space-time, not merely a limit on the speed of matter.

General relativity proceeds to explain gravitation in terms of curvature of space-time, this curvature being induced by the presence of mass-energy. This curvature is described by the Einstein field equations, which may be expressed as

$$G^{\alpha\beta} = 8\pi T^{\alpha\beta} \quad (3)$$

where $G^{\alpha\beta}$ is the space-time curvature tensor and $T^{\alpha\beta}$ is the stress-energy tensor (including the presence of mass-energy). Since these four-by-four tensors are symmetric, this expression describes ten coupled non-linear partial differential equations. Note that this formulation uses geometrized units (i.e. $G \equiv 1$ and $c \equiv 1$) and sets the cosmological constant to 0.

As discussed by Misner, Thorne, and Wheeler [1], this description of gravitation in terms of space-time curvature models space-time as a differentiable manifold. This manifold is locally flat or Minkowskian, but in general is globally curved. The fact that the manifold is locally flat is an expression of the equivalence principle, which states that freely falling frames are equivalent to inertial frames. In postulating such an equivalence, general relativity replaces the concept of a gravitational force in the freely falling frame with that of the influence of space-time curvature.

In the Newtonian formulation of physics, a particle moving under the influence of no forces moves in a straight line. In general relativity, a particle or free test mass moving under the influence of no forces moves along a geodesic, which is locally a straight line but conforms to any curvature of the space-time manifold. Such a geodesic is "time-like". This space-time curvature takes the place of gravity (which was a force in the Newtonian formulation).

B. Gravitational waves

Gravitational waves are a consequence of general relativity and may most simply be described as ripples in the curvature of space-time. They were immediately recognized as implications of the theory, although it was some time before an adequate theory of gravitational waves was developed. Given that changes in space-time curvature can only be communicated from the source at the speed of light, such waves represent the delayed effect at a distance of a change in space-time curvature—which in turn results from a change in mass-energy configuration.

A more specific development follows, based on the discussion by Schutz [2]. If we consider the Einstein equations in vacuum ($T^{\alpha\beta} = 0$) in a weak field approximation and gauge condition $\overline{h}^{\alpha\beta}_{,b} = 0$, we have

$$\left(-\frac{\partial^2}{\partial t^2} + \nabla^2\right)\overline{h}^{\alpha\beta} = 0. \quad (4)$$

This has the solution

$$\overline{h}^{\alpha\beta} = A^{\alpha\beta} \exp(i k_\alpha x^\alpha) \quad (5)$$

with k_α necessarily a null one-form and $A^{\alpha\beta}$ necessarily orthogonal to k_α. This solution is a plane transverse wave with direction k_α and amplitude the real part of $A^{\alpha\beta}$. The fact that k_α is a null one-form corresponds to the fact that the propagation speed of the gravitational wave is the speed of light. It can be shown that it is possible to change the gauge to express $\overline{h}$ in a transverse-traceless (TT) form such that

$$A^{TT}_{\alpha\beta} = \begin{bmatrix} 0 & 0 & 0 & 0 \\ 0 & A_{xx} & A_{xy} & 0 \\ 0 & A_{xy} & -A_{xx} & 0 \\ 0 & 0 & 0 & 0 \end{bmatrix} \quad (6)$$

i.e. with only two independent constants. These two constants describe two possible polarizations of gravitational waves; to understand these polarizations we first consider the effect of a gravitational wave.

The effect of gravitational wave is to stretch or compress the space-time metric. This is only observable by comparison of two (or more) separated free test masses. In directions perpendicular to the direction of wave propagation, the separation of a pair of test masses will oscillate about the rest separation (given an appropriately oriented pair). Consider a singly polarized gravitational wave propagating in a direction perpendicular to the circular array of test masses in figure 1. Test masses along one diameter oscillate radially about their rest positions, while masses along the perpendicular diameter do likewise except out of phase. The alternate polarization is depicted in figure 1 and is like the first except rotated by 45°. These two polarizations are called plus (+) and cross (×) polarizations. Note that this contrasts with the case of electromagnetic waves, where the two polarizations differ by 90°: this difference reflects the quadrupole nature of gravitational sources.

It may be noted that alternate theories of gravitation exist which provide for gravitational waves; however, general relativity is uniquely consistent with observations, assumes no prior geometry to space-time, and

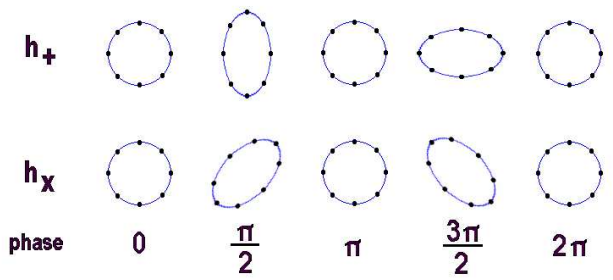

FIG. 1: Gravitational wave polarizations: Effect of singly-polarized gravitational waves propagating perpendicular to a ring of free test masses, for + polarization (top) and × polarization (bottom).

invokes no force to explain gravitation (Misner, Thorne, and Wheeler [1]). Observations of gravitational waves would potentially provide tests of the general theory of relativity.

C. Gravitational wave sources

The most detectable gravitational wave sources are astrophysical sources, and specifically such sources involving relativistic motion and/or compact masses. As an illustration, Misner, Thorne, and Wheeler [1] calculate the power radiated by a hypothetical laboratory generator of gravitational waves. For a 20-m long, 490-ton steel beam rotating at a speed constrained by tensile strength, they obtain a power of $L_{GW} = 2.2 \times 10^{-22}$ erg/s. This would give a flux of about 2×10^{-31} erg/s cm^2 at a distance of 100 m. In contrast, their calculated flux of gravitational wave energy from some representative binary stars is of order 2×10^{-12} erg/s cm^2. Detectability weighs even more in favor of astrophysical sources when it is considered that methods currently devised for potentially detecting gravitational waves are sensitive to wave amplitude, not wave energy. Since wave amplitude is inversely proportional to source distance (in contrast to the inverse of square of distance in the case of wave energy), the advantage of nearby sources is diminished. Note that due to the conservation of mass-energy and momentum, gravitational waves can only be produced by sources which are not spherically symmetric. In reviewing possible sources, we will highlight those relevant to a triggered burst search.

The orbital motion of binary compact objects, such as black holes and neutron stars, would produce circularly polarized gravitational wave signals of a periodic long-term nature. Consider a pair of neutron stars or stellar-mass black holes orbiting each other in a circular orbit. For such objects the maximum strain amplitude h is given by Thorne [3] as

$$h = 4.1\times10^{-21}\left(\frac{\mu}{M_\odot}\right)^{1/2}\left(\frac{M}{M_\odot}\right)^{1/3}\left(\frac{10\ \mathrm{Mpc}}{r}\right)\left(\frac{100\ \mathrm{Hz}}{f}\right)^{1/6} \quad (7)$$

where $M = M_1 + M_2$ is the total mass of the binary components, $\mu = M_1 M_2/M$ is the mass function, r is the source distance, and f is the gravitational wave frequency which is twice the orbital frequency. Maximum possible values of f are of order 1 kHz for binary neutron stars. (Note that radiation of gravitational waves will cause such binaries to inspiral; this is discussed below.)

Other binary systems would produce gravitational waves. Binary white dwarfs would be weaker but far more common sources; collectively, they may contribute to a stochastic background of gravitational waves at frequencies well below 1 Hz (Benacquista *et al.* [4]). Another potential source of stochastic gravitational waves is primordial gravitational waves, representing a relic of the big bang. Such gravitational waves would be analogous to the cosmic microwave background in the electromagnetic spectrum. Observation of the energy-frequency spectrum of such gravitational waves would provide constraints on big bang models.

Pulsars are also potential periodic sources. A rotating neutron star will produce gravitational waves if the star is not axisymmetric, which could result from deformations in the solid crust or deformations resulting from strong magnetic fields or rapid rotation. Observed rates of pulsar spindowns may be used to calculate upper limits on the radiation of gravitational waves if it is assumed that all dissipated rotational energy is converted to gravitational waves. Such upper limits for known pulsars are of order $h = 10^{-24}$ to 10^{-26} at frequencies between 10 Hz and 1 kHz (Allen and Woan [5]). Palomba [6] gives tighter constraints by modeling the combined contributions of electromagnetic and gravitational radiation to spindown, finding an upper limit of $h = 5.5 \times 10^{-25}$ in the case of the Crab pulsar.

For the binary objects discussed above, gravitational waves carry energy from the system, resulting in their inspiral and eventual merger into a single object—a black hole in the case of systems of neutron stars or black holes. Such inspiral (well short of merger) was first indirectly observed in the case of binary pulsar PSR B1913+16, discovered by Hulse and Taylor. Timing observations of the observable pulsar component demonstrated inspiral at a rate consistent with that predicted based on gravitational wave energy removal (Weisberg and Taylor [7]). As the binary components spiral closer together, the rate of inspiral will increase, causing the gravitational wave signal to rapidly increase in both frequency and amplitude in the last minutes before final inspiral. The binary components would finally approach to within the closest stable orbit, leading to their merger into a single black hole. Following the very brief merger (lasting of order ms), a brief ringdown would occur as the black hole's event horizon stabilizes. The inspiral and ringdown phases are

fairly well modeled, but the merger phase requires numerical techniques to estimate gravitational wave signals produced.

Cutler and Thorne [8] indicate that for binary black hole mergers with component black holes much larger than $10M_\odot$, the merger and ringdown is expected to represent most of the gravitational wave signal, in contrast to the case for binaries with smaller black holes or neutron stars. For gravitational waves in the frequency range of maximum sensitivity for first-generation detectors, they suggest strain amplitudes of order

$$h = 5 \times 10^{-23} \left(\frac{10 \text{ Mpc}}{r} \right) \text{ for neutron stars,}$$

$$h = 3 \times 10^{-22} \left(\frac{10 \text{ Mpc}}{r} \right) \text{ for two 10 } M_\odot \text{ black holes.}$$

Burgay *et al.* [9] recently identified pulsar PSR J0737-3039 as a binary neutron star system estimated as only 85 Myr short of inspiral merger. By incorporating this and other known systems into models of binary neutron star populations and detectability, Kalogera *et al.* [10] obtain most probable rates of detectable inspirals of 0.004 to 0.2 per year for first-generation detectors and 20-1000 per year for planned second-generation detectors.

Similarly, stars or stellar remnants orbiting supermassive black holes in galactic cores—or orbiting intermediate black holes in globular clusters—will spiral into the black hole. Although stars would generally be tidally disrupted before the final plunge, the orbital motion and inspiral is still a potential source of gravitational waves. Such plunges would give waves with strain amplitude and frequency of order

$$h = 2 \times 10^{-21} \left(\frac{M_*}{M_\odot} \right) \left(\frac{10 \text{ Mpc}}{r} \right) \quad (8)$$

$$f = 10^{-4} \text{ Hz} \left(\frac{10^8 M_\odot}{M} \right) \quad (9)$$

(Thorne [3]) where M is the mass of the supermassive black hole (10^6 to $10^9 M_\odot$ for suspected galactic core black holes) and M_* is the mass of the star.

Supernovae from stellar collapse are another potential source, whether the end product is a neutron star or a black hole. If the collapse is spherically symmetric, no gravitational waves would be produced. However, the star itself is generally non-spherical due to its rotation, contributing to non-spherical collapse. In order to produce significant gravitational waves, there must be deviations from even this rotational axisymmetry. For supernovae which produce a neutron star, additional asymmetries may result from core bounce, or the production of a shock wave as infalling material impacts the newly formed neutron star (this shock wave eventually produces the supernova explosion), from convection between the neutron star surface and the shock front, and from resultant asymmetries in neutrino emissions. Recent models suggest that the strongest source of gravitational waves within a supernova collapse could be neutrino-induced convection and not core bounce. Fryer and Warren [11] and Fryer, Holz, and Hughes [12] report maximum amplitudes, based on their models, of order

$$h = (1 \text{ to } 4) \times 10^{-25} \left(\frac{10 \text{ Mpc}}{r} \right). \quad (10)$$

Supernovae and compact binary inspiral are the most promising burst sources for current searches, although it should be noted that burst searches are generalized to detect bursts from previously unrecognized sources. Supernovae and binary inspiral are known candidates for triggered burst searches because the presumed production of gravitational waves is coincident with independently observable phenomena. Supernovae produce an obvious multispectral electromagnetic signature, but this follows at a significant time delay from the gravitational wave signal: the optical signature of a supernova is associated with explosion of the star's outer layers due to the shock wave from core bounce and from decay of radioactive elements produced in the explosion. However, neutrino emissions and gravitational waves signals would be more nearly coincident in time, so that detection of neutrinos would better constrain the possible time of a gravitational wave signal (Arnaud *et al.* [13]). Binary inspiral as well as some supernovae may be associated with gamma ray bursts, as discussed below.

D. Gamma ray bursts

Astronomical gammas ray bursts (GRBs) were first reported in 1973, but only recently have observations begun to identify their sources. The first GRB was detected in 1967 by Vela satellites, military satellites tasked with detection of terrestrial nuclear explosions. Besides being of short overall duration (of order seconds or less), GRBs were observed to vary in intensity over periods of order ms. Since causality arguments lead to the conclusion that the timescale of such variability must set an upper limit on the light-travel time across the source region, this constrained GRB source regions to sizes of at most a few hundred km. Subsequently other satellites made additional GRBs detections, and in a few cases X-ray emissions were also observed. However, little else was known until the beginning of observations by the Compton Gamma-Ray Observatory (CGRO), in orbit from 1991 to 2000. The Burst and Transient Experiment, or BATSE sensor, aboard Compton identified a total of about 2700 GRBs. This data indicated a uniform sky distribution, eliminating any association with the Milky Way Galaxy. BATSE data further indicated that GRBs included two distinct classes: "short" GRBs with durations less than 2 s (some less than 0.1 s) and "long" GRBs lasting more than 2 s up to a few minutes (Mészáros [14]).

Follow-up observations in other electromagnetic energies eventually provided additional information on

GRBs. The Gamma Ray Burst Coordinates Network (GCN) was developed to automatically notify astronomers of GRB detections to aid in rapid followup (Barthelmy [15]). X-ray flashes (XRFs) have been observed and linked to GRBs. With BeppoSAX satellite and other satellite observations in X-rays, improved source locations for GRBs were obtained. Such information allowed observations of optical afterglows of GRBs beginning in 1997. Automated systems involving the GCN have improved the response time, as illustrated by the ROTSE-1 team which obtained automatic observations of GRB 990123 in 1999 within seconds of the gamma ray burst itself. In turn, afterglow observations served to identify presumed host galaxies for some GRBs, with redshift measurements giving typical distances of several Gpc. With GRBs established as occuring at cosmological distances, energy releases could be calculated as up to 10^{54} ergs, or the energy equivalent of one solar mass, if the energy emission was anisotropic. Another key development was development of evidence linking GRBs and supernovae. This connection was proposed in the case of GRB 980425 and SN 1998bw in 1998, but established in the case of GRB 030329 in 2003, based on observations of the afterglow (Willingale *et al.* [16]). As of 2002 over 40 GRB afterglows had been observed, with host galaxies identified in over 30 cases (see review by Mészáros [14]), and through 2004 associated redshift measurements have been obtained for over 30 GRBs. Spacecraft currently providing GRB obserations include HETE, INTEGRAL, RXTE, and Ulysses. NASA's Swift satellite to be orbited in late 2004 is expected to significantly extend detection and observation capabilities. During its two year mission, Swift's gamma-ray detectors will provide arc minute accurate positions within about 10 s of a GRB, then direct its onboard X-ray and optical/UV telescopes onto the GRB within 20-70 s for follow-up observations (NASA [17]).

Together, these observations have led to collapsar models for long GRBs which explain them as a special type of supernova. In these models, the core of a massive collapsing star forms a black hole, and rapidly infalling material forms an accretion disk. Either due to the star's rapid rotation or strong magnetic fields or both, particles and radiation preferentially escape in jets perpendicular to the accretion disk. As these jets collide with stellar material or surrounding gas at Lorenz factors up to 1000, they produce beamed gamma-ray and X-ray bursts. While the degree of beaming remains unclear, beaming is demonstrated by the intensity decay of GRB afterglows. The rate of this decay abruptly increases at a particular point in time, corresponding to the end of spreading of the relativistic beaming effect. It is also suggested that observed X-ray flashes are slightly off-axis GRBs. In attempting to relate observed energy fluxes to energy available in a stellar collapse, beaming is a key factor. If beaming occurs, this would reduce the required source energies by a factor of 100 or more, to levels that correspond with such collapse models.

Short GRBs, however, remain poorly modeled because of the lack of follow-up observations that might provide observational constraints, this lack due to their short duration. One possibility is that they result from the final merger of a binary neutron star into a black hole, either with or without gamma rays preferentially emitted in jets perpendicular to a short-lived accretion disk. Alternately, the source could be unrecognized in nature.

In the cases of both types of GRBs, they appear to be promising sources of gravitational waves, given the indications of relativistic motion of compact masses. They are currently the most studied event for triggered burst searches of gravitational waves due to their frequency, the current ability to identify source location, and the relatively short time delay between the GRB trigger and the gravitational wave signal. Observable GRBs are typically at distances of several Gpc, much more distant that some other potential burst sources.

III. DETECTION OF GRAVITATIONAL WAVES

A. Introduction

Expected gravitational wave sources will produce signals of order $h = 10^{-21}$ or less. Detection of such gravitational waves presents significant challenges. Consider that even for test masses separated by the diameter of the Earth, the above strain produces a change in relative displacement which is an order of magnitude smaller than an atom. Two principal methods have been pursued to detect such signals: bar detectors and interferometric detectors. These will be described, with subsequent discussion focusing on interferometric detectors to cover antenna patterns, noise, data analysis, and detection tests.

B. Bar detectors

Resonant bar detectors were the first proposed means of detecting gravitational waves. Consider a bar with its axis perpendicular to a gravitational wave's direction of propagation. For gravitational waves of a frequency near the natural vibrational frequency of the bar, the gravitational waves would excite vibrations in the bar. These mechanical oscillations can be measured with transducers. Weber first experimented with such bars in the 1960s; while he claimed coincident detections (Weber [18]), they were unconfirmed by other observers. However, similar detectors were subsequently built by several independent groups. These second-generation bar detectors are operated in vacuum chambers and cryogenically cooled to minimize thermal noise.

Several such bar detectors are in operation, including ALLEGRO in Louisiana (Heng *et al.* [19]), AURIGA (Zendri *et al.* [20]) and NAUTILUS in Italy (Astone *et al.* [21]), EXPLORER in Switzerland (Astone *et al.* [22]),

and NIOBE in Australia (Coward *et al.* [23]). (See appendix B for additional information.) These all have peak sensitivities near 900 Hz with the exception of NIOBE which has peak sensitivity near 700 Hz. These five detectors form the International Gravitational Event Collaboration (IGEC) in seeking coincident signals (Astone *et al.* [24]). Correlations with interferometric detectors are feasible at these narrow bands. Figure 2 is an image of the ALLEGRO bar detector taken while the cryogenic container was open for maintenance, viewing from one of the bar.

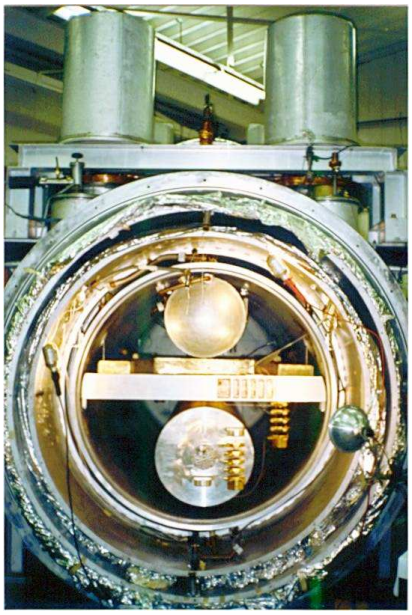

FIG. 2: ALLEGRO bar detector: View of ALLEGRO bar detector with cryogenic dewar open. Image from ALLEGRO [25].

Resonant detectors of other shapes have been proposed, specifically spherical detectors. None of these are yet in operation. Such detectors would have omni-directional sensitivity, in contrast to bar detectors (Pizzella [26]).

Bar detectors are severely limited by the very narrow band sensitivity, confined to near the natural resonance frequency of the bar. Interferometers are not so limited.

C. Interferometric detectors

The first prototype laser interferometric detector was completed in 1972 by a team led by Forward (Forward [27]). Such detectors employ a Michelson interferometer, with the laser beam split at a corner test mass and reflected from a pair of orthogonally located mirror test masses at the end of each arm. The passage of a gravitational wave (from an appropriate direction) will induce relative changes in the length of the arms, i.e. the distance between each arm's end test mass and the corner test mass. The recombined laser beam's interference pattern is then used to compare arm lengths and potentially detect very slight changes in relative length.

In describing the practical aspects of such detectors we consider in particular those of the LIGO project (Barish and Weiss [28]). LIGO, for Laser Interferometer Gravitational Wave Observatory, is a project involving three detectors at two well-separated locations, one at Hanford in Washington state (LIGO Hanford Observatory or LHO) and one near Livingston, Louisiana (LIGO Livingston Observatory or LLO). LIGO began collecting scientific data during its first science run in August-September 2002.

Figure 3 is an aerial view of the LIGO Livingston Observatory, showing the corner station with one 4-km arm extending towards the horizon.

FIG. 3: LIGO Livingston Observatory: Aerial view of LHO site. Image from LIGO [29].

In practice, each arm is set up as a Fabry-Perot cavity, with the laser beam trapped between the respective end mirror and a semi-transparent mirror near the corner beam splitter (see figure 4). The arm lengths are adjusted to produce destructive interference of the recombined beam at the detector. A recycling mirror located between the laser and the beam-splitter further increases the laser power within the interferometer and reduces noise.

For each LIGO site, the interferometer arms are 4 km in length and contained in an ultrahigh vacuum assembly. Test masses/optics are suspended within this assembly and seismically isolated by a four-layered passive isolation apparatus (Barish [30]). The entire system is isolated from electrical noise, and a variety of sensors monitor the internal and external environment in terms of potential noise sources. The LHO facility contains two independent interferometers within the same vacuum assembly, having arm lengths of 4 km (LHO-4k) and 2 km (LHO-2k).

Several other such detectors are in operation as well,

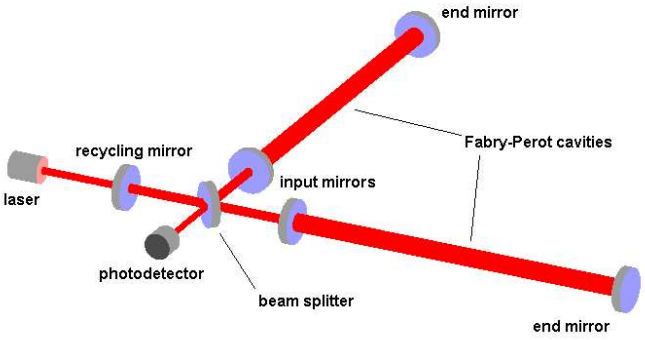

FIG. 4: Laser interferometer configuration

notably VIRGO in Italy (Acernese *et al.* [31]), GEO in Germany (Willke *et al.* [32]), and TAMA-300 in Japan (Ando *et al.* [33]). AIGO (Blair [34]), an additional project in Australia operated by ACIGA, is under development; currently it is operating a testbed version with 80 meter arms. Data regarding these detectors are listed in appendix B. VIRGO, GEO, and TAMA were completed between 2001 and 2003. LIGO, GEO, and TAMA have run coincident searches (VIRGO has not yet operated in science mode). At this stage, the interferometers generally gather scientific data continually only during science runs of limited duration, with engineering work performed between these runs.

These detectors have maximum sensitivities in the range of 50 Hz to a few kHz. The limitations will be discussed further in section 3.5 in reference to noise. GEO, however, is being converted to a dual-recycling configuration which will give it a narrow band sensitivity quite different in form from other IFOs (Malec *et al.* [35]). The general similarity of the LIGO, VIRGO, and TAMA detectors has implications for coincident analysis that will be discussed below.

A space-based interferometric detector is being developed by NASA and ESA. This Laser Interferometer Space Antenna (LISA) (Danzmann and Rüdiger [36]) would comprise three probes in solar orbit roughly forming a equilateral triangle 5×10^6 km on a side. Each probe would serve as both end test mass and laser source. LISA would be sensitive to gravitational waves of far lower frequencies (10^{-3} to 10^{-1} Hz) than the ground-based detectors currently in operation.

During the anticipated 3-year LISA mission, the design sensitivity would guarantee detection of a variety of gravitational wave signals, such as signals from binary supermassive black holes or stars orbiting supermassive black holes. At the lower end of its sensitivity window, LISA will be limited by the stochastic noise from galactic white dwarf binaries (Benacquista *et al.* [4]).

D. Orientation and antenna patterns

An individual interferometric detector cannot identify the direction of a gravitational wave source. However, the sensitivity of such a detector to a given gravitational wave is dependent on the detector's orientation relative to the direction of the source. Consider a detector with the corner station located at the origin and detector arms oriented along the positive x- and y-axes. A gravitational wave of plus polarization (in the detector frame) directed along the z-axis will induce a stretching of one arm and a shortening of the other. This orientation provides for maximum sensitivity. Note that the effect in the detector is independent of whether the source direction is in the positive z direction or negative z direction.

Alternately, consider a cross polarized gravitational wave directed at the same detector also along the z-axis. In this case, the end masses will be displaced equally and comparison of arms lengths will show no relative change. Thus such a gravitational wave is undetectable in this orientation. The results are similar for gravitational waves (of either polarization) directed either along the bisector of the detector arms or orthogonal to this bisector. Note in the latter case we assume a gravitational wave wavelength that is large compared to the size of the detector. From here on, it is assumed that the wavelength of the gravitational waves is large compared to the size of the detector; in the case of LIGO, this limits us to frequencies below about 10 kHz.

The directional sensitivity of interferometric detectors to the two polarizations, referred to as antenna patterns, are discussed by Rakhmanov and Klimenko [37]. Consider a gravitational wave with polarization components $h_+(t)$ and $h_\times(t)$ with respect to some fixed frame. The detector's ideal response (in the absence of noise) will be

$$h(t) = F_+(t)h_+(t) + F_\times(t)h_\times(t) \tag{11}$$

where F_+ and $F_\times$ are the detector response functions and are functions of the detector's orientation with respect to the source direction and frame, i.e. functions of detector latitude, longitude, orientation, angle between arms, and source right ascension, declination, gravitational wave polarization, and local time. The time dependence of F_+ and $F_\times$ involves specifying the detector's location in space on the rotating Earth.

To determine the detector response as it depends on these factors, we can take the previous solution for the strain tensor from section 2.2 as it depends on $A^{TT}_{\alpha\beta}$. Neglecting the time dependence and separating the plus and cross polarization components gives an expression for the gravitational wave strain tensor of

$$\mathbf{h_s} = h_+ \begin{bmatrix} 1 & 0 & 0 \\ 0 & -1 & 0 \\ 0 & 0 & 0 \end{bmatrix} + h_\times \begin{bmatrix} 0 & 1 & 0 \\ 1 & 0 & 0 \\ 0 & 0 & 0 \end{bmatrix} = h_+\mathbf{m} + h_\times\mathbf{n}. \tag{12}$$

This result is in the coordinate frame defined by the source direction and polarization and must be trans-

formed to the frame defined by the detector. For interferometer detectors, a detector frame is naturally defined by the two arms, defined as the x- and y-axes. The signal in the detector is proportional to the difference in length of the two arms, or proportional to

$$\overline{s} = \frac{1}{2}\mathrm{Tr}[\mathbf{mh}] \tag{13}$$

in terms of $\mathbf{h}$, the strain tensor in the detector frame. This is related to the strain tensor $\mathbf{h_s}$ in the source frame by a rotational transformation:

$$\mathbf{h} = \mathbf{R}^T\mathbf{h_s}\mathbf{R}. \tag{14}$$

The rotational transformation can be described by three Euler rotations (see figure 5). Consider the source direction to be described by θ, angle from detector zenith, and ϕ, angle from detector x-arm direction to source azimuth. The rotation $\mathbf{R}$ is

$$\mathbf{R} = \mathbf{R}_z(\psi)\mathbf{R}_y(\theta)\mathbf{R}_z(\phi) \tag{15}$$

describing a rotation about the detector z-axis to align the source with the detector x-axis, a rotation about the new y-axis to rotate the source to the detector zenith, and a rotation about the z-axis by the polarization angle to align the frames.

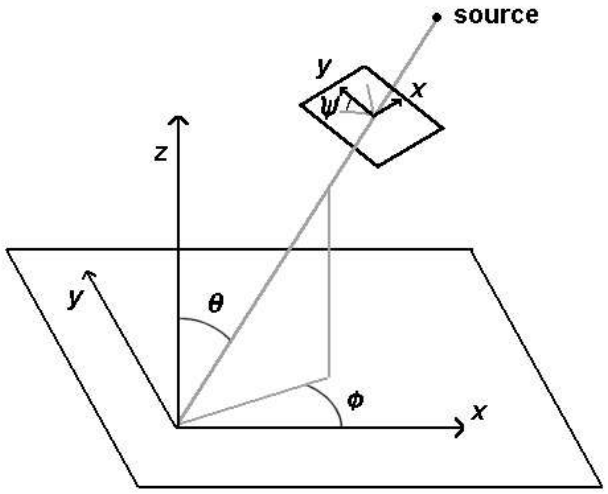

FIG. 5: Rotations from source frame to detector frame: See text for explanation. After Rakhmanov and Klimenko [37].

To illustrate the antenna patterns consider this in the detector frame defined above, with source direction given by θ and ϕ and polarization angle by ψ. In this case the response functions are

$$\begin{aligned} F_+ &= \frac{1}{2}\cos 2\phi(1+\cos^2\theta)\cos 2\psi - \sin 2\phi\cos\theta\sin 2\psi, \\ F_\times &= \frac{1}{2}\cos 2\phi(1+\cos^2\theta)\sin 2\psi - \sin 2\phi\cos\theta\cos 2\psi. \end{aligned}$$

Figure 6 shows the magnitudes of these responses as a radius vector over all possible sky positions (polarization angle is fixed at $\psi = 0$).

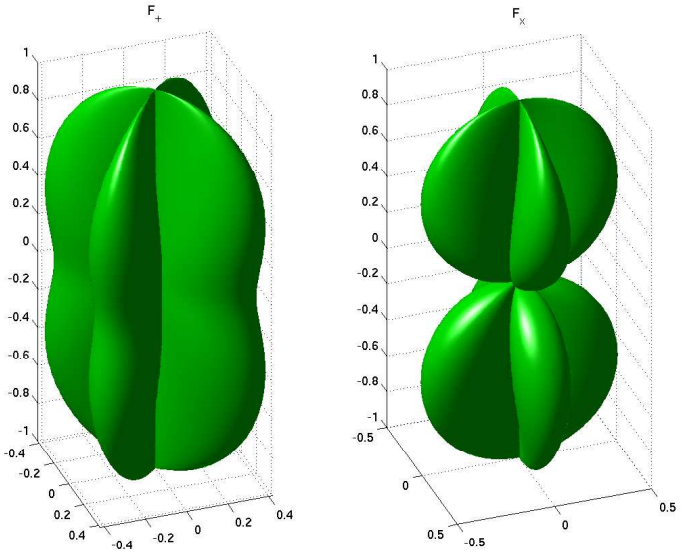

FIG. 6: Antenna patterns: Idealized antenna patterns for interferometer detector, for + polarizations (left) and × polarizations (right).

In practice, additional rotations are needed to incorporate the conventional source and detector data; the resultant expressions below are developed by Jaranowski, Królak, and Schutz [38]. Source direction is specified by celestial coordinates: right ascension α and declination δ. Detector location is given by geographic latitude λ and longitude L, the angle between the arms is ξ, and its orientation may be described by angle γ measured from due east counter-clockwise to the bisector of the detector arms. Polarization angle ψ is defined in the source frame (related to the detector frame by the previously described rotations).

Finally, the time-dependent aspect of the detector's orientation must be specified as it depends on the Earth's rotation. This is necessary to relate the source's sky position to the detection's geographical location on the rotating Earth; we consider this to be a fixed quantity for a given burst. For simplicity, we may define

$$\phi' = L + \phi_0 + \Omega_r(t - t_0) \tag{16}$$

where Ω_r is the angular velocity of the Earth's rotation, ϕ_0 is the celestial right ascension aligned with the Greenwich meridian at time t_0, and t is the current time. Then detector responses may be expressed as

$$F_+(t) = \sin\xi[a(t)\cos 2\psi + b(t)\sin 2\psi] \tag{17}$$

$$F_\times(t) = \sin\xi[b(t)\cos 2\psi - a(t)\sin 2\psi] \tag{18}$$

where

$$\begin{aligned} a(t) &= \frac{1}{16}\sin 2\gamma(3-\cos 2\lambda)(3-\cos 2\delta)\cos[2(\alpha-\phi')] \\ &\quad -\frac{1}{4}\cos 2\gamma \sin\lambda(3-\cos 2\delta)\sin[2(\alpha-\phi')] \\ &\quad +\frac{1}{4}\sin 2\gamma \sin 2\lambda \sin 2\delta \cos(\alpha-\phi') \\ &\quad -\frac{1}{2}\cos 2\gamma \cos\lambda \sin 2\delta \sin(\alpha-\phi') \\ &\quad +\frac{3}{4}\sin 2\gamma \cos^2\lambda \cos^2\delta \end{aligned} \tag{19}$$

$$\begin{aligned} b(t) &= \cos 2\gamma \sin\lambda \sin\delta \cos[2(\alpha-\phi')] \\ &\quad +\frac{1}{4}\sin 2\gamma(3-\cos 2\lambda)\sin\delta \sin[2(\alpha-\phi')] \\ &\quad +\cos 2\gamma \cos\lambda \cos\delta \cos(\alpha-\phi') \\ &\quad +\frac{1}{2}\sin 2\gamma \sin 2\lambda \cos\delta \sin(\alpha-\phi'). \end{aligned} \tag{20}$$

Note that $\sin\xi = 1$ for detectors with orthogonal arms.

It was noted above that a single detector cannot identify source direction for an unknown signal. However, the delay in arrival time among multiple detectors potentially provides directional information; additionally, it must be accounted for in comparing results from individual detectors. Gravitational waves propagate at the speed of light; thus, the separation of the LLO and LHO detectors, for example, corresponds to a time delay of up to 10 ms, depending on source direction.

E. Noise

Before addressing methods of identifying a signal, we first examine the nature of noise in the detectors. Here we first define noise and noise power spectral density, use this to describe the sensitivity of the various detectors, then detail the sources of noise in LIGO and finally comment on the statistical nature of this noise. Statistical aspects of noise are further discussed by van Trees [39].

Detector noise is most basically the random background of detector output, resulting from the physical and technical constraints of the detector and environmental effects (both local and non-local) that affect output. In a variety of situations noise can be approximated as Gaussian or normally distributed, where individual samples of the series $n(i)$ are drawn from a distribution described by

$$P(n(i):\mu,\sigma^2) = \frac{1}{\sqrt{2\pi\sigma^2}} e^{-(n(i)-\mu)^2/2\sigma^2}. \tag{21}$$

The parameters μ and σ^2 are the mean and variance of the distribution, respectively, defined as

$$\mu = E[x(i)] \tag{22}$$

$$\sigma^2 = E[(n(i)-\mu)^2]. \tag{23}$$

Noise RMS (root mean square), or standard deviation σ, is the square root of the noise variance.

Generally, the various samples $n(i)$ are not independent of each other but are correlated. This is described by the covariance function

$$K(i,j) \equiv E[(n(i)-\mu)(n(j)-\mu)] \tag{24}$$

where μ is the mean referenced above. For a discretely sampled time series of finite length, this information is conveyed by the covariance matrix

$$\mathbf{C}_{ij} \equiv E[(n(i)-\mu)(n(j)-\mu)] \tag{25}$$

which for a series with N samples will be an N by N matrix. If the individual samples are independent of each other, the covariance matrix is simply

$$(C)_{ij} = \sigma^2\delta(i-j) \tag{26}$$

and the noise is called white. Otherwise, the noise is called colored.

Additionally, the noise is described as stationary if these statistical properties (such as μ and σ^2) are unchanging in time. This includes the covariance function; the noise is specifically covariance-stationary if the covariance function depends only on $|i-j|$ and not on i or j individually.

In practice, detector noise is far from ideal: it is non-Gaussian, colored, and non-stationary. Consider first the colored nature of noise in detectors such as LIGO. This is the consequence of the frequency-dependent sensitivity of such a detector, which is most often expressed as power spectral density (PSD), or variance per unit bandwidth. This is defined as

$$S(f) = \int_{-\infty}^{\infty} R(\tau) e^{-i2\pi f\tau} d\tau \tag{27}$$

where $R(\tau)$ is the auto-correlation function for the detector, and $\tau = |i-j|\Delta t$ is the time difference between the samples with sampling at intervals of Δt. This is related to the previously described covariance function by

$$K(i,j) = R(i,j) - \mu^2 = R(\tau) - \mu^2. \tag{28}$$

Strain PSD is then frequency dependent and may be expressed in $\sqrt{\mathrm{Hz}^{-1}}$. Figure 7 compares the PSDs for ALLEGRO (a representative bar detector), LIGO (a representative ground-based IFO detector), and LISA. Figure 8 shows PSDs for the various ground-based IFO detectors discussed previously, along with LIGO II. LIGO II, or Advanced LIGO, is a planned upgrade of LIGO and is discussed below.

In the case of the LIGO detectors, the design sensitivity for first generation LIGO is at best $h(f) = 10^{-22}$ per root Hz. Given the 4 km arm length this corresponds to a relative displacement of the test masses of order 10^{-17} m.

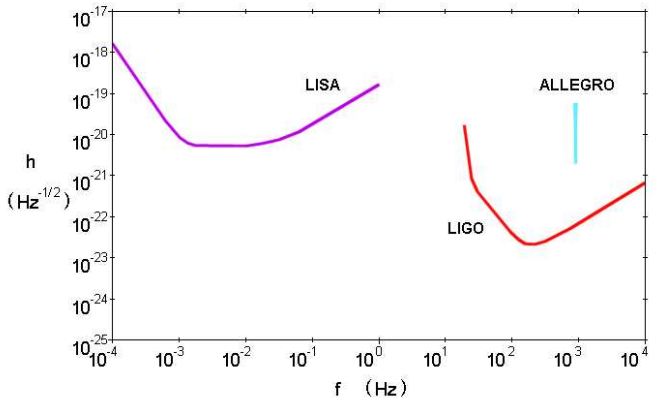

FIG. 7: Detector power spectral densities: LISA, LIGO, ALLEGRO: After Sathyaprakash and Winkler [40] and Hamilton *et al.* [41].

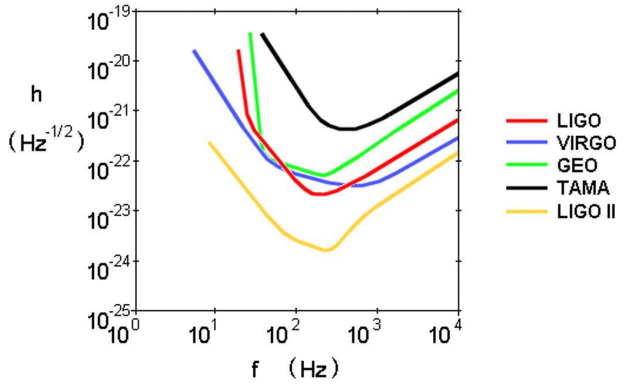

FIG. 8: Detector power spectral densities, ground-based IFOs: After Sathyaprakash and Winkler [40] and Torres [42].

The LIGO PSD is depicted in figure 9. From several hundred Hz and above, increasing with higher frequency, LIGO sensitivity is limited by photon shot noise, or the quantization of the laser beam into individual photons which introduces uncertainty into intensity measurements by the photodetector. High laser power, including the results of beam recycling plus the Fabry-Perot cavity assembly, serves to reduce the ratio of this noise to total measured power. The floor at maximum sensitivity around 300 Hz includes the effects of thermal vibrations of atoms in the test masses and in the suspension system. In the neighborhood of 50 Hz, sensitivity rapidly diminishes due to seismic noise. In the current generation LIGO, this represents low frequency vibrations from both natural and anthropogenic sources.

Future upgrades to LIGO are planned, referred to as LIGO II. The planned sensitivity will be improved over that of LIGO I by a factor of 10 or more (depending

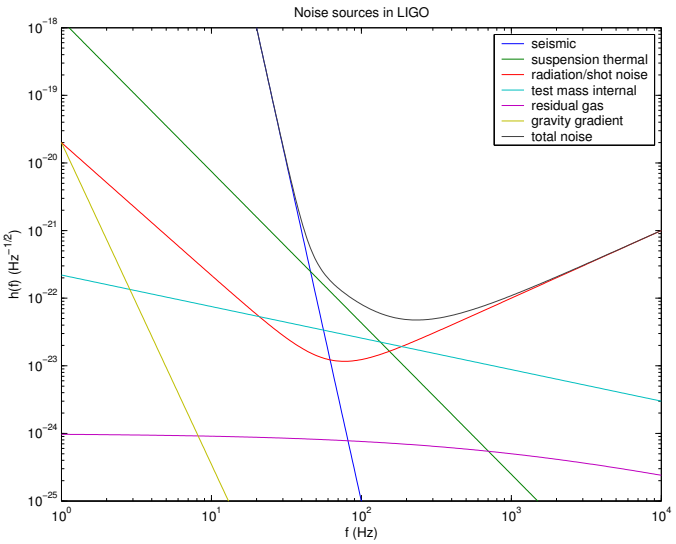

FIG. 9: LIGO sensitivity and noise sources: After Hughes *et al.* [43].

on frequency) and the "seismic wall" or low-frequency cutoff will be pushed back to around 20 Hz. LIGO II system improvements will improve sensitivity by addressing all of these noise sources; this includes superior seismic isolation, higher laser power, improved optics, and more massive test masses. An additional noise source which may then become an issue at low frequencies is gravity gradient noise. Seismic waves traveling past the detector test masses displace the ground mass. In particular Rayleigh waves displace the surface in a rolling motion (combined transverse and longitudinal motion). This produces a time-varying change in the Newtonian gravitational forces from the ground on the test masses. Since the effect is conveyed to the test masses gravitationally and not acoustically, seismic isolation does not address this phenomenon. If it proves to be an issue, arrayed seismometers may allow subtraction of this effect (Johnston [44]). Noise from residual gas molecules in the detector arms and radiation pressure are also potential noise issues for LIGO II.

Narrow band higher noise sources include electrical noise, including spikes at multiples of 60 Hz associated with noise from the electric power supply, and resonances in the suspension system.

The colored nature of detector noise can be addressed for many applications by data whitening. Additionally, detector noise is in practice non-Gaussian and non-stationary. In particular, bursts of noise with higher than average variance are common. LIGO concurrently records data from environmental sensors to help isolate affected data segments. Still, data analysis must consider the non-ideal nature of the noise.

F. Data analysis

Data analysis efforts for LIGO are organized into separate groups, each addressing a different type of signal: Inspirals, Periodic (Pulsar), Burst, and Stochastic Sources. This reflects the different statistical and analytic strategies involved for these differing target signals.

The Periodic sources subgroup is looking for periodic signals (relatively) unchanging in time in terms of frequency; pulsar phenomena are leading potential sources. The Inspiral sources subgroup seeks to detect the chirp of frequency changing in the last moments before binary neutron stars or black holes plunge together, along with the merger phenomena. The Stochastic sources subgroup is concerned with a random background of signal. The long-term nature of periodic and stochastic signals allows these analyses to integrate signals over long time periods.

The Burst sources subgroup seeks any short burst of gravitational waves. In a single detector this would in general be indistinguishable from non-stationary noise in that detector. This necessitates comparison (correlation) of results from two or more detectors.

The current burst analysis pipeline is described in LSC [45]. Data segments where all three detectors were operating in science mode are identified. For each LIGO interferometer, the output data stream is validated and filtered. This prepared data is then subjected to two parallel algorithms to identify event triggers. For the same time segments, data from auxiliary interferometer channels is used to identify anomalous environmental or detector events which could be misinterpreted as bursts. Events identified here are used to veto any corresponding event triggers. The surviving set of single IFO event triggers is then compared to the sets from the other three detectors. Events must be coincident in multiple detectors, with coincidence defined in terms of time, clustering, and frequency cuts. This produces a smaller set of event candidates. To evaluate the frequency of false alarms, checks include offsetting the different IFO event triggers in time to test for background "burst" rates. Hardware and software injections are also applied to each interferometer at the front end of the analysis pipeline for testing.

G. Triggered burst analysis

Burst searches based on independent triggers are a special type of burst search to which this project most relates, so we examine it in some detail. The Triggered Burst subgroup is concerned with possible gravitational wave bursts associated with independent observations of transient astrophysical phenomena, notably GRBs. Such searches have some advantages over untriggered searches. The sensitivity is greater because the ability to target a specific time segment reduces false alarms, plus the independently observed trigger may suggest a particular waveform for the particular signal. Data analysis for such searches is significantly different than many searches in that the source location is (generally) known from the independent trigger. As a result, both the time delay and the direction-dependence of individual detector response functions can be factored out.

Currently, GRBs are used as triggers for such searches because of their frequency of detection (about 1 per day) and because current models suggest a small delay between the trigger signal and the gravitational wave signal. Specifically, collapsar models suggest that the GRB will lag about 100 seconds or less behind the gravitational wave emission (this delay represents the time for the jets to reach surrounding gas and produce gamma ray emissions).

The analysis pipeline is described by Mohanty *et al.* [46] and may be summarized as follows. GRB trigger information is obtained from the GCN. Since this includes source sky location, the corresponding time for each detector involved may be determined. Note that while the detection of a GRB is reported within seconds, accurate sky location information may take a few hours or more to become available. Corrections include propagation time between detectors and between the detecting spacecraft and the detectors, as well as timing corrections particular to detectors. Comparison of source direction to detector antenna patterns allows a quality factor to be assigned based on the potential detectability of a given signal.

For each trigger, on-source data segments are identified from each detector, with adjustments for propagation time delay. These segments cover a range in time before and after the trigger since most models suggest a time delay between the GRB and production of gravitational waves. Remaining data segments form the off-source data set.

Data conditioning precedes application of search algorithms and includes line removal, or filtering to eliminate narrow bands of high noise (from sources such as electrical system noise). Bandpass filtering eliminates noise at lower frequencies where seismic noise dominates and at higher frequencies where system noise increases (and fewer gravitational wave signals are expected). The data is also whitened to simplify subsequent analysis.

Mohanty *et al.* [46] develop a statistical indicator comparable to the cross-correlation of limited length time series between two detectors, but normalized with off-signal data. This indicator has free parameters corresponding to start time, relative shift between the two detectors, and the length of the time series. These three parameters define a three-dimensional S-volume, and several different methods are used to collapse this to two-dimensional maps dependent on start time and time series length.

The real-time notice of GRBs via the GCN is not critical to gravitational wave observations, since detector data is stored, but could have applications. In particular, notification of detector operators can permit requests that detector lock status be maintained or extended.

H. Hypotheses testing

The search for gravitational waves using detectors such as LIGO involves signals which are of small amplitude compared to the noise RMS. Statistical tests are a necessary means of detecting a signal.

Consider two detectors with uncorrelated noise $n_1(t)$ and $n_2(t)$ for detectors $j = 1, 2$. In general the gravitational wave signal will be different in the two detectors; this will be $h_1(t)$ and $h_2(t)$ in the respective detectors. These signals will differ due to the (generally) different antenna patterns for the detectors as well as the relative time shift due to difference in signal arrival time at the two detectors. The observed signals in the two detectors may be written

$$x_1(t) = h_1(t) + n_1(t) \quad (29)$$
$$x_2(t) = h_2(t) + n_2(t). \quad (30)$$

Initially we will consider the case of a pair of identical, co-located, co-aligned detectors. In this case $h_1(t) = h_2(t) \equiv h(t)$.

By making a comparison of the two signals, the effects of individual uncorrelated noise may be minimized, increasing the potential of detecting a signal. One statistical test for such a comparison is the cross-correlation, defined (for two detectors) as

$$\Lambda_{CC} \equiv < \overline{x}_1, \overline{x}_2 > = \sum_{m=1}^{N} x_1(m) x_2(m) \quad (31)$$

for a discretely sampled time series with N samples. Λ_{CC} is the test statistic, which is the quantitative result of the test. Figure 10 gives a schematic illustration of cross-correlation. The signal (top series) is observed by two detectors amidst uncorrelated noise (middle figures), making direct identification of the signal difficult. A cross-correlation of the two detector series for various time offsets, however, shows a noticably higher result for Λ near zero time offset (bottom figure). The value of Λ will tend toward zero if no correlated signal is present (assuming uncorrelated noise of zero mean), but will have positive values for correlated signals, increasing in magnitude with stronger signals. In this sense, such statistical methods serve to increase detector sensitivity.

Another test is the matched filter. A known or postulated signal waveform is here correlated with a detector signal; a high statistic value results if the detector signal contains a signal corresponding to the filter.

For the matched filter test, signal-to-noise ratio (SNR) may be defined as follows in the case of Gaussian stationary noise with mutually independent samples:

$$(SNR)_{MF} = \frac{\sum_{i=1}^{N} h^2(i)}{\sum_{i=1}^{N} n^2(i)} = \frac{< \overline{h}, \overline{h} >}{\sigma^2} \quad (32)$$

for a known signal $h(i)$, detector signal $x(i)$, and noise $n(i)$ having variance σ^2 and zero mean μ.

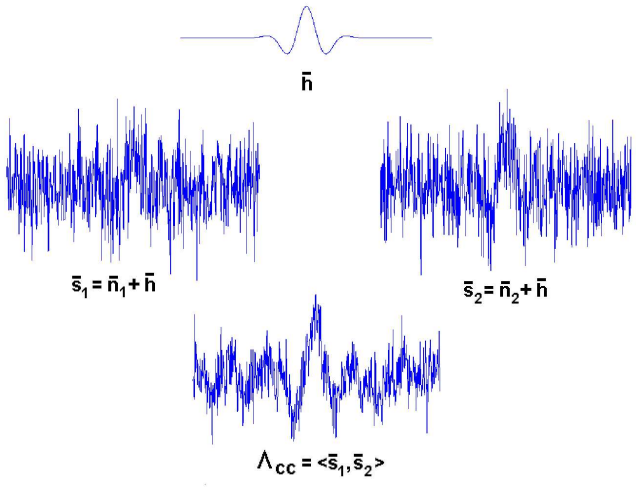

FIG. 10: Illustration of cross-correlation: See text for explanation.

The performance of different tests can be compared using the receiver operating characteristic (ROC) curve, which is the relation of the probabilities (P):

$$P\{\Lambda > k \text{ given a signal is present } \} \text{ vs. } P\{\Lambda > k \text{ given no signal } \}$$

for a specified threshold k, where Λ is the test statistic.

A further test is based on the likelihood ratio. The generalized likelihood ratio test is an optimized statistical test in the frequentist sense. Details are discussed by van Trees [39]. Consider data $\overline{X}$ with a probability distribution $P(\overline{x}|\overline{a})$ as a function of parameters $\overline{a}$ drawn from parameter space A. In the case here, A would be the set of all possible signals with each $\overline{a}$ describing a particular signal; we may indicate the parameters corresponding to the absence of any signal by A_0. Suppose we have a pair of hypotheses

$$H_0 : \overline{a} \in A_0 \text{ vs. } H_1 : \overline{a} \notin A_0 \quad (33)$$

which here would be that no signal is present H_0 vs. that a signal is present H_1. The likelihood ratio is defined as

$$\Lambda = \frac{P(\overline{x}|\overline{a}) : \overline{a} \notin A_0}{P(\overline{x}|\overline{a}) : \overline{a} \in A_0}. \quad (34)$$

This ratio gives small values in the case of the second hypothesis H_1. Maximizing the statistic $\Lambda(x)$ with respect to $\overline{a}$ favors the first hypothesis H_0. This is then a generalized means of hypothesis testing.

Applying this to the case of two detectors considered here, if the maximized likelihood ratio test statistic for two detectors is generalized to unknown signal $\overline{h}$:

$$\Lambda(\overline{x}|\overline{h}) = \max_{\overline{h}} \frac{P_1(\overline{x}_1, \overline{x}_2|\overline{h})}{P_0(\overline{x}_1, \overline{x}_2)} \quad (35)$$

which may be maximized by maximizing $\ln(\Lambda)$, and

$$\ln(\Lambda) = \sum_{m=1}^{N} x_1(m)h(m) + \sum_{m=1}^{N} x_2(m)h(m) - \sum_{m=1}^{N} h^2(m). \tag{36}$$

Note that the noise is assumed Gaussian and white. This result is maximized if

$$\frac{\partial}{\partial h(n)} \sum_{m=1}^{N} \Big(x_1(m)h(m) + x_2(m)h(m) - h^2(m) \Big) = 0 \tag{37}$$

which yields

$$h(m) = \frac{x_1(m) + x_2(m)}{2}. \tag{38}$$

Substituting this result for $h(m)$ above gives a maximized statistic

$$\ln(\Lambda) = \left\langle \frac{\overline{x}_1 + \overline{x}_2}{2}, \frac{\overline{x}_1 + \overline{x}_2}{2} \right\rangle \tag{39}$$

which can be compared to a specified threshold k. For details of this derivation see appendix C.

This analysis involves a variety of simplifications. For example, we assume above that the detectors are physically identical and noise is stationary and white. In seeking a burst signal based on a trigger, a relatively short time segment is searched and thus the noise may be relatively stationary. Non-stationarity may be more of an issue in comparing the on-source sample to off-source samples (when checking for false alarm rate).

Additionally, only the LLO and LHO-4k detectors are physically identical, and the PSDs of the various detectors differ somewhat—even LLO and LHO differ slightly in PSD due to their different noise environments. The consequence is that the covariance matrix for a specified detector pair must be incorporated into calculations of cross-correlation:

$$\ln(\Lambda) = \overline{x}_1 \mathbf{C}^{-1} \overline{x}_2^T \tag{40}$$

Auto-correlation terms are similarly affected by the colored nature of the noise.

However, for an analysis confined to the IFO detectors, a first approximation may be made without considering these issues. Note that the LIGO, VIRGO, and TAMA detectors have approximately similar PSD except for a scale factor. This is a consequence of the generally similar construction of these detectors, introducing similar engineering and environmental constraints. The analysis below will consider such representation of the PSD differences.

IV. LIKELIHOOD RATIO TEST FOR BURST SIGNAL DETECTION

A. Introduction

The goal of this research was to identify optimal tests in a network of detectors for a signal associated with an external trigger. The first objective (discussed in this chapter) was to compare several statistical tests for a pair of identical co-located co-aligned detectors. Selected tests included the cross-correlation test, the likelihood ratio test, and the sum of the individual variances. This would be done analytically (for ideal noise) and by simulation (for ideal noise and a realistic noise model). For non-Gaussian noise, the cross-correlation test proved superior to the likelihood ratio test. This would motivate the method of the next stage (discussed in chapter 5), which would be development of the optimal test. There, the likelihood ratio method was used to develop optimal weightings of the various cross-correlation and auto-correlation terms within a network; then, applying the previous findings regarding cross-correlation, only those terms would be retained to form an optimal statistic.

B. Analytical derivation

The issue is to identify an optimal statistic for multi-detector correlations. Initially, the standard cross-correlation and likelihood ratio tests were compared. At this stage identical co-located co-aligned detectors were considered, simplifying the likelihood ratio test to the inner product of the average of the detector signals (as in the derivation in section 3.8). As an additional comparison, the sum of the individual auto-correlations (sum of variances for each detector) was also considered. Note that the likelihood ratio statistic is a linear combination of the cross-correlation term and the sum of variances (for the case considered here).

Recall that for a pair of identical detectors co-located and co-aligned, the signal in detector i = 1,2 is described as

$$s_i(m) = n_i(m) + h(m) \tag{41}$$

for the mth sample of N total samples, where $n_i(m)$ is the noise in detector i and $h(m)$ is the signal (same for both detectors in this initial case). In the absence of any signal, $x_i(m) = n_i(m)$. Noise is assumed to be Gaussian and uncorrelated, with mean $\mu = 0$ and variance $\sigma^2 = 1$.

First, the ROC curves were constructed by analytical treatment of these test statistics, assuming a white stationary Gaussian noise distribution. Given an arbitrary but deterministic signal and this simple noise distribution, the probability distribution of the statistic with or without a signal can be obtained. In either case each statistic has a Gaussian distribution by the central limit theorem as the number of time series samples approaches infinity. A summary of the analysis follows:

The cross-correlation statistic is defined as:

$$\Lambda_{CC} \equiv < \overline{x}_1, \overline{x}_2 > . \tag{42}$$

In terms of $n_i(m)$ and $h(m)$ this becomes, for the cases

without and with signal, respectively:

$$\Lambda_{CC} = \sum_{m=1}^{N} n_1(m)n_2(m) \tag{43}$$

and

$$\Lambda'_{CC} = \sum_{m=1}^{N} \Big[n_1(m)n_2(m) + n_1(m)h(m) + n_2(m)h(m) + h^2(m) \Big]. \tag{44}$$

Note that the term

$$\sum_{m=1}^{N} h^2(m) \equiv C \tag{45}$$

is a constant for a specified signal.

The likelihood ratio test statistic in this case is:

$$\Lambda_{LR} = \left\langle \frac{\overline{x}_1 + \overline{x}_2}{2}, \frac{\overline{x}_1 + \overline{x}_2}{2} \right\rangle = \frac{1}{4} < \overline{x}_1, \overline{x}_1 > + \frac{1}{4} < \overline{x}_2, \overline{x}_2 > + \frac{1}{2} < \overline{x}_1, \overline{x}_2 > .$$

With no signal present, this is

$$\Lambda_{LR} = \frac{1}{4}\sum_{m=1}^{N} n_1^2(m) + \frac{1}{4}\sum_{m=1}^{N} n_2^2(m) + \frac{1}{2}\sum_{m=1}^{N} n_1(m)n_2(m) \tag{46}$$

and with signal present is

$$\Lambda'_{LR} = \frac{1}{4}\sum_{m=1}^{N} n_1^2(m) + \frac{1}{4}\sum_{m=1}^{N} n_2^2(m) + \frac{1}{2}\sum_{m=1}^{N} n_1(m)n_2(m) + \sum_{m=1}^{N} n_1(m)h(m) + \sum_{m=1}^{N} n_2(m)h(m) + C \tag{47}$$

where C was defined in equation 4.5.

The final test used was the sum of the variances (or auto-correlations):

$$\Lambda_{VS} \equiv < \overline{x}_1, \overline{x}_1 > + < \overline{x}_2, \overline{x}_2 > . \tag{48}$$

With no signal present, this is

$$\Lambda_{VS} = \sum_{m=1}^{N} n_1^2(m) + \sum_{m=1}^{N} n_2^2(m) \tag{49}$$

and with signal present is

$$\Lambda'_{VS} = \sum_{m=1}^{N} n_1^2(m) + \sum_{m=1}^{N} n_2^2(m) + 2\sum_{m=1}^{N} n_1(m)h(m) + 2\sum_{m=1}^{N} n_2(m)h(m) + 2C.$$

TABLE I: Analytic mean and variance for tests examined

test	signal absent	signal present
cross-correlation	$\mu = 0$ $\sigma^2 = N$	$\mu = C$ $\sigma^2 = N + 2C$
likelihood ratio	$\mu = \frac{1}{2}N$ $\sigma^2 = \frac{1}{2}N$	$\mu = \frac{1}{2}N + C$ $\sigma^2 = \frac{1}{2}N + 2C$
variance sum	$\mu = 2N$ $\sigma^2 = 4N$	$\mu = 2N + 2C$ $\sigma^2 = 4N + 8C$

The full derivations are included in appendix D, and the analytic results are summarized in table 4.1. Again, in each case the statistics have a Gaussian distribution described by the tabulated parameters, as the number of samples N becomes sufficiently large.

Using these results construction of the ROC curves is straightforward. The ROC curve is detection probability versus false alarm probability, or probability that the statistic exceeds a threshold in the presence of a signal versus the probability that the statistic exceeds the same threshold in the absence of a signal.

Since the statistics in this case (ideal noise) have a Gaussian distribution, the ROC curves are obtained as follows. Given a detection threshold x, the probability that a given statistic Λ is less than the threshold, i.e. the probability that $\Lambda < x$, is

$$D(x) = \frac{1}{2}\left[1 + \mathrm{erf}\left(\frac{x-\mu}{\sqrt{x\sigma^2}}\right)\right]. \tag{50}$$

The probability of a positive test result (a detection if a signal is present, or a false alarm if no signal is present) is then

$$P(x) = \frac{1}{2} - \frac{1}{2}\mathrm{erf}\left[\frac{x-\mu}{\sqrt{2\sigma^2}}\right] \tag{51}$$

in terms of the parameters derived previously.

To obtain the desired function, detection probability as a function of false alarm probability, we can solve the above equation to find the threshold that gives a specified false alarm probability, then substitute that threshold value to determine the corresponding detection probability. The above equation solved for threshold value is

$$x = \mu + \sqrt{2\sigma^2}\ \mathrm{erfinv}\ \Big[1 - 2P(x)\Big]. \tag{52}$$

For all three statistics, the fact that the noise is stationary with zero mean leads to the result

$$\sum_{i=1}^{N} n_i(m)h(m) = 0. \tag{53}$$

Thus each statistic is a sum of terms, each term either a product of the noise variance and number of samples, or the previously defined C. Since C is proportional to the

signal-to-noise ratio, the statistics are uniformly independent of the shape of the signal apart from a dependence on the signal-to-noise ratio. This is of course only true for this ideal (Gaussian) noise case.

To illustrate these analytic results, several resulting ROC curves are plotted in figure 11. This plot shows detector performance for three different values of SNR. Note that the variance sum test results are identical to the cross-correlation test results for these analytic results with Gaussian noise. In the context of our initial searches for gravitational waves, it is most desirable to minimize the false alarm probability. Given this restriction, the figure illustrates that for lower SNR values the consequence will be a low detection probability. Figure 12 shows the detection probability versus SNR for various fixed false alarm probabilities. For the false alarm probabilities depicted, a detection probability of at least 50 percent requires an SNR of at least 4 to 10.

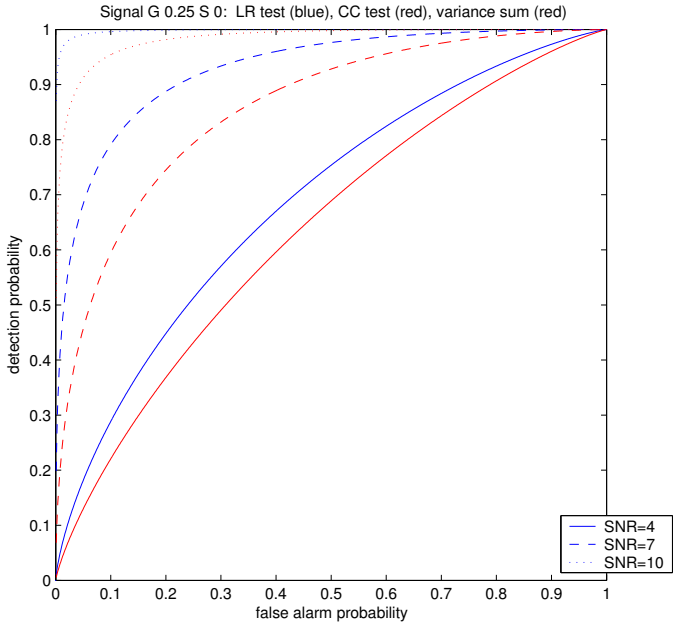

FIG. 11: Analytic ROC curve, Gaussian noise

C. Simulation, Gaussian noise

In parallel, a Monte Carlo simulation was used and its results compared to the analytic results discussed above. The simulation code was written in Matlab and is included as appendix I. Several simple burst signals were considered of two forms: a Gaussian signal or a sine-Gaussian, with varying duration, amplitude, and (in the latter case) modulation frequency. For individual trials, signals were generated by producing a vector of 1024 time samples, with noise produced as a Gaussian distribution and, in the signal present case, added to the generated

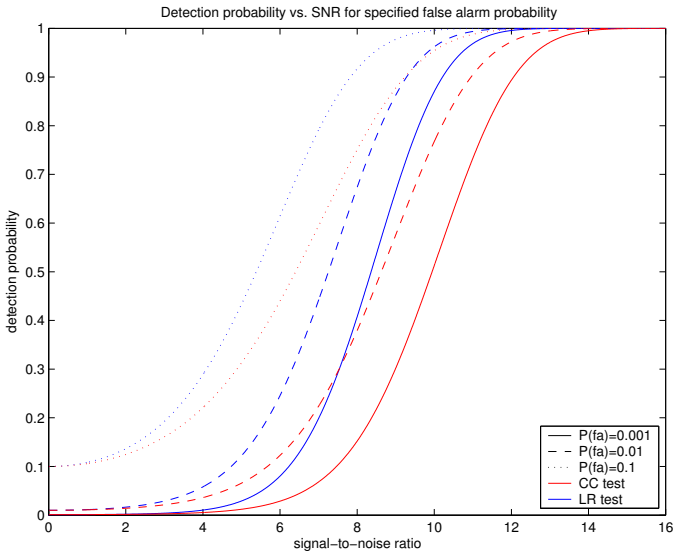

FIG. 12: Analytic detection probability vs. SNR for fixed false alarm probabilities, Gaussian noise

signal. Noise was independently generated for the signal present and signal absent cases. The three statistics were then calculated for each of the two cases from the definitions given previously. Statistic values were stored for a number of trials (typically 10^3 to 10^4), with probabilities of a statistic exceeding a specified threshold calculated from counts of these statistic values.

Simulation results were consistent with the analytic results, affirming the simulation code. The likelihood ratio test consistently outperformed the other tests, both with high SNR and low SNR. The results indicate that for the case of ideal Gaussian noise the likelihood ratio test is superior to the cross-correlation test, and that the relative performance of these tests is independent of the form of the signal beyond dependence on the SNR.

Figure 13 shows the ROC curve for a sine-Gaussian signal for a 10^4-trial simulation with SNR=2 and SNR=7. Figure 14 shows the ROC curve for a Gaussian signal with the same SNR values, but plotted with a semilog axis to emphasize performance at low false alarm probabilities. Since low false alarm probability is a priority for gravitational wave searches, performance in this regime is of particular interest.

D. Simulation, realistic noise

Next, the simulations were repeated with a more realistic noise model. The model used was a mixed Gaussian noise model, in which a random small fraction α of the time samples have noise drawn from a Gaussian distribution with standard deviation (or noise RMS) larger by

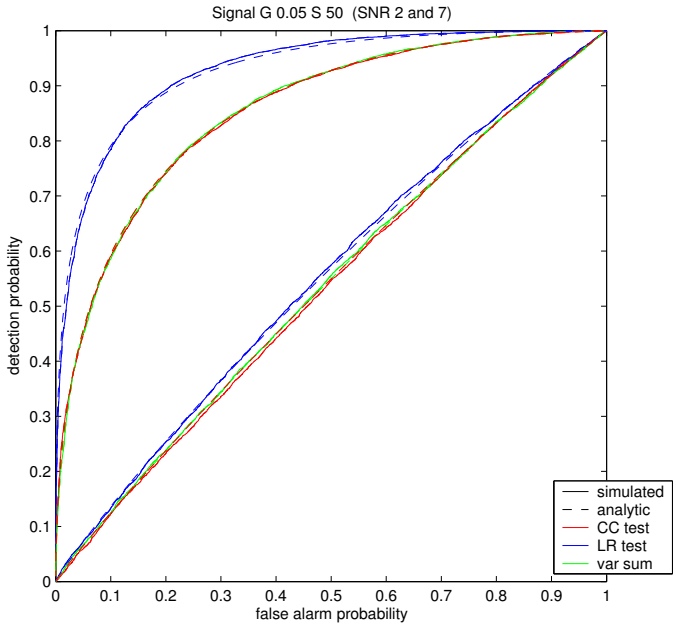

FIG. 13: ROC curve for sine-Gaussian signal, Gaussian noise: Comparison of analytic results (dashed lines) and Monte Carlo results (solid lines).

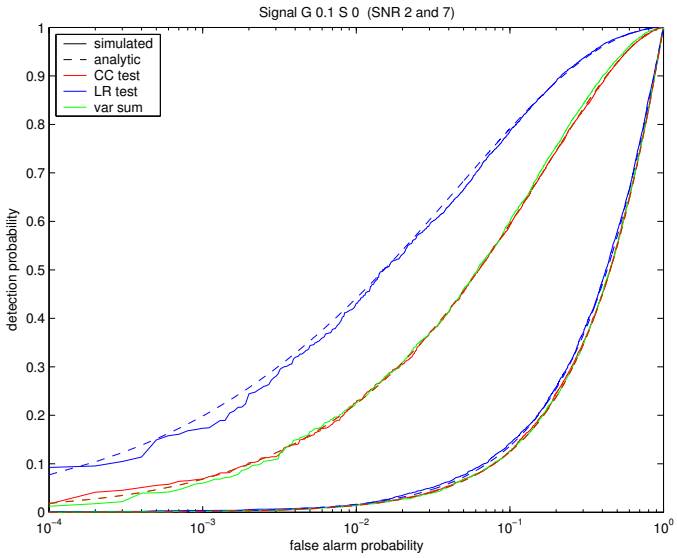

FIG. 14: ROC curve for Gaussian signal, semilog, Gaussian noise: Comparison of analytic and Monte Carlo results.

a factor k:

$$k \equiv \frac{\sigma_2}{\sigma_1}, \qquad \sigma_1 < \sigma_2 \tag{54}$$

The ratio of the variances then is $k^2 = \sigma_2^2/\sigma_1^2$. This model is moderately realistic in that interferometer noise tends to include occasional bursts of higher-variance samples.

These simulations found that for sufficiently low SNR, the cross-correlation test outperformed the other tests. The reason for this is that the non-Gaussian noise element significantly increases the auto-correlations (or variances) of individual detectors, eliminating the usefulness of this term in the likelihood ratio statistic. Plots illustrating conditions of best tests from simulations are in figures 15 and 16, with different signals (sine-Gaussian and Gaussian signals, respectively).

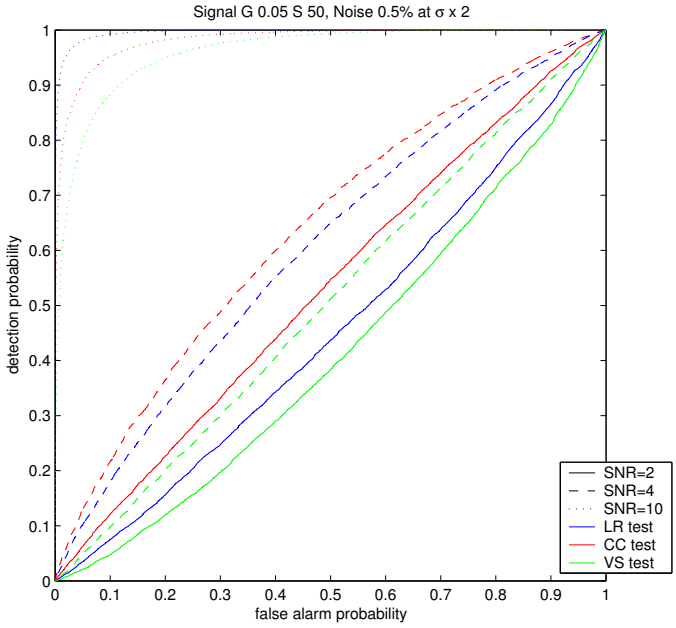

FIG. 15: ROC curve for signal, mixed Gaussian noise: Comparison of tests from Monte Carlo simulations (10^4 trials), for a mixed Gaussian noise distribution (random 0.005 of samples with variance times 2). Signal is sine-Gaussian.

Figure 17 shows simulation results on a semilog plot to highlight performance at low false alarm probabilities. The plot includes results for a fixed SNR and fixed fraction of high variance noise, but the noise RMS ratio k varies. This illustrates clearly that there is relatively little change in the performance of the cross-correlation test as the nature of the noise changes, while the likelihood ratio test performance deteriorates more rapidly with increasing high noise component. For these conditions (SNR = 5, fraction of high noise $\alpha = 10^{-3}$), the two tests have comparable performance for $k = 4$, with the cross-correlation test proving superior as k increases.

Applied to mixed Gaussian noise, the Monte Carlo simulations show that at low SNR the cross-correlation test is superior in performance, even if the high noise samples comprise less than one percent of the time series. Figure 18 shows which test performs best, cross-correlation (red) or likelihood ratio (blue), for various values of f (fraction of high noise samples) and SNR. Each point indicates which test performed best in a 10^4-trial Monte Carlo simulation using the specified parameters (varying f and SNR). Note that the left edge of the plot corre-

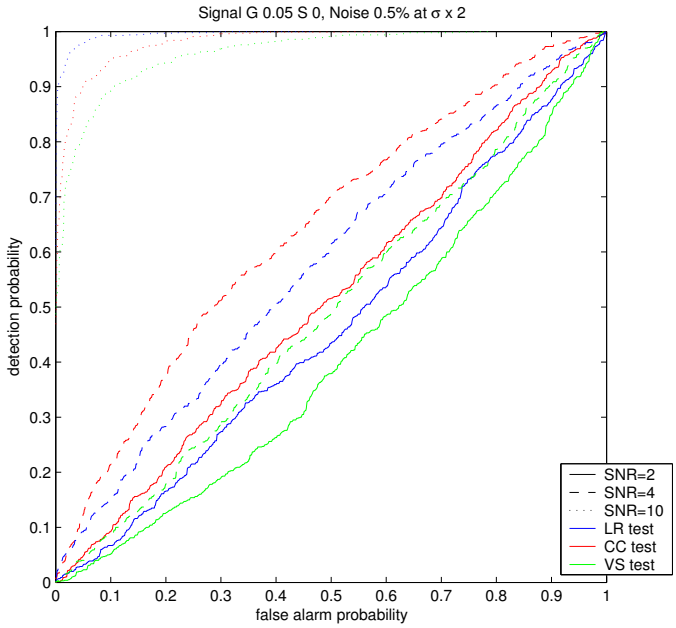

FIG. 16: ROC curve for signal, mixed Gaussian noise: Comparison of tests from Monte Carlo simulations (10^3 trials), for a mixed Gaussian noise distribution (random 0.005 of samples with variance times 2). Signal is Gaussian.

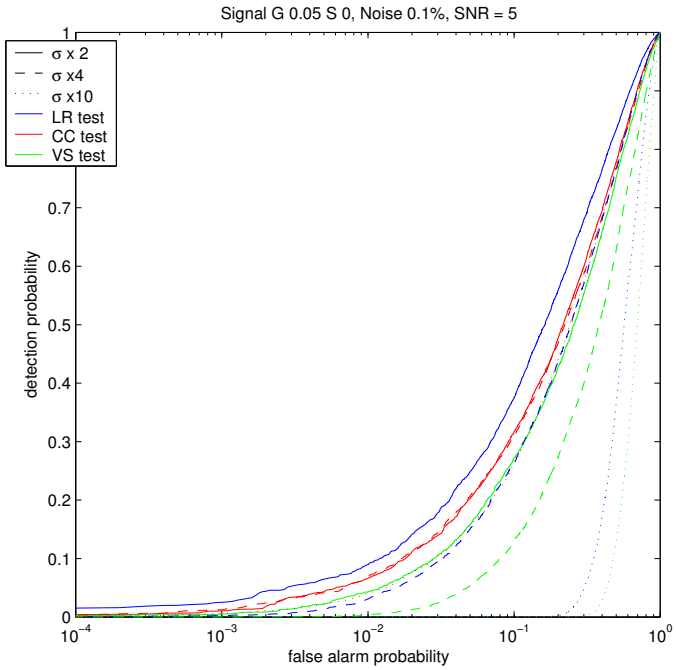

FIG. 17: ROC curve for signal, mixed Gaussian noise: Comparison of tests from Monte Carlo simulations (10^3 trials), for a mixed Gaussian noise distribution (random 0.001 of samples with k = 2, 4, or 10). Signal is Gaussian, SNR=5.

sponds to uniform Gaussian noise ($\sigma_2/\sigma_1 = 1$), and the bottom edge of the plot corresponds to negligible presence of high variance noise.

As the probability of any high variance noise samples drops, the likelihood ratio test performs best: for $\alpha < 3 \times 10^{-4}$, the simulations tend to have few if any high noise samples. Since the number of time samples $N = 1024$, many of the trials for such values of α have no high noise samples. This leaves the series as uniform Gaussian noise (or nearly so), a case in which the likelihood ratio test consistently performs best. On the other hand, once high noise samples begin to appear even in very small numbers, the cross-correlation test becomes superior. For $\alpha = 10^{-3}$, the cross-correlation test is best for noise RMS ratios k of 3-4 or greater; for $\alpha = 10^{-2}$, it is best for values of k greater than about 2.

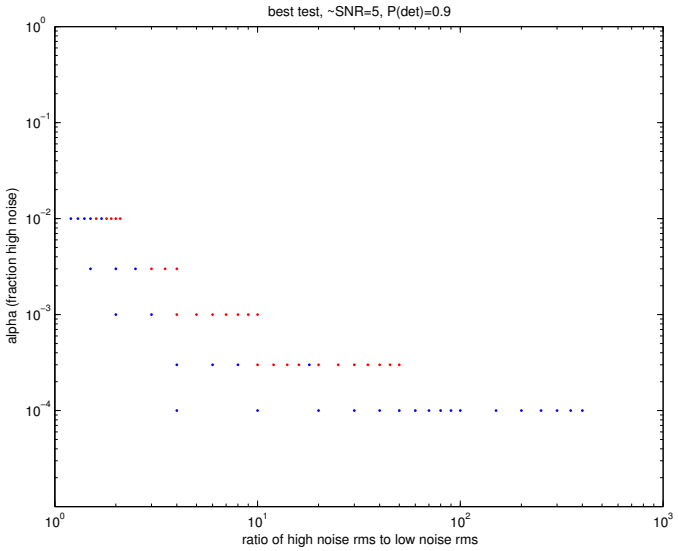

FIG. 18: Best test, Monte Carlo results: Best test from Monte Carlo results (10^4 trials each), for cross-correlation (red) or likelihood ratio (blue).

Thus even these slight departures from ideal uniform Gaussian noise are sufficient to cause the traditional likelihood ratio test to perform worse than the cross-correlation test. As noted previously, this is because the likelihood ratio statistic is highly dependent on the character of the noise, and this is due to the effect on the auto-correlation terms contributions as this type of noise is encountered. This motivates the steps to follow in identifying a more generally ideal test statistic.

V. GENERAL NETWORKS OF DETECTORS

A. Introduction

In the previous section it was demonstrated that the cross-correlation test performs better than the likelihood ratio test for low SNR and non-Gaussian noise. This is

now used in constructing an optimal statistic for detector networks. The likelihood ratio method is used to obtain a test statistic, then only the cross-correlation terms are retained with the derived weightings. This is done for the two detector case, then for larger networks of detectors.

B. Likelihood ratio statistic for two detectors

First the likelihood ratio method was used to construct the optimal test statistic for a pair of detectors physically identical but neither co-located nor co-aligned. Thus the signal in each detector is a function of the signal's two polarization components (identical for physically identical detectors) and the given detector's response function. Using this method we construct the signal components as a function of detector signals and response functions. The full derivation is in appendix E. Noise is assumed white and uncorrelated between the detectors, but no assumptions regarding the signal are made. The signal in detector $j = 1, 2$ is then

$$x_j(m) = n_j(m) + F_{+j}h_+(m) + F_{\times j}h_\times(m) \tag{55}$$

in terms of the detector response functions F_{+j}, $F_{\times j}$ and the signal polarization components. The response functions are time dependent since the detector antenna patterns change relative to the source as the Earth rotates. However, we assume here in the context of burst signals that the burst is of sufficiently short duration to ignore this time dependence.

The likelihood ratio statistic for two detectors is

$$\Lambda(\overline{x}|\overline{h}) = \max_{\overline{h}} \frac{P_1(\overline{x}_1, \overline{x}_2|\overline{h})}{P_0(\overline{x}_1, \overline{x}_2)} \tag{56}$$

and following the procedure previously described and detailed in appendix E the result for the likelihood ratio statistic for two detectors is

$$\ln(\Lambda) = \sum_{i=1}^{N} \left[\frac{1}{2}x_{1,i}^2 + \frac{1}{2}x_{2,i}^2 \right]. \tag{57}$$

There are two points to note regarding this result. First, this result is not valid for a pair of co-located, co-aligned detectors since the derivation produces an undefined result (due to division by zero) in such a case. This is not surprising, since such a detector pair will have identical signals and hence yield only one independent measurement of the signal. Thus it cannot produce a solution for the two polarization components of the gravitational wave signal.

Second, this optimal statistic is merely the sum of the individual auto-correlation terms with no contribution from the cross-correlation. This is counter-intuitive, since this holds even for nearly co-located co-aligned detectors. In such a case, the cross-correlation term should be significant. But with the above result, even for a detector pair infinitesimally misaligned, no cross-correlation term remains. This occurs because the signal components are completely unconstrained by this purely mathematical approach. As a result, the optimization method obtains a solution where individual detector signals may bear no relation to the nature of the solution for source signal. In other words, the method used produces a mathematically optimal solution without regard to its physical plausibility, since the entire possible signal space is treated as equally likely.

To address this issue, one possible approach would be to introduce an additional constraint in the solution, such as that the polarization components of the signal be of the same order of magnitude as the signals in the detectors. Such a constraint is ad hoc, but it may be possible to identify a constraint which is physically required (as opposed to merely most likely). For example, the detector response functions $F_{+}j$, $F_{\times j}$ are each constrained to values between -1 and 1.

C. Likelihood ratio statistic for multiple detectors

The derivation of test statistic was expanded to three detectors to see if the cross-correlation terms would be present in this case. The likelihood ratio optimal statistic for three detectors, which is

$$\Lambda(\overline{x}|\overline{h}) = \max_{\overline{h}} \frac{P_1(\overline{x}_1, \overline{x}_2, \overline{x}_3|\overline{h})}{P_0(\overline{x}_1, \overline{x}_2, \overline{x}_3)}, \tag{58}$$

is fully derived in appendix F. The final result may be written as

$$\begin{aligned} \ln(\Lambda) \;=\; & \sum_{i=1}^{N} \Big[\kappa_{11}x_{1,i}^2 + \kappa_{22}x_{2,i}^2 + \kappa_{33}x_{3,i}^2 \\ & + \kappa_{12}x_{1,i}x_{2,i} + \kappa_{13}x_{1,i}x_{3,i} + \kappa_{23}x_{2,i}x_{3,i} \Big] \end{aligned} \tag{59}$$

where

$$\kappa_{11} = \frac{1}{2\beta}\left(f_{12}^2 + f_{13}^2 \right), \tag{60}$$

$$\kappa_{22} = \frac{1}{2\beta}\left(f_{12}^2 + f_{23}^2 \right), \tag{61}$$

$$\kappa_{33} = \frac{1}{2\beta}\left(f_{13}^2 + f_{23}^2 \right), \tag{62}$$

$$\kappa_{12} = \frac{1}{\beta} f_{13} f_{23}, \tag{63}$$

$$\kappa_{13} = -\frac{1}{\beta} f_{12} f_{23}, \qquad \text{and} \tag{64}$$

$$\kappa_{23} = \frac{1}{\beta} f_{12} f_{13} \tag{65}$$

using the definitions

$$f_{pq} = F_{+p}F_{\times q} - F_{+q}F_{\times p} \qquad \text{and} \tag{66}$$

$$\beta = f_{12}^2 + f_{13}^2 + f_{23}^2. \tag{67}$$

Note that $\kappa_{pp} > 0$, that $\kappa_{11} + \kappa_{22} + \kappa_{33} = 1$, and that κ_{pq} for p not equal to q may be either positive, negative, or zero. Negative values of the cross-correlation term coefficients describe anti-correlation between the two detectors' signals. The absolute magnitude of the coefficient may be used to identify the relative contribution of a given term to the final statistic.

Consider the above result for the case of three detectors of which two ($j = 1, 2$) are co-incident and co-aligned. This is somewhat analogous to the three LIGO detectors, ignoring (for now) the different sensitivity of the LHO-2k detector. In this case $f_{12} = 0$, giving these values for the coefficients:

$$\kappa_{11} = \kappa_{22} = \frac{1}{4},\ \kappa_{33} = \kappa_{12} = \frac{1}{2},\ \text{and}\ \kappa_{13} = \kappa_{23} = 0. \tag{68}$$

In this case, the cross-correlation term for the co-aligned co-located detectors remains, but the other cross-correlation terms do not.

As mentioned in section 3.8, if the detectors have similarly shaped PSD curves in the most sensitive region apart from a relative scaling of the noise (this is true for similar detectors, such as LIGO, VIRGO, and TAMA), we may modify the above treatment. For each detector, suppose we express the signal $\overline{x}_j$ by normalizing with respect to the noise. Then $\overline{x}_j$ may be expressed

$$x_j(m) = n_j(m) + g_j h_j(m) \tag{69}$$

where g_j is (assumed) a constant scale factor. In the derivation of the likelihood ratio statistic we may simply replace F_{+j} with $g_j F_{+j}$ and $F_{\times j}$ with $g_j F_{\times j}$. The result is

$$f_{pq} = g_p g_q (F_{+p} F_{\times q} - F_{+q} F_{\times p}) \tag{70}$$

and the previous expressions for β and κ_{pq} are unchanged.

To apply this result, consider the three LIGO detectors as discussed above, but now more realistically. Let $i = 1, 2, 3$ refer to the LHO-4k, LHO-2k, and LLO detectors, respectively. If $g_1 \equiv 1$, then $g_2 = 0.5$ and $g_3 = 1$. As before, $f_{12} = 0$, but now $f_{23} = \frac{1}{2} f_{13}$, giving these values for the coefficients:

$$\kappa_{11} = \frac{2}{5} = \kappa_{12}, \qquad \kappa_{22} = \frac{1}{10}, \tag{71}$$

$$\kappa_{33} = \frac{1}{2}, \qquad \text{and} \qquad \kappa_{13} = \kappa_{23} = 0. \tag{72}$$

In this case, the auto-correlation contribution of the LHO-4k detector is unsurprisingly four times that of the LHO-2k detector. Cross-correlation terms between either LHO detector and the LLO detector. Just as in the previous two detector case, here only two of the three detectors provide independent data.

The result is expanded to n detectors in appendix F. In this case the result is

$$\ln(\Lambda) = \sum_{i=1}^{N} \left[\sum_{j=1}^{n} \kappa_{jj} x_{j,i}^2 + \sum_{j=1}^{n} \sum_{k=1}^{j-1} \kappa_{jk} x_{j,i} x_{k,i} \right] \tag{73}$$

where

$$\kappa_{jj} = \frac{1}{2\beta} \sum_{k \neq j}^{n} f_{jk}^2, \tag{74}$$

$$\kappa_{jk} = \frac{1}{\beta} \sum_{p \neq j,k}^{n} f_{jp} f_{kp}, \tag{75}$$

$$\beta = \sum_{j=1}^{n} \sum_{k=1}^{j-1} f_{jk}^2, \qquad \text{and} \tag{76}$$

$$f_{pq} = F_{+p} F_{\times q} - F_{+q} F_{\times p}. \tag{77}$$

In the case of four detectors there are 4 auto-correlation terms and 6 cross-correlation terms. If (only) two detectors are co-located and co-aligned, all the terms remain non-zero.

Again, to a first approximation we may consider the various IFO detectors to have similar PSDs after adjustment by a scale factor g_j for each detector. The various values of g_j could be estimated by integrating the PSD curves over the frequency range of interest. Here, as a first approximation, values of g_j were simply estimated by comparing approximate design sensitivity at a frequency selected (200 Hz) near maximum sensitivity. Defining the factors in terms of LLO with $g_j = 1$, this gives approximate values of 1 for LHO-4k, 0.5 for LHO-2k, 0.75 for VIRGO, 0.5 for GEO, and 0.17 for TAMA.

D. Dependence on polarization angle

It should be noted that the above derivations have assumed known and fixed values of ψ, the gravitational wave polarization angle. Tests suggest that the effect of changes to the polarization angle is minimal. This is as expected: the gravitational waveforms h_+ and $h_\times$ represent a breakdown of the gravitational wave signal with respect to a designated frame, this frame characterized by choice of polarization angle ψ (Gürsel and Tinto [47]). The gravitational waveforms are thus dependent on the choice of polarization angle. For arbitrary burst waveforms, polarization angle is not a particularly useful quantity and may be absorbed in the waveform solutions. For certain waveforms, such as signals from binary neutron stars or black holes, the polarization angle is usefully related to source properties (such as orientation of the binary orbit). The following discussion is thus more applicable to such cases of waveforms well related to source characteristics.

In principle it should be possible to obtain the likelihood ratio statistic including ψ as a variable over which to maximize, given that we have at least three independent detectors. This would not be possible with two detectors.

Consider the likelihood ratio statistic derivation, but retaining the dependence on polarization angle, which

may be separated within the response functions as:

$$F_{+j} = Q_j \cos 2\psi + R_j \sin 2\psi \quad (78)$$
$$F_{\times j} = R_j \cos 2\psi - Q_j \sin 2\psi. \quad (79)$$

The results are detailed in appendix G. Whereas in previous cases we obtained a set of coupled linear equations, here we obtain non-linear equations involving the signal samples h_{+i}, $h_{\times i}$ and the polarization angle ψ_i, which in general for an unknown burst wave form could vary with time. However, the substitutions $X_i = \cos 2\psi_i$ and $Y_i = \sin 2\psi_i$ reduce the equations to a set of quadratic equations. If ψ is assumed constant in time, the equations become

$$0 = \gamma_1 X + \gamma_2 Y - a_1 X^2 h_{+i} - a_2 Y^2 h_{+i} - 2b_1 XY h_{+i} + (a_1 - a_2) XY h_{\times i} - b_1 (X^2 - Y^2) h_{\times i} \quad (80)$$

$$0 = \gamma_2 X + \gamma_1 Y - a_2 X^2 h_{\times i} - a_1 Y^2 h_{\times i} - 2b_1 XY h_{\times i} + (a_1 - a_2) XY h_{+i} - b_1 (X^2 - Y^2) h_{+i} \quad (81)$$

$$0 = -\gamma_1 Y h_{+i} + \gamma_2 X h_{+i} - \gamma_2 Y h_{\times i} - \gamma_1 X h_{\times i} + (h_{+i}^2 - h_{\times i}^2)[(a_1 - a_2) XY + b_1 (X^2 - Y^2)] + h_{+i} h_{\times i} [(a_1 - a_2)(X^2 - Y^2) + 4b_1 XY] \quad (82)$$

$$0 = X^2 + Y^2 - 1 \quad (83)$$

where

$$a_1 = \sum_{j=1}^{d} Q_j^2, \qquad a_2 = \sum_{j=1}^{d} R_j^2, \qquad b_1 = \sum_{j=1}^{d} Q_j R_j,$$

$$\gamma_1 = \sum_{j=1}^{d} Q_j x_{j,i}, \qquad \text{and} \qquad \gamma_2 = \sum_{j=1}^{d} R_j x_{j,i}. \quad (84)$$

For a polarization angle varying over time, X and Y would become X_i and Y_i.

E. Mapping weightings

Concentrating on the cross-correlation terms for the multi-detector network results, these results can be used to generate sky maps comparing the contributions of specified terms to the test statistic. A code was written in Matlab to accomplish this and is included in appendix J. For detector networks of four detectors selected from a list of seven IFOs (LLO, LHO-4k, LHO-2k, VIRGO, GEO, TAMA, AIGO), it produces a sky map indicating which cross-correlation term has the greatest magnitude. The code stores values of all coefficients (including auto-correlation terms) and can handle detector networks of three to seven detectors (with adjustments to color mapping and plot legends).

A sample map produced with this code is shown as the top map of figure 19. Note that if the two LHO detectors are used, this cross-correlation term has the largest magnitude coefficient for most source directions. This map (as well as those in appendix H) incorporates the adjustments for varying detector sensitivity previously described. The bottom map in figure 19 shows the same four detector network but without this adjustment. Note that in the adjusted map, the LLO/LHO/VIRGO cross-correlations have the greatest weightings over much larger sky areas, reflecting their greater potential sensitivity compared to correlations with less sensitive detectors. However, there remain sky directions where correlations with the less sensitive detectors contribute the most. The sky maps in appendix H, which cover all possible 4-detector correlations involving the LIGO detectors, VIRGO, GEO, and TAMA, identify several cases where such correlations are important over large areas of the sky.

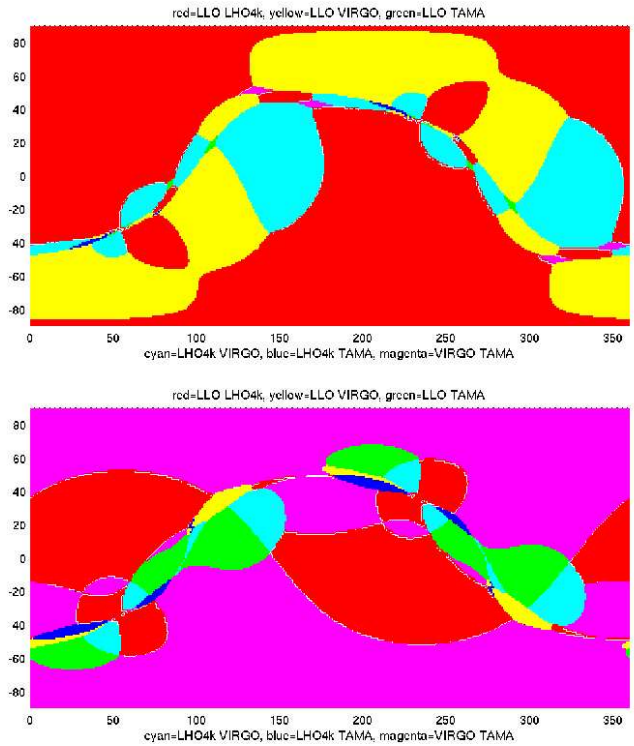

FIG. 19: Highest weight cross-correlation term: For LLO/LHO/GEO/VIRGO correlation, the cross-correlation term with the greatest magnitude coefficient from the derived statistic. The top map is adjusted for detector sensitivities as discussed in the text; the bottom map is not, effectively assuming identical detectors.

Note that these maps simply identify the cross-correlation term that contributes the most to the likelihood ratio statistic. This term may or may not be significantly greater than the next greatest term, and the

cross-correlation terms for some sky directions in some cases may collectively contribute much less than the auto-correlation terms. To illustrate, figure 20 depicts the magnitude of each cross-correlation term over all sky directions. For this four-detector correlation, the two LHO detectors are included.

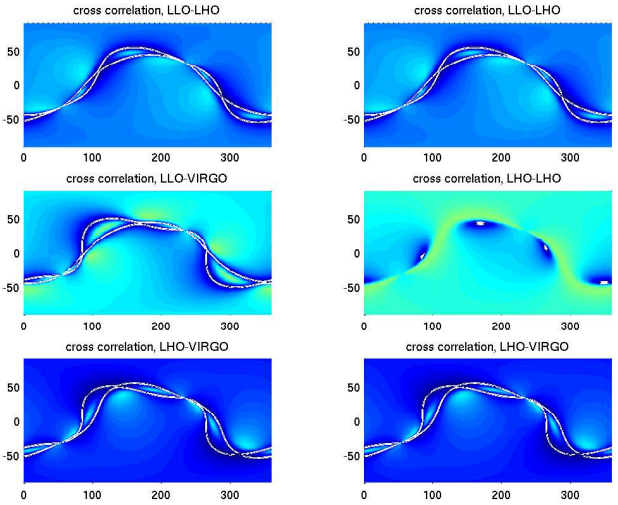

FIG. 20: Illustrative maps of weightings for individual cross-correlation terms: Sky maps of magnitude of cross-correlation term coefficients for a network including LLO, LHO-4k, LHO-2k, and VIRGO. Color indicates magnitude, ranging from 0 (blue) to 1 (red).

To further illustrate the variation of these coefficients, figure 21 depicts the values of each coefficient in a three-detector network for a fixed value of declination. Recall that the right ascension in the sky maps must be adjusted for local solar time; in other words, without specifying local time with respect to the source, we can specify the source's declination but not its east-west sky location relative to the detector. Figure 21 thus illustrates weightings for a fixed sky position, with the rotational position of the Earth accounting for the horizontal axis. The auto-correlation terms are all positive, whereas the cross-correlation terms may be positive or negative, since for some configurations and source directions the respective signals are anti-correlated.

These plots illustrate this statistic as a step towards weighing the various detector contributions for signal searches. The practical application of a validated optimal statistic would be to define weightings for cross-correlation and auto-correlation terms for a specific sky direction, corresponding to a particular detection of a burst trigger. These weightings would then potentially allow an optimal test for the detection of a corresponding gravitational wave burst.

Several issues remain before this objective can be attained; these include resolving the issues with additional physical constraints on the signals and optimizing for the

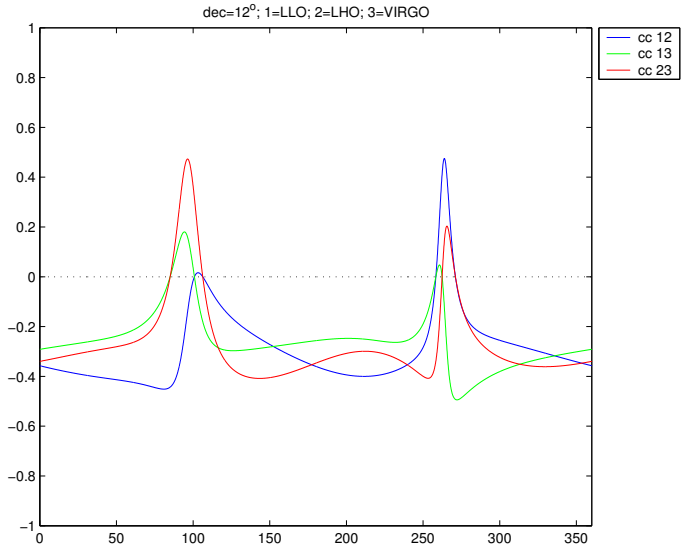

FIG. 21: Coefficients of individual terms vs. right ascension for fixed declination: Coefficients of cross-correlation terms for detector network including LLO, LHO, and VIRGO, for fixed celestial declination of 12°.

polarization angle. In the former case, this is needed to check the results against the simple cases of nearly co-aligned, co-located detectors.

F. Comparison to other works on optimized detection

Among the more directly comparable previous works is that of Anderson *et al.* [48], who develop an excess power method for detecting short bursts, uncharacterized other than by short duration, of gravitational waves in a network of detectors. Their treatment analyzes data in the frequency domain and is generalized to detectors with differing responses. Their optimal statistic is optimized over unknown source direction, since their search method is for untriggered bursts, in contrast to this work which is concerned with triggered bursts, providing known source direction. Their likelihood ratio result, prior to this optimization, may be compared to the result obtained here in section 5.2. Viceré [49] develops a method in the case of Gaussian noise (also for the more general untriggered burst search), but here we seek to generalize to more realistic noise environments.

VI. CONCLUSIONS AND DIRECTIONS FOR FURTHER DEVELOPMENT

In seeking an optimal statistical test for triggered burst searches, we first considered the simple case of two identical co-located co-aligned detectors. While the likelihood ratio test performs best for ideal Gaussian noise, it does

not in certain cases for more realistic noise. Specifically, for mixed Gaussian noise the cross-correlation test performs best for low SNR even for very low fractions of high variance noise.

This leads us to analytically develop an optimal likelihood ratio statistic. Here, we find for the two detector case that the likelihood ratio method (assuming fixed polarization angle but otherwise unconstrained signal components) yields the sum of the auto-correlation terms with no cross-correlation contribution. This is because the method maximizes over the space of possible signals without regard to physical plausibility.

When expanded to networks of three or more detectors, the likelihood ratio method produces a statistic that does include cross-correlation terms. Using this statistic we can identify weighings for terms as a function of source direction. These results can also be easily adjusted for the differing sensitivities of the various detectors, treating the individual PSDs as similar except for a scale factor. These results are illustrated by sky maps comparing the term coefficients, which give expected results for correlations involving less sensitive detectors.

Polarization angle is not an independent factor in these weightings, since it defines a frame for separating the polarization components. Should it be desirable for certain sources, initial calculations do suggest a route for developing a likelihood ratio statistic incorporating polarization angle as an unknown quantity.

A number of simplifying assumptions have been used, and a variety of issues beg further analysis. Further work is needed to determine if the optimal statistic can be developed to recover the expected behavior for a pair of nearly aligned detectors, possibly by constraining the form of the unknown signal to more physically likely solutions. Polarization angle should be considered fully. Also, the statistic should be generalized to detectors that are not identical, by incorporating the correlation matrices in derivation.

The eventual goal is to obtain an optimal statistic for correlations between multiple detectors looking for a gravitational wave burst from a known trigger. Results obtained here begin to address how to grant preference to certain correlation terms when statistically testing for a signal. They incidentally suggest that all IFOs are potentially important to this effort. If these questions are resolved, this may provide information on weighting for cross-correlations among three or more detectors, assisting in this promising area of gravitational wave searches.

VII. ACKNOWLEDGMENTS

They are too many to list, but all the faculty, staff, and students of the UTB Physics and Astronomy Department have been consistently supportive and instructive, besides being good friends; I thank them all. In particular I thank my supervisor Dr. Soumya Mohanty for his inestimable help and instruction in this project. Also I thank Dr. Malik Rakhmanov and Dr. Isabel Leonor for helpfully answering questions on issues encountered here. I thank Charlie Torres for his help; he paved the way symbolically and practically for such a dual-university degree. I thank also those faculty and staff at UTEP with whom I've had the opportunity to interact with, even from a distance; they have been great. I thank the many teachers and instructors who have personally inspired a love of learning. I thank my parents, Wm. Ronnal Johnston and Linda Lee Johnston, for being supportive so long in many ways. They along with my grandmother Betty Landreth I also thank for particular last-minute support. My brother Jeffrey Johnston I thank for proofreading this work. Finally—but most of all—I thank my wife, Victoria, who inspired me to see this through to the end. I acknowledge financial support for this work from the NSF through Grant NSF-PHY-0140326 and from NASA through Grant NASA-URC-Brownsville (NAG5-13396).

[1] Charles W. Misner, Kip S. Thorne, and John Archibald Wheeler, *Gravitation* (W. H. Freeman and Co., New York, NY, 1973).

[2] Bernard F. Schutz, *A First Course in General Relativity* (Cambridge Univ. Press, New York, NY, 1986).

[3] Kip S. Thorne, "Gravitational radiation," in *300 Years of Gravitation*, 330-458, ed. by Stephen W. Hawking and Werne Israel (Univ. of Chicago Press, Chicago, IL, 1987).

[4] M. J. Benacquista, J. DeGoes, and D. Lunder, "A simulation of the laser interferometer space antenna data stream from galactic white dwarf binaries," *Classical and Quantum Gravity*, **21**, S509-S514 (2004).

[5] B. Allen and G. Woan for LIGO Scientific Collaboration, "Upper limits on the strength of periodic gravitational waves from PSR J1939+2134," *Classical and Quantum Gravity*, **21**, S671-S676 (2004).

[6] C. Palomba, "Pulsars ellipticity revised," *Astronomy and Astrophysics*, **354**, 163-168 (2000).

[7] Joel M. Weisberg and Joseph H. Taylor, "The relativistic binary pulsar B1913+16," in *Radio Pulsars: ASP Conference Proceedings, Vol. 302*, 93, ed. by Matthew Bailes, David J. Nice, and Stephen E. Thorsett (Astronomical Society of the Pacific, San Francisco, CA), astro-ph/0211217 (2003).

[8] Curt Cutler and Kip S. Thorne, "An overview of gravitational-wave sources," gr-qc/0204090 (2002).

[9] M. Burgay *et al.*, "An increased estimate of the merger rate of double neutron stars from observations of a highly relativistic system," *Nature*, **426**, 531-533 (2003).

[10] V. Kalogera, C. Kim, D. R. Lorimer, M. Burgay, N. D'Amico, A. Possenti, R. N. Manchester, A. G. Lyne, B. C. Joshi, M. A. McLaughlin, M. Kramer, J. M. Sarkissian, and F. Camilo, "The cosmic coalescence rates for double neutron star binaries," *The Astrophysical*

Journal, **601**, L179-L182 (2004).

[11] Chris L. Fryer and Michael S. Warren, "The collapse of rotating massive stars in three dimensions," *Astronomical Journal*, **601**, 391-404 (2004).

[12] Chris L. Fryer, Daniel E. Holz, and Scott A. Hughes, "Gravitational waves from stellar collapse: correlations to explosion asymmetries," gr-qc/0403188 (2004).

[13] N. Arnaud, M. Barsuglia, M. A. Bizouard, F. Cavalier, M. Davier, P. Hello, and T. Pradier, "Gravity wave and neutrino bursts from stellar collapse: a sensitive test of neutrino masses," *Physical Review D*, **65**, 033010, hep-ph/0109027 (2002).

[14] P. Mészáros, "Theories of gamma-ray bursts," *Annual Reviews of Astronomy and Astrophysics*, **40**, 137-169 (2002).

[15] Scott Barthelmy, "GCN: The GRB Coordinates Network," `http://gcn.gsfc.nasa.gov/` (2003).

[16] R. Willingale, J. P. Osborne, P. T. O'Brien, M. J. Ward, A. Levan, and K. L. Page, "The X-ray, optical and radio evolution of the GRB 030329 afterglow and the associated SN2003dh," *Monthly Notices of the Royal Astronomical Society*, **349**, 31-38 (2004).

[17] NASA, "Swift: Catching gamma ray bursts on the fly...", `http://swift.gsfc.nasa.gov/` (2004).

[18] Joseph Weber, "Evidence for discovery of gravitational radiation," *Physical Review Letters*, **22**, 1320-1324 (1969).

[19] I. S. Heng, E. Daw, J. Giaime, W. O. Hamilton, M. P. Mchugh, and W. W. Johnson, "Allegro: noise performance and the ongoing search for gravitational waves," *Classical and Quantum Gravity*, **19**, 1889-1895 (2002).

[20] J.-P. Zendri *et al.*, "Status report and near future prospects for the gravitational wave detector AURIGA," *Classical and Quantum Gravity*, **19**, 1925-1933 (2002).

[21] P. Astone *et al.*, "The next science run of the gravitational wave detector NAUTILUS," *Classical and Quantum Gravity*, **19**, 1911-1917 (2002).

[22] P. Astone *et al.*, "The EXPLORER gravitational wave antenna: recent improvements and performances," *Classical and Quantum Gravity*, **19**, 1905-1910 (2002).

[23] David Coward, David Blair, Roger Clay, and Giovanni Mazzitelli, "Improved sensitivity of NIOBÉ in 2001 and the search for anomalous cosmic ray events," *Classical and Quantum Gravity*, **19**, 1871-1875 (2002).

[24] P. Astone, "Methods and results of the IGEC search for burst gravitational waves in the years 1997-2000," *Physical Review D*, **68**, 022001 (2003).

[25] ALLEGRO, "LSU Gravity: ALLEGRO Group," `http://gravity.phys.lsu.edu/` (2004).

[26] G. Pizzella, "Resonant detectors for the search for gravitational waves," *Classical and Quantum Gravity*, **14**, 1481-1485 (1997).

[27] Robert Forward, "Wideband laser-interferometer gravitational-radiation experiment," *Physical Review D*, **17**, 379-390 (1978).

[28] B. Barish and R. Weiss, "LIGO and the detection of gravitational waves," *Physics Today*, **52**, 44 (1999).

[29] LIGO, "LIGO Livingston," `http://www.ligo-la.caltech.edu/public.htm` (2004).

[30] Barry C. Barish, "The Laser Interferometer Gravitational-Wave Observatory LIGO," *Advanced Space Research*, **25**, 1165-1169 (2000).

[31] F. Acernese *et al.*, "The present status of the VIRGO central interferometer," *Classical and Quantum Gravity*, **19**, 1421-1428 (2002).

[32] B. Willke *et al.*, "The GEO 600 gravitational wave detector," *Classical and Quantum Gravity*, **19**, 1377-1387 (2002).

[33] Masaki Ando and the TAMA collaboration, "Current status of TAMA," *Classical and Quantum Gravity*, **19**, 1409-1419 (2002).

[34] David G. Blair for ACIGA, "The first stage of the laser interferometer gravitational wave observatory in Australia," *General Relativity and Gravitation*, **32**, 371 (2000).

[35] M. Malec, H. Grote, A. Freise, G. Heinzel, K. A. Strain, J. Hough, and K. Danzmann, "Towards dual recycling with the aid of time and frequency domain simulation," *Classical and Quantum Gravity*, **21**, S991-S998 (2004).

[36] Karsten Danzmann and Albrecht Rüdiger, "LISA technology—concept, status, prospects," *Classical and Quantum Gravity*, **20**, S1-S9 (2003).

[37] M. Rakhmanov and S. Klimenko, "Angular correlation of LIGO Hanford and Livingston interferometers," LIGO Technical Note LIGO-T030215-00-D (2003).

[38] Piotr Jaranowski, Andrzej Królak, and Bernard F. Schutz, "Data analysis of gravitational-wave signals from spinning neutron stars. I. The signal and its detection," *Physical Review D*, **58**, 063001, gr-qc/9804014 (1998).

[39] Harry L. van Trees, *Detection, Estimation, and Modulation Theory, Part I* (John Wiley and Sons, New York, NY, 2001).

[40] B. S. Sathyaprakash and Walter Winkler, "Gravitational waves," *Europhysics News*, **32**, no. 6 (2001).

[41] W. O. Hamilton, M. A. Burgamy, D. M. Busby, E. J. Daw, J. Duran, J. A. Giaime, J. Hanson, I. S. Heng, W. W. Johnson, M. P. McHugh, P. Miller, D. Nettles, and J. T. Whelan, "Resonant detectors and interferometers can work together," *Proceedings of SPIE, Vol. 4856: Gravitational-Wave Detection* (SPIE, Bellingham, WA, 2002).

[42] Charlie W. Torres Jr., "Some topics in the statistical analysis of LIGO data in the search for a stochastic background of gravitational radiation," M.S. thesis (2001).

[43] Scott A. Hughes, Szabolcs Márka, Peter L. Bender, and Craig J. Hogan, "New physics and astronomy with the new gravitational-wave observatories," LIGO document LIGO-P010029-00-D, astro-ph/0110349 (2001).

[44] Wm. Robert Johnston, "Gravity gradient noise from ground waves," unpublished (2002).

[45] LIGO Scientific Collaboration, "First upper limits from LIGO on gravitational wave bursts," LIGO preprint LIGO-P030011, gr-qc/0312056 (2004).

[46] Soumya D. Mohanty, Sz. Marka, R. Rahkola, S. Mukherjee, I. Leonor, R. Frey, J. Cannizzo, and J. Camp, "Gamma ray bursts and gravitational waves: triggered search strategy in the LIGO science runs," *Classical and Quantum Gravity*, **20**, 1-10 (2003).

[47] Yekta Gürsel and Massimo Tinto, "Near optimal solution to the inverse problem for gravitational-wave bursts," *Physical Review D*, **40**, 3884-3938 (1989).

[48] Warren G. Anderson, Patrick R. Brady, Jolien D. E. Creighton, and Éanna É. Flanagan, "An excess power statistic for detection of burst sources of gravitational radiation," *Physical Review D*, **63**, 042003, gr-qc/0008066 (2001).

[49] Andrea Viceré, "Optimal detection of burst events in gravitational wave interferometric observations," gr-qc/0112013 (2001).
[50] Biplab Bhawal and S. V. Dhurandhar, "Coincident detection of broadband signals by networks of the planned interferometric gravitational wave detectors," gr-qc/9509042 (1995).
[51] David Blair, personal communication (2004).
[52] J. A. Lobo and M. Montero, "All-sky search algorithms for monochromatic signals in resonant bar GW detector data," *Monthly Notices of the Royal Astronomical Society*, **301**, 729-744 (1998).
[53] The Math Works, *Matlab* (The Math Works, Natick, MA).

APPENDIX A: LIST OF ABBREVIATIONS

ACIGA Australian Consortium for Interferometric Gravitational Astronomy

AIGO Australian International Gravitational Observatory

BATSE Burst and Transient Experiment

CC cross-correlation

CGRO Compton Gamma-Ray Observatory

CGWA Center for Gravitational Wave Astronomy

GCN Gamma Ray Burst Coordinates Network

GRB gamma ray burst

GW gravitational wave

HETE High Energy Transient Explorer

IFO interferometer

IGEC International Gravitational Event Collaboration

INTEGRAL International Gamma-Ray Astrophysics Laboratory

LHO LIGO Hanford Observatory

LHO-2k LHO 2 km interferometer

LHO-4k LHO 4 km interferometer

LIGO Laser Interferometer Gravitational-Wave Observatory

LISA Laser Interferometer Space Antenna

LLO LIGO Livingston Observatory

LR likelihood ratio

LSC LIGO Scientific Collaboration

NASA National Aeronautics and Space Administration
NSF National Science Foundation

PSD power spectral density

ROC receiver operating characteristic

RXTE Rossi X-Ray Timing Explorer

RMS root-mean-square

SNR signal-to-noise ratio

XRF X-ray flash

APPENDIX B: LIST OF GRAVITATIONAL WAVE DETECTORS

detector	location	arm length (km)	latitude ° N	longitude ° W	orientation °
LLO	Louisiana, USA	4.0	30.56	90.77	243.0
LHO (4k)	Washington, USA	4.0	46.45	119.41	171.8
LHO (2k)	Washington, USA	2.0	46.45	119.41	171.8
VIRGO	Italy	3.0	43.63	-10.50	116.5
TAMA-300	Japan	0.3	35.68	-139.54	225.0
GEO-600	Germany	0.6	52.25	-9.81	68.8
AIGO	Australia	0.08	-31.4	-115.7	315

TABLE II: Laser interferometer detectors. Note: All detectors have perpendicular arms with the exception of the GEO-600 detector, which has arms separated by 94.33°. Orientation refers to direction of bisector of arms measured counter-clockwise from east. Data from Jaranowski, Królak, and Schutz [38] except for AIGO data which is from Bhawal and Dhurandhar [50], Blair [34], and Blair [51].

detector	location	latitude ° N	longitude ° W	orientation °
ALLEGRO	Louisiana, USA	30.45	91.17	130
AURIGA	Italy	45.35	-11.95	46
EXPLORER	Switzerland	46.45	-6.20	51
NAUTILUS	Italy	41.82	-12.67	46
NIOBE	Australia	-31.93	115.82	90

TABLE III: Resonant bar detectors. Note: Orietation refers to bar alignment measured counter-clockwise from east. Data from Lobo and Montero [52].

APPENDIX C: LIKELIHOOD RATIO STATISTIC FOR TWO CO-LOCATED CO-ALIGNED DETECTORS

Consider the likelihood ratio test statistic for two detectors is generalized to unknown signal $\overline{h}$:

$$\Lambda(\overline{x}|\overline{h}) = \max_{\overline{h}} \frac{P_1(\overline{x}_1, \overline{x}_2|\overline{h})}{P_0(\overline{x}_1, \overline{x}_2)}. \tag{C1}$$

Since individual samples are uncorrelated, these probabilities are

$$\begin{aligned} P_1 &= \prod_{i=1}^{N} \exp\left(-\frac{(x_{1,i}-h_i)^2}{2}\right) \exp\left(-\frac{(x_{2,i}-h_i)^2}{2}\right), \\ P_0 &= \prod_{i=1}^{N} \exp\left(-\frac{x_{1,i}^2}{2}\right) \exp\left(-\frac{x_{2,i}^2}{2}\right), \end{aligned}$$

This statistic Λ can be maximized by maximizing $\ln(\Lambda)$. Substituting the above expressions for P_1 and P_0 and taking the logarithm, we obtain

$$\begin{aligned} \ln(\Lambda) &= -\sum_{i=1}^{N} \frac{(x_{1,i}-h_i)^2}{2} - \sum_{i=1}^{N} \frac{(x_{2,i}-h_i)^2}{2} \\ &\quad + \sum_{i=1}^{N} \frac{x_{1,i}^2}{2} + \sum_{i=1}^{N} \frac{x_{2,i}^2}{2} \qquad \text{(C2)} \\ &= \sum_{i=1}^{N} x_{1,i}h_i + \sum_{i=1}^{N} x_{2,i}h_i - \sum_{i=1}^{N} h_i^2. \qquad \text{(C3)} \end{aligned}$$

To maximize Λ requires

$$\frac{\partial}{\partial h_j} \sum_{i=1}^{N} (x_{1,i}h_i + x_{2,i}h_i - h_i^2) = 0 \tag{C4}$$

which gives

$$\begin{aligned} x_{1,j} + x_{2,j} - 2h_j = 0, \qquad &\text{or} \qquad \text{(C5)} \\ h_j = \frac{x_{1,j} + x_{2,j}}{2}. \qquad &\text{(C6)} \end{aligned}$$

Substituting this result for h_i above gives the following maximized statistic:

$$\begin{aligned} \max \ln(\Lambda) &= \sum_{i=1}^{N} (x_{1,i} + x_{2,i}) \left(\frac{x_{1,i} + x_{2,i}}{2}\right) \\ &\quad - \sum_{i=1}^{N} \left(\frac{x_{1,i} + x_{2,i}}{2}\right)^2 \qquad \text{(C7)} \\ \ln(\Lambda) &= \sum_{i=1}^{N} \left(\frac{(x_{1,i} + x_{2,i})}{2}\right)^2 \qquad \text{(C8)} \\ &= \left\langle \frac{\overline{x}_1 + \overline{x}_2}{2}, \frac{\overline{x}_1 + \overline{x}_2}{2} \right\rangle \qquad \text{(C9)} \end{aligned}$$

This statistic can be compared to a specified theshold k.

APPENDIX D: DERIVATION OF MEANS AND VARIANCES FOR SAMPLE TESTS

We first assume a pair of identical detectors co-located and co-aligned. The signal in detector $i = 1,2$ is described as

$$x_i(m) = n_i(m) + h(m) \tag{D1}$$

for the mth sample of N total samples, where $n_i(m)$ is the noise in detector i and h is the signal (same for both detectors in this initial case). In the absence of any signal $x_i(m) = n_i(m)$.

Noise is assumed to be Gaussian and uncorrelated, with $\mu = 0$ and $\sigma^2 = 1$.

We note here the following:

$$\begin{aligned} E[n_i^2(m)] &= 1, \qquad \text{(D2)} \\ \text{var}[n_i^2(m)] &= 2, \qquad \text{(D3)} \\ E[n_1(m)n_2(m)] &= 0, \qquad \text{(D4)} \\ \text{var}[n_1(m)n_2(m)] &= 1, \qquad \text{(D5)} \\ E[n_i(m)h(m)] &= 0, \qquad \text{(D6)} \\ \text{var}[n_i(m)h(m)] &= h^2(m), \qquad \text{(D7)} \end{aligned}$$

for $n = 1, 2$.

1. Cross-correlation test

The cross-correlation statistic is defined as:

$$\Lambda_{CC} \equiv < \overline{x}_1, \overline{x}_2 > = \sum_{m=1}^{N} x_1(m)x_2(m) \tag{D8}$$

For simplicity, hereafter this will be written

$$\Lambda_{CC} = \sum_{m} x_1(m)x_2(m) \tag{D9}$$

With no signal present, this is

$$\Lambda_{CC} = \sum_m n_1(m)n_2(m) \tag{D10}$$

and with signal present is

$$\begin{aligned}\Lambda'_{CC} &= \sum_m \Big[n_1(m)+h(m)\Big]\Big[n_2(m)+h(m)\Big] &\text{(D11)}\\ &= \sum_m n_1(m)n_2(m) + \sum_m n_1(m)h(m) \\ &\quad + \sum_m n_2(m)h(m) + \sum_m h^2(m) &\text{(D12)}\end{aligned}$$

Note that $\sum_m h^2(m) = C$ is a constant for a specified signal.

For a large number of samples N, the central limit theorem dictates that Λ_{CC} and Λ'_{CC} will have Gaussian distributions, with μ and σ^2 simply related to the respective values for individual terms. For the case of no signal we obtain:

$$\begin{aligned}E[\Lambda_{CC}] &= E\Big[\sum_m n_1 n_2\Big] = \sum_m E[n_1 n_2] &\text{(D13)}\\ \mu &= 0 &\text{(D14)}\end{aligned}$$

and

$$\begin{aligned}\text{var}[\Lambda_{CC}] &= E[\Lambda_{CC}^2] - (E[\Lambda_{CC}])^2 &\text{(D15)}\\ &= E\Big[\sum_m n_1 n_2 \sum_p n_1 n_2\Big] - 0 &\text{(D16)}\\ &= \sum_m E[n_1^2 n_2^2] = \sum_m 1 &\text{(D17)}\\ \sigma^2 &= N &\text{(D18)}\end{aligned}$$

Note that in obtaining the variance, the product of summation terms involves independent summations (summed over sample indices m and p, respectively); these are uncorrelated (giving a product of 0) except for the case $m = p$.

For the case with signal present, and letting $C = \sum_m h^2$, we obtain

$$\begin{aligned}E[\Lambda'_{CC}] &= E\Big[\sum_m n_1 n_2\Big] + E\Big[\sum_m n_1 h\Big] + E\Big[\sum_m n_2 h\Big] + E\Big[\sum_m h^2\Big] &\text{(D19)}\\ &= \sum_m E[n_1 n_2] + \sum_m E[n_1]h + \sum_m E[n_2]h + C &\text{(D20)}\\ \mu &= 0 + C = C &\text{(D21)}\\ & &\text{(D22)}\end{aligned}$$

and

$$\begin{aligned}\text{var}[\Lambda'_{CC}] &= E[(\Lambda'_{CC})^2] - (E[\Lambda'_{CC}])^2 &\text{(D23)}\\ &= E\Big[\Big(\sum_m n_1 n_2 + \sum_m n_1 h + \sum_m n_2 h + C\Big)^2\Big] - C^2 &\text{(D24)}\\ &= -C^2 E\Big[\sum_m n_1 n_2 \sum_p n_1 n_2 + \sum_m n_1 h \sum_p n_1 h + \sum_m n_2 h \sum_p n_2 h + C^2 + 2\sum_m n_1 n_2 \sum_p n_1 h \\ &\quad + 2\sum_m n_1 n_2 \sum_p n_2 h + 2C\sum_m n_1 n_2 + 2\sum_m n_1 h \sum_p n_2 h + 2C\sum_m n_1 h + 2C\sum_m n_2 h &\text{(D25)}\\ &= -C^2 + N + C + C + C^2 + 0 + 0 + 0 + 0 + 0 + 0 &\text{(D26)}\\ \sigma^2 &= N + 2C &\text{(D27)}\end{aligned}$$

2. Likelihood ratio test

The likelihood ratio test statistic is:

$$\Lambda_{LR} = \left\langle \frac{\overline{x}_1 + \overline{x}_2}{2}, \frac{\overline{x}_1 + \overline{x}_2}{2} \right\rangle \tag{D28}$$

$$\begin{aligned}&= \frac{1}{4} < \overline{x}_1, \overline{x}_1 > + \frac{1}{4} < \overline{x}_2, \overline{x}_2 > + \frac{1}{2} < \overline{x}_1, \overline{x}_2 > \\ &= \frac{1}{4}\sum_m x_1^2(m) + \frac{1}{4}\sum_m x_2^2(m) + \frac{1}{2}\sum_m x_1(m)x_2(m)\end{aligned}$$

With no signal present, this is

$$\Lambda_{LR} = \frac{1}{4}\sum_m n_1^2(m) + \frac{1}{4}\sum_m n_2^2(m) + \frac{1}{2}\sum_m n_1(m)n_2(m) \tag{D29}$$

and with signal present is

$$\begin{aligned}\Lambda'_{LR} &= \frac{1}{4}\sum_m \Big[n_1(m)+h(m)\Big]^2 + \frac{1}{4}\sum_m \Big[n_2(m)+h(m)\Big]^2 \\ &\quad + \frac{1}{2}\sum_m \Big[n_1(m)+h(m)\Big]\Big[n_2(m)+h(m)\Big] \qquad \text{(D30)} \\ &= \frac{1}{4}\sum_m n_1^2(m) + \frac{1}{4}\sum_m n_2^2(m) + \sum_m n_1(m)h(m) \\ &\quad + \sum_m n_2(m)h(m) + \sum_m h^2(m) \\ &\quad + \frac{1}{2}\sum_m n_1(m)n_2(m) \qquad \text{(D31)}\end{aligned}$$

For the case of no signal, the mean and variance are

$$\begin{aligned}E[\Lambda_{LR}] &= E\left[\frac{1}{4}\sum_m n_1^2\right] + E\left[\frac{1}{4}\sum_m n_2^2\right] + E\left[\frac{1}{2}\sum_m n_1 n_2\right] \\ &= \frac{1}{4}\sum_m E[n_1^2] + \frac{1}{4}\sum_m E[n_2^2] + \frac{1}{2}\sum_m E[n_1 n_2] \\ &= \frac{1}{4}N + \frac{1}{4}N + 0 \qquad \text{(D32)} \\ \mu &= \frac{1}{2}N \qquad \text{(D33)}\end{aligned}$$

and

$$\begin{aligned}\mathrm{var}[\Lambda_{LR}] &= E[\Lambda_{LR}^2] - (E[\Lambda_{LR}])^2 \qquad \text{(D34)} \\ &= E\left[\left(\frac{1}{4}\sum_m n_1^2 + \frac{1}{4}\sum_m n_2^2 + \frac{1}{2}\sum_m n_1 n_2\right)^2\right] - \frac{1}{4}N^2 \qquad \text{(D35)} \\ &= -\frac{1}{4}N^2 + E\left[\frac{1}{16}\sum_m n_1^2\sum_p n_1^2 + \frac{1}{16}\sum_m n_2^2\sum_p n_2^2 + \frac{1}{4}\sum_m n_1 n_2\sum_p n_1 n_2 + \frac{1}{8}\sum_m n_1^2\sum_p n_2^2\right. \\ &\quad \left. + \frac{1}{4}\sum_m n_1^2\sum_p n_1 n_2 + \frac{1}{4}\sum_m n_2^2\sum_p n_1 n_2\right] \qquad \text{(D36)} \\ &= -\frac{1}{4}N^2 + \left(\frac{1}{8}N + \frac{1}{16}N^2\right) + \left(\frac{1}{8}N + \frac{1}{16}N^2\right) + \frac{1}{4}N + 0 + \frac{1}{8}N^2 \qquad \text{(D37)} \\ \sigma^2 &= \frac{1}{2}N \qquad \text{(D38)}\end{aligned}$$

For the case with signal, we obtain:

$$\begin{aligned}E[\Lambda'_{LR}] &= E\left[\frac{1}{4}\sum_m n_1^2\right] + E\left[\frac{1}{4}\sum_m n_2^2\right] + E\left[\sum_m n_1 h\right] + E\left[\sum_m n_1 h\right] + E\left[\frac{1}{2}\sum_m n_1 n_2\right] + C \qquad \text{(D39)} \\ &= \frac{1}{4}\sum_m E[n_1^2] + \frac{1}{4}\sum_m E[n_2^2] + \sum_m E[n_2 h] + \sum_m E[n_2 h] + \frac{1}{2}\sum_m E[n_1 n_2] + C \qquad \text{(D40)} \\ &= \frac{1}{4}N + \frac{1}{4}N + 0 + 0 + 0 + C \qquad \text{(D41)} \\ \mu &= \frac{1}{2}N + C \qquad \text{(D42)}\end{aligned}$$

and

$$\begin{aligned}\mathrm{var}[\Lambda'_{LR}] &= E[(\Lambda'_{LR})^2] - (E[\Lambda'_{LR}])^2 \qquad \text{(D43)} \\ &= E\left[\left(\frac{1}{4}\sum_m n_1^2 + \frac{1}{4}\sum_m n_2^2 + \sum_m n_2 h + \sum_m n_2 h + \frac{1}{2}\sum_m n_1 n_2 + C\right)^2\right] - \left(\frac{1}{2}N + C\right)^2 \\ &\qquad \text{(D44)}\end{aligned}$$

$$= -\frac{1}{4}N^2 - NC - C^2 + E\Bigg[\frac{1}{16}\sum_m n_1^2 \sum_p n_1^2 + \frac{1}{16}\sum_m n_2^2 \sum_p n_2^2 + \sum_m n_1 h \sum_p n_1 h + \sum_m n_2 h \sum_p n_2 h$$
$$+\frac{1}{4}\sum_m n_1 n_2 \sum_p n_1 n_2 + C^2 + \frac{1}{8}\sum_m n_1^2 \sum_p n_2^2 + \frac{1}{2}\sum_m n_1^2 \sum_p n_1 h + \frac{1}{2}\sum_m n_1^2 \sum_p n_2 h$$
$$+\frac{1}{4}\sum_m n_1^2 \sum_p n_1 n_2 + \frac{1}{2}\sum_m n_1^2 C + \frac{1}{2}\sum_m n_2^2 \sum_p n_1 h + \frac{1}{2}\sum_m n_2^2 \sum_p n_2 h + \frac{1}{4}\sum_m n_2^2 \sum_p n_1 n_2 + \frac{1}{2}\sum_m n_2^2 C$$
$$+2\sum_m n_1 h \sum_p n_2 h + \sum_m n_1 h \sum_p n_1 n_2 + 2\sum_m n_1 h C + \sum_m n_2 h \sum_p n_1 n_2 + 2\sum_m n_2 h C + \sum_m n_1 n_2 C\Bigg] \quad \text{(D45)}$$

$$= -\frac{1}{4}N^2 - NC - C^2 + \left(\frac{1}{8}N + \frac{1}{16}N^2\right) + \left(\frac{1}{8}N + \frac{1}{16}N^2\right) + C + C + \frac{1}{4}N + C^2 + \frac{1}{8}N^2$$
$$+0 + 0 + 0 + \frac{1}{2}NC + 0 + 0 + 0 + \frac{1}{2}NC + 0 + 0 + 0 + 0 + 0 + 0 \quad \text{(D46)}$$

$$\sigma^2 = \frac{1}{2}N + 2C \quad \text{(D47)}$$

3. Variance sum test

A final test is constructed from the sum of the variances:

$$\Lambda_{VS} \equiv <\overline{x}_1, \overline{x}_1> + <\overline{x}_2, \overline{x}_2> \quad \text{(D48)}$$
$$= \sum_m x_1^2(m) + \sum_m x_2^2(m) \quad \text{(D49)}$$

With no signal present, this is

$$\Lambda_{VS} = \sum_m n_1^2(m) + \sum_m n_2^2(m) \quad \text{(D50)}$$

and with signal present is

$$\Lambda'_{VS} = \sum_m \Big[n_1(m) + h(m)\Big]^2 + \sum_m \Big[n_2(m) + h(m)\Big]^2$$
$$= \sum_m n_1^2(m) + \sum_m n_2^2(m) + 2\sum_m n_1(m)h(m)$$
$$+2\sum_m n_2(m)h(m) + 2\sum_m h^2(m) \quad \text{(D51)}$$

As before, for a large number of samples N, Λ_{VS} and Λ'_{VS} will have gaussian distributions. For the case of no signal, the following results are found:

$$E[\Lambda_{VS}] = E\Big[\sum_m n_1^2\Big] + E\Big[\sum_m n_2^2\Big] \quad \text{(D52)}$$
$$= \sum_m E[n_1^2] + \sum_m E[n_2^2] \quad \text{(D53)}$$
$$\mu = 2N \quad \text{(D54)}$$

$$\text{var}[\Lambda_{VS}] = E[\Lambda_{VS}^2] - (E[\Lambda_{VS}])^2 \quad \text{(D55)}$$
$$= E\left[\left(\sum_m n_1^2 + \sum_m n_2^2\right)^2\right] - (2N)^2 \quad \text{(D56)}$$
$$= E\Bigg[\sum_m n_1^2 \sum_p n_1^2 + \sum_m n_2^2 \sum_p n_2^2$$
$$+2\sum_m n_1^2 \sum_p n_2^2\Bigg] - 4N^2 \quad \text{(D57)}$$
$$= (2N + N^2) + (2N + N^2) + 2N^2 - 4N^2$$
$$\sigma^2 = 4N \quad \text{(D58)}$$

For the case with signal:

$$E[\Lambda'_{VS}] = E\Big[\sum_m n_1^2\Big] + E\Big[\sum_m n_2^2\Big] + 2E\Big[\sum_m n_1 h\Big]$$
$$+2E\Big[\sum_m n_2 h\Big] + 2E\Big[\sum_m h^2\Big] \quad \text{(D59)}$$
$$\mu = N + N + 0 + 0 + 2C = 2N + 2C \quad \text{(D60)}$$
$$\quad \text{(D61)}$$

and

$$\text{var}[\Lambda'_{VS}] = E[(\Lambda'_{VS})^2] - (E[\Lambda'_{VS}])^2 \quad \text{(D62)}$$

$$\mathrm{var}[\Lambda'_{VS}] = E\left[\left(\sum_m n_1^2 + \sum_m n_2^2 + 2\sum_m n_1 h + 2\sum_m n_2 h + 2C\right)^2\right] - (2N+2C)^2 \quad \text{(D63)}$$

$$\begin{aligned} &= -4N^2 - 4C^2 - 8NC + 4C^2 + E\Bigg[\sum_m n_1^2 \sum_p n_1^2 + \sum_m n_2^2 \sum_p n_2^2 + 4\sum_m n_1 h \sum_p n_1 h \\ &\quad + 4\sum_m n_2 h \sum_p n_2 h + 2\sum_m n_1^2 \sum_p n_2^2 + 4\sum_m n_1^2 \sum_p n_1 h + 4\sum_m n_1^2 \sum_p n_2 h + 4\sum_m n_1^2 C \\ &\quad + 4\sum_m n_2^2 \sum_p n_1 h + 4\sum_m n_2^2 \sum_p n_2 h + 4\sum_m n_2^2 C + 8\sum_m n_1 h \sum_p n_2 h + 8\sum_m n_1 h C + 8\sum_m n_2 h C \end{aligned}$$

$$= -4N^2 - 8NC + (2N+N^2) + (2N+N^2) + 4C + 4C + 2N^2 + 4NC + 4NC \quad \text{(D64)}$$

$$\sigma^2 = 4N + 8C \quad \text{(D65)}$$

APPENDIX E: LIKELIHOOD RATIO OPTIMUM STATISTIC FOR A PAIR OF DETECTORS

1. General assumptions

We again consider the likelihood ratio test statistic for two detectors, but in this case generalized to different signals in each detector. With detectors of differing locations and alignments, the signals in the two detectors will (generally) be different. The signal in detector j = 1,2 is described as

$$x_j(m) = n_j(m) + h_j(m) \quad \text{(E1)}$$

for the mth sample of N total samples, where $n_j(m)$ is the noise and h_j the signal in detector j. In the absence of any signal $x_j(m) = n_j(m)$. Noise is assumed to be uncorrelated.

The signal h_j in detector j is of the form

$$h_j = F_{+j} h_+ + F_{\times j} h_\times \quad \text{(E2)}$$

where h_+ and $h_\times$ are the plus and cross polarized components of the gravitational wave, respectively, in some frame of reference external to both detectors, and F_{+j} and $F_{\times j}$ describe the response of detector j to these plus and cross polarized gravitational wave components, respectively. The responses F are a function of the detectors' location and orientation on the Earth's surface relative to the celestial location of the gravitational wave source. Note that this is time dependent, since the Earth's rotation presents different detector orientations to the gravitational wave. (For this analysis, the time dependence will be ignored since a gravitational wave burst is assumed to be of short duration compared to the change in orientation produced by the Earth's rotation.)

2. Deriving the likelihood ratio statistic for the generalized two detector case

The likelihood ratio statistic is:

$$\Lambda(\overline{x}|\overline{h}) = \max_{\overline{h}} \frac{P_1(\overline{x}_1, \overline{x}_2|\overline{h})}{P_0(\overline{x}_1, \overline{x}_2)}. \quad \text{(E3)}$$

Individual samples are uncorrelated, so these probabilities are

$$P_1 = \prod_{i=1}^{N} \exp\left(-\frac{(x_{1,i} - h_{1,i})^2}{2}\right) \exp\left(-\frac{(x_{2,i} - h_{2,i})^2}{2}\right),$$

$$P_0 = \prod_{i=1}^{N} \exp\left(-\frac{x_{1,i}^2}{2}\right) \exp\left(-\frac{x_{2,i}^2}{2}\right),$$

Note that in this case $h_{1,i}$ and $h_{2,i}$ represent different signals for two detectors with different locations and orientations (different response functions in general). These signals can be expressed in terms of the polarization components of the gravitational wave in a particular external frame:

$$h_{1,i} = F_{+1} h_{+,i} + F_{\times 1} h_{\times,i} \quad \text{(E4)}$$

$$h_{2,i} = F_{+2} h_{+,i} + F_{\times 2} h_{\times,i} \quad \text{(E5)}$$

This statistic Λ can be maximized by maximizing $\ln(\Lambda)$, which is equal to

$$\begin{aligned} \ln(\Lambda) &= -\sum_{i=1}^{N} \frac{(x_{1,i} - h_{1,i})^2}{2} - \sum_{i=1}^{N} \frac{(x_{2,i} - h_{2,i})^2}{2} \quad \text{(E6)} \\ &\quad + \sum_{i=1}^{N} \frac{x_{1,i}^2}{2} + \sum_{i=1}^{N} \frac{x_{2,i}^2}{2} \\ &= \sum_{i=1}^{N} x_{1,i} h_{1,i} + \sum_{i=1}^{N} x_{2,i} h_{2,i} - \frac{1}{2}\sum_{i=1}^{N} h_{1,i}^2 - \frac{1}{2}\sum_{i=1}^{N} h_{2,i}^2. \end{aligned}$$

Substituting the above expressions for $h_{1,i}$ and $h_{2,1}$ gives

$$\ln\Lambda = \sum_{i=1}^{N} x_{1,i}(F_{+1}h_{+,i} + F_{\times 1}h_{\times,i}) + \sum_{i=1}^{N} x_{2,i}(F_{+2}h_{+,i} + F_{\times 2}h_{\times,i}) - \frac{1}{2}\sum_{i=1}^{N}(F_{+1}h_{+,i} + F_{\times 1}h_{\times,i})^2$$
$$-\frac{1}{2}\sum_{i=1}^{N}(F_{+2}h_{+,i} + F_{\times 2}h_{\times,i})^2 \tag{E7}$$

$$= \sum_{i=1}^{N}\Big[(F_{+1}x_{1,i} + F_{+2}x_{2,i})h_{+,i} + (F_{\times 1}x_{1,i} + F_{\times 2}x_{2,i})h_{\times,i} - \frac{1}{2}(F_{+1}^2 + F_{+2}^2)h_{+,i}^2 - \frac{1}{2}(F_{\times 1}^2 + F_{\times 2}^2)h_{\times,i}^2$$
$$-(F_{+1}F_{\times 1} + F_{+2}F_{\times 2})h_{+,i}h_{\times,i}\Big] \tag{E8}$$

To maximize Λ requires

$$\frac{\partial}{\partial h_{+,i}}\ln\Lambda = 0 \quad \text{and} \quad \frac{\partial}{\partial h_{\times,i}}\ln\Lambda = 0 \tag{E9}$$

which gives

$$x_{1,i}F_{+1} + x_{2,i}F_{+2} - (F_{+1}^2 + F_{+2}^2)h_{+,1} - (F_{+1}F_{\times 1} + F_{+2}F_{\times 2})h_{\times,i} = 0 \tag{E10}$$

and

$$x_{1,i}F_{\times 1} + x_{2,i}F_{\times 2} - (F_{\times 1}^2 + F_{\times 2}^2)h_{\times,1} - (F_{+1}F_{\times 1} + F_{+2}F_{\times 2})h_{+,i} = 0 \tag{E11}$$

These equations can be solved for $h_{+,i}$ and $h_{\times,i}$ using matrix representation:

$$\begin{bmatrix} F_{+1}^2 + F_{+2}^2 & F_{+1}F_{\times 1} + F_{+2}F_{\times 2} \\ F_{+1}F_{\times 1} + F_{+2}F_{\times 2} & F_{\times 1}^2 + F_{\times 2}^2 \end{bmatrix}\begin{bmatrix} h_{+,i} \\ h_{\times,i} \end{bmatrix} = \begin{bmatrix} F_{+1}x_{1,i} + F_{+2}x_{2,i} \\ F_{\times 1}x_{1,i} + F_{\times 2}x_{2,i} \end{bmatrix} \tag{E12}$$

$$\begin{bmatrix} h_{+,i} \\ h_{\times,i} \end{bmatrix} = \frac{1}{\beta}\begin{bmatrix} F_{\times 1}^2 + F_{\times 2}^2 & -F_{+1}F_{\times 1} - F_{+2}F_{\times 2} \\ -F_{+1}F_{\times 1} - F_{+2}F_{\times 2} & F_{+1}^2 + F_{+2}^2 \end{bmatrix}\begin{bmatrix} F_{+1}x_{1,i} + F_{+2}x_{2,i} \\ F_{\times 1}x_{1,i} + F_{\times 2}x_{2,i} \end{bmatrix} \tag{E13}$$

where

$$\beta = (F_{+1}^2 + F_{+2}^2)(F_{\times 1}^2 + F_{\times 2}^2) - (F_{+1}F_{\times 1} + F_{+2}F_{\times 2})^2 \tag{E14}$$
$$= F_{+1}^2F_{\times 1}^2 + F_{+2}^2F_{\times 1}^2 + F_{+1}^2F_{\times 2}^2 + F_{+2}^2F_{\times 2}^2 - F_{+1}^2F_{\times 1}^2 - 2F_{+1}F_{+2}F_{\times 1}F_{\times 2} - F_{+2}^2F_{\times 2}^2 \tag{E15}$$
$$= (F_{+2}F_{\times 1} - F_{+1}F_{\times 2})^2 \tag{E16}$$

Note that there is no solution if $\beta = 0$.
Taking the product of the above matrices gives

$$\begin{bmatrix} h_{+,i} \\ h_{\times,i} \end{bmatrix} = \frac{1}{\beta}\begin{bmatrix} q \\ r \end{bmatrix} \tag{E17}$$

where

$$q = (F_{\times 1}^2 + F_{\times 2}^2)(F_{+1}x_{1,i} + F_{+2}x_{2,i}) - (F_{+1}F_{\times 1} + F_{+2}F_{\times 2})(F_{\times 1}x_{1,i} + F_{\times 2}x_{2,i}) \tag{E18}$$
$$= (F_{+1}F_{\times 1}^2 + F_{+1}F_{\times 2}^2 - F_{+1}F_{\times 1}^2 - F_{+2}F_{\times 1}F_{\times 2})x_{1,i} + (F_{+2}F_{\times 1}^2 + F_{+2}F_{\times 2}^2 - F_{+2}F_{\times 2}^2 - F_{+1}F_{\times 1}F_{\times 2})x_{2,i}$$
$$= -(F_{+2}F_{\times 1} - F_{+1}F_{\times 2})F_{\times 2}x_{1,i} + (F_{+2}F_{\times 1} - F_{+1}F_{\times 2})F_{\times 1}x_{2,i} \tag{E19}$$

and

$$r = -(F_{+1}F_{\times 1} + F_{+2}F_{\times 2})(F_{+1}x_{1,i} + F_{+2}x_{2,i}) + (F_{+1}^2 + F_{+2}^2)(F_{\times 1}x_{1,i} + F_{\times 2}x_{2,i}) \quad \text{(E20)}$$

$$= (-F_{+1}^2F_{\times 1} - F_{+1}F_{+2}F_{\times 2} + F_{+1}^2F_{\times 1} + F_{+2}^2F_{\times 1})x_{1,i} + (-F_{+1}F_{+2}F_{\times 1} - F_{+2}^2F_{\times 2} + F_{+1}^2F_{\times 2} + F_{+2}^2F_{\times 2})x_{2,i}$$

$$= (F_{+2}F_{\times 1} - F_{+1}F_{\times 2})F_{+2}x_{1,i} - (F_{+2}F_{\times 1} - F_{+1}F_{\times 2})F_{+1}x_{2,i} \quad \text{(E21)}$$

Combining these results gives

$$\begin{bmatrix} h_{+,i} \\ h_{\times,i} \end{bmatrix} = \frac{1}{(F_{+2}F_{\times 1} - F_{+1}F_{\times 2})} \begin{bmatrix} -F_{\times 2}x_{1,i} + F_{\times 1}x_{2,i} \\ F_{+2}x_{1,i} - F_{+1}x_{2,i} \end{bmatrix} \quad \text{(E22)}$$

or

$$h_{+,i} = \frac{-F_{\times 2}x_{1,i} + F_{\times 1}x_{2,i}}{F_{+2}F_{\times 1} - F_{+1}F_{\times 2}} \quad \text{(E23)}$$

and

$$h_{\times,i} = \frac{F_{+2}x_{1,i} - F_{+1}x_{2,i}}{F_{+2}F_{\times 1} - F_{+1}F_{\times 2}} \quad \text{(E24)}$$

When these are substituted into the previous expression for $\ln(\Lambda)$ we obtain

$$\ln(\Lambda) = \sum_{i=1}^{N}\Bigg[(x_{1,i}F_{+1} + x_{2,i}F_{+2})\frac{F_{\times 2}x_{1,i} - F_{\times 1}x_{2,i}}{F_{+1}F_{\times 2} - F_{+2}F_{\times 1}} + (x_{1,i}F_{\times 1} + x_{2,i}F_{\times 2})\frac{F_{+1}x_{2,i} - F_{+2}x_{1,i}}{F_{+1}F_{\times 2} - F_{+2}F_{\times 1}}$$
$$-\frac{1}{2}(F_{+1}^2 + F_{+2}^2)\frac{(F_{\times 2}x_{1,i} - F_{\times 1}x_{2,i})^2}{(F_{+1}F_{\times 2} - F_{+2}F_{\times 1})^2} - \frac{1}{2}(F_{\times 1}^2 + F_{\times 2}^2)\frac{(F_{+1}x_{2,i} - F_{+2}x_{1,i})^2}{(F_{+1}F_{\times 2} - F_{+2}F_{\times 1})^2}$$
$$-(F_{+1}F_{\times 1} + F_{+2}F_{\times 2})\frac{(F_{\times 2}x_{1,i} - F_{\times 1}x_{2,i})(F_{+1}x_{2,i} - F_{+2}x_{1,i})}{(F_{+1}F_{\times 2} - F_{+2}F_{\times 1})^2}\Bigg] \quad \text{(E25)}$$

$$= \frac{1}{(F_{+1}F_{\times 2} - F_{+2}F_{\times 1})^2}\sum_{i=1}^{N}\left[x_{1,i}^2\frac{1}{2}(F_{+1}F_{\times 2} - F_{+2}F_{\times 1})^2 + x_{2,i}^2\frac{1}{2}(F_{+1}F_{\times 2} - F_{+2}F_{\times 1})^2\right] \quad \text{(E26)}$$

$$= \frac{1}{2}\sum_{i=1}^{N}x_{1,i}^2 + \frac{1}{2}\sum_{i=1}^{N}x_{2,i}^2 \quad \text{(E27)}$$

APPENDIX F: DERIVATION OF OPTIMUM STATISTIC FOR THREE OR MORE DETECTORS

Here we obtain the likelihood ratio statistic for the generalized case of three or more detectors at different locations and arbitrary orientations.

1. General assumptions

With detectors of differing locations and alignments, the signals in the three detectors will (generally) be different. The signal in detector j = 1,2,3 is described as

$$x_j(m) = n_j(m) + h_j(m) \quad \text{(F1)}$$

for the mth sample of N total samples, where $n_j(m)$ is the noise and h_j the signal in detector j. In the absence of any signal $x_j(m) = n_j(m)$.

Noise is assumed to be uncorrelated.

The signal h_j in detector j is of the form

$$h_j = F_{+j}h_+ + F_{\times j}h_\times \quad \text{(F2)}$$

as before.

2. Deriving the likelihood ratio statistic for the generalized three detector case

The general likelihood ratio test statistic for three detectors is

$$\Lambda(\overline{x}|\overline{h}) = \max_{\overline{h}} \frac{P_1(\overline{x}_1, \overline{x}_2, \overline{x}_3|\overline{h})}{P_0(\overline{x}_1, \overline{x}_2, \overline{x}_3)}. \tag{F3}$$

Individual samples are uncorrelated, so these probabilities are

$$\begin{aligned} P_1 &= \prod_{i=1}^{N} \exp\left(-\frac{(x_{1,i}-h_{1,i})^2}{2}\right) \exp\left(-\frac{(x_{2,i}-h_{2,i})^2}{2}\right) \exp\left(-\frac{(x_{3,i}-h_{3,i})^2}{2}\right), \\ P_0 &= \prod_{i=1}^{N} \exp\left(-\frac{x_{1,i}^2}{2}\right) \exp\left(-\frac{x_{2,i}^2}{2}\right) \exp\left(-\frac{x_{3,i}^2}{2}\right), \end{aligned} \tag{F4}$$

Note that in this case the signals $h_{j,i}$ represent different signals for each detectors—each with different location and orientation (different response functions in general). These signals can be expressed in terms of the polarization components of the gravitational wave in a particular external frame:

$$h_{j,i} = F_{+j}h_{+,i} + F_{\times j}h_{\times,i} \tag{F5}$$

This statistic Λ can be maximized by maximizing $\ln(\Lambda)$, which is equal to

$$\ln(\Lambda) = -\sum_{i=1}^{N} \frac{(x_{1,i}-h_{1,i})^2}{2} - \sum_{i=1}^{N} \frac{(x_{2,i}-h_{2,i})^2}{2} - \sum_{i=1}^{N} \frac{x_{3,i}-h_{3,i}{}^2}{2} + \sum_{i=1}^{N} \frac{x_{1,i}^2}{2} + \sum_{i=1}^{N} \frac{x_{2,i}^2}{2} + \sum_{i=1}^{N} \frac{x_{3,i}^2}{2} \tag{F6}$$

$$= \sum_{i=1}^{N} \left[x_{1,i}h_{1,i} + x_{2,i}h_{2,i} + x_{3,i}h_{3,i} - \frac{1}{2}h_{1,i}^2 - \frac{1}{2}h_{2,i}^2 - \frac{1}{2}h_{3,i}^2 \right]. \tag{F7}$$

Substituting the corresponding expressions for the $h_{j,i}$'s and rearranging terms gives

$$\begin{aligned} \ln\Lambda = \sum_{i=1}^{N} \Big[& h_{+,i}(F_{+1}x_{1,i} + F_{+2}x_{2,i} + F_{+3}x_{3,i}) + h_{\times,i}(F_{\times 1}x_{1,i} + F_{\times 2}x_{2,i} + F_{\times 3}x_{3,i}) \\ & -\frac{1}{2}h_{+,i}^2(F_{+1}^2 + F_{+2}^2 + F_{+3}^2) - \frac{1}{2}h_{\times,i}^2(F_{\times 1}^2 + F_{\times 2}^2 + F_{\times 3}^2) - h_{+,i}h_{\times,i}(F_{+1}F_{\times 1} + F_{+2}F_{\times 2} + F_{+3}F_{\times 3}) \Big] \end{aligned} \tag{F8}$$

To maximize Λ requires

$$\frac{\partial}{\partial h_{+,i}} \ln\Lambda = 0 \quad \text{and} \quad \frac{\partial}{\partial h_{\times,i}} \ln\Lambda = 0 \tag{F9}$$

which gives

$$\begin{aligned} F_{+1}x_{1,i} + F_{+2}x_{2,i} + F_{+3}x_{3,i} - (F_{+1}^2 + F_{+2}^2 + F_{+3}^2)h_{+,1} - (F_{+1}F_{\times 1} + F_{+2}F_{\times 2} + F_{+3}F_{\times 3})h_{\times,i} &= 0 \text{ and} \\ F_{\times 1}x_{1,i} + F_{\times 2}x_{2,i} + F_{\times 3}x_{3,i} - (F_{\times 1}^2 + F_{\times 2}^2 + F_{\times 3}^2)h_{\times,1} - (F_{+1}F_{\times 1} + F_{+2}F_{\times 2} + F_{+3}F_{\times 3})h_{+,i} &= 0 \end{aligned} \tag{F10}$$

These equations can be solved for $h_{+,i}$ and $h_{\times,i}$ using matrix representation:

$$\begin{bmatrix} F_{+1}^2 + F_{+2}^2 + F_{+3}^2 & F_{+1}F_{\times 1} + F_{+2}F_{\times 2} + F_{+3}F_{\times 3} \\ F_{+1}F_{\times 1} + F_{+2}F_{\times 2} + F_{+3}F_{\times 3} & F_{\times 1}^2 + F_{\times 2}^2 + F_{\times 3}^2 \end{bmatrix} \begin{bmatrix} h_{+,i} \\ h_{\times,i} \end{bmatrix} = \begin{bmatrix} F_{+1}x_{1,i} + F_{+2}x_{2,i} + F_{+3}x_{3,i} \\ F_{\times 1}x_{1,i} + F_{\times 2}x_{2,i} + F_{\times 3}x_{3,i} \end{bmatrix} \tag{F11}$$

For simplicity, the following variables are defined:

$$a_1 = F_{\times 1}^2 + F_{\times 2}^2 + F_{\times 3}^2, \tag{F12}$$

$$a_2 = F_{+1}^2 + F_{+2}^2 + F_{+3}^2, \tag{F13}$$

$$b_1 = F_{+1}F_{\times 1} + F_{+2}F_{\times 2} + F_{+3}F_{\times 3}, \tag{F14}$$

$$\gamma_1 = F_{+1}x_{1,i} + F_{+2}x_{2,i} + F_{+3}x_{3,i}, \tag{F15}$$

$$\gamma_2 = F_{\times 1}x_{1,i} + F_{\times 2}x_{2,i} + F_{\times 3}x_{3,i}, \quad \text{and} \tag{F16}$$

$$\beta = a_1a_2 - b_1^2. \tag{F17}$$

Using this notation, the matrix solution for $h_{+,i}$ and $h_{\times,i}$ is

$$\begin{bmatrix} h_{+,i} \\ h_{\times,i} \end{bmatrix} = \frac{1}{\beta} \begin{bmatrix} a_1 & -b_1 \\ -b_1 & a_2 \end{bmatrix} \begin{bmatrix} \gamma_1 \\ \gamma_2 \end{bmatrix} \tag{F18}$$

Taking the product of the above matrices yields solutions for $h_{+,i}$ and $h_{\times,i}$:

$$h_{+,i} = \frac{1}{\beta}(a_1\gamma_1 - b_1\gamma_2), \tag{F19}$$

$$h_{\times,i} = \frac{1}{\beta}(-b_1\gamma_1 + a_2\gamma_2) \tag{F20}$$

Substituting in the above expression for $\ln(\Lambda)$ gives

$$\begin{aligned}
\ln\Lambda &= \sum_{i=1}^{N}\Bigg[\frac{1}{\beta}(a_1\gamma_1 - b_1\gamma_2)\gamma_1 + \frac{1}{\beta}(-b_1\gamma_1 + a_2\gamma_2)\gamma_2 - \frac{1}{2}\left(\frac{1}{\beta}(a_1\gamma_1 - b_1\gamma_2)\right)^2 a_2 - \frac{1}{2}\left(\frac{1}{\beta}(-b_1\gamma_1 + a_2\gamma_2)\right)^2 a_1 \\
&\quad -\frac{1}{\beta}(a_1\gamma_1 - b_1\gamma_2)\frac{1}{\beta}(-b_1\gamma_1 + a_2\gamma_2)b_1\Bigg] \qquad \text{(F21)} \\
&= \frac{1}{\beta}\sum_{i=1}^{N}\Big[a_1\gamma_1^2 - 2b_1\gamma_1\gamma_2 + a_2\gamma_2^2\Big] - \frac{1}{\beta^2}\sum_{i=1}^{N}\Bigg[\frac{1}{2}a_2(a_1^2\gamma_1^2 - 2a_1b_1\gamma_1\gamma_2 \\
&\quad +b_1^2\gamma_2^2) + \frac{1}{2}a_1(a_2^2\gamma_2^2 - 2a_2b_1\gamma_1\gamma_2 + b_1^2\gamma_1^2) + b_1(a_1a_2\gamma_1\gamma_2 - a_1b_1\gamma_1^2 - a_2b_1\gamma_2^2 + b_1^2\gamma_1\gamma_2)\Bigg] \qquad \text{(F22)} \\
&= \frac{1}{\beta}\sum_{i=1}^{N}\Big[a_1\gamma_1^2 - 2b_1\gamma_1\gamma_2 + a_2\gamma_2^2\Big] - \frac{1}{\beta^2}\sum_{i=1}^{N}\Bigg[\left(\frac{1}{2}a_1^2a_2 + \frac{1}{2}a_1b_1^2 - a_1b_1^2\right)\gamma_1^2 + \left(\frac{1}{2}a_2b_1^2 + \frac{1}{2}a_1a_2^2 - a_2b_1^2\right)\gamma_2^2 \\
&\quad +\left(-a_1a_2b_1 - a_1a_2b_1 + a_1a_2b_1 + b_1^3\right)\gamma_1\gamma_2\Bigg] \qquad \text{(F23)} \\
&= \frac{1}{\beta}\sum_{i=1}^{N}\Big[a_1\gamma_1^2 - 2b_1\gamma_1\gamma_2 + a_2\gamma_2^2\Big] - \frac{1}{\beta^2}\sum_{i=1}^{N}\Big[\frac{a_1}{2}\beta\gamma_1^2 + \frac{a_2}{2}\beta\gamma_2^2 - b_1\beta\gamma_1\gamma_2\Big] \qquad \text{(F24)} \\
&= \frac{1}{\beta}\sum_{i=1}^{N}\Big[a_1\gamma_1^2 - 2b_1\gamma_1\gamma_2 + a_2\gamma_2^2 - \frac{a_1}{2}\gamma_1^2 + b_1\gamma_1\gamma_2 - \frac{a_2}{2}\gamma_2^2\Big] \qquad \text{(F25)} \\
\ln\Lambda &= \frac{1}{\beta}\sum_{i=1}^{N}\Big[\frac{a_1}{2}\gamma_1^2 + \frac{a_2}{2}\gamma_2^2 - b_1\gamma_1\gamma_2\Big] \qquad \text{(F26)}
\end{aligned}$$

Now substituting for γ_1 and γ_2 gives

$$\begin{aligned}
\ln(\Lambda) &= \frac{1}{\beta}\sum_{i=1}^{N}\Bigg[a_1\left(\frac{1}{2}(F_{+1}^2x_{1,i}^2 + F_{+2}^2x_{2,i}^2 + F_{+3}^2x_{3,i}^2) + F_{+1}F_{+2}x_{1,i}x_{2,i} + F_{+1}F_{+3}x_{1,i}x_{3,i} + F_{+2}F_{+3}x_{2,i}x_{3,i}\right) \\
&\quad +a_2\left(\frac{1}{2}(F_{\times1}^2x_{1,i}^2 + F_{\times2}^2x_{2,i}^2 + F_{\times3}^2x_{3,i}^2) + F_{\times1}F_{\times2}x_{1,i}x_{2,i} + F_{\times1}F_{\times3}x_{1,i}x_{3,i} + F_{\times2}F_{\times3}x_{2,i}x_{3,i}\right) \\
&\quad -b_1\Bigg(F_{+1}F_{\times1}x_{1,i}^2 + F_{+2}F_{\times2}x_{2,i}^2 + F_{+3}F_{\times3}x_{3,i}^2 + (F_{+1}F_{\times2} + F_{+2}F_{\times1})x_{1,i}x_{2,i} \\
&\qquad +(F_{+1}F_{\times3} + F_{+3}F_{\times1})x_{1,i}x_{3,i} + (F_{+2}F_{\times3} + F_{+3}F_{\times2})x_{2,i}x_{3,i}\Bigg)\Bigg] \qquad \text{(F27)} \\
&= \frac{1}{\beta}\sum_{i=1}^{N}\Bigg[\frac{1}{2}x_{1,i}^2(a_1F_{+1}^2 + a_2F_{\times1}^2 - 2b_1F_{+1}F_{\times1}) + \frac{1}{2}x_{2,i}^2(a_1F_{+2}^2 + a_2F_{\times2}^2 - 2b_1F_{+2}F_{\times2}) \\
&\quad +\frac{1}{2}x_{3,i}^2(a_1F_{+3}^2 + a_2F_{\times3}^2 - 2b_1F_{+3}F_{\times3}) + x_{1,i}x_{2,i}\left(a_1F_{+1}F_{+2} + a_2F_{\times1}F_{\times2} - b_1(F_{+1}F_{\times2} + F_{+2}F_{\times1})\right) \\
&\quad +x_{1,i}x_{3,i}\left(a_1F_{+1}F_{+3} + a_2F_{\times1}F_{\times3} - b_1(F_{+1}F_{\times3} + F_{+3}F_{\times1})\right) \\
&\quad +x_{2,i}x_{3,i}\left(a_1F_{+2}F_{+3} + a_2F_{\times2}F_{\times3} - b_1(F_{+2}F_{\times3} + F_{+3}F_{\times2})\right)\Bigg] \qquad \text{(F28)}
\end{aligned}$$

Expansion and factoring of the coefficients on the $x_{j,i}$ terms yields

$$\begin{aligned}\ln(\Lambda) &= \frac{1}{\beta}\sum_{i=1}^{N}\Bigg[\frac{1}{2}x_{1,i}^2\Big((F_{+1}F_{\times 2}-F_{+2}F_{\times 1})^2+(F_{+1}F_{\times 3}-F_{+3}F_{\times 1})^2\Big)+\frac{1}{2}x_{2,i}^2\Big((F_{+1}F_{\times 2}-F_{+2}F_{\times 1})^2+(F_{+2}F_{\times 3}-F_{+3}F_{\times 2})^2\Big)\\ &+\frac{1}{2}x_{3,i}^2\Big((F_{+1}F_{\times 3}-F_{+3}F_{\times 1})^2+(F_{+2}F_{\times 3}-F_{+3}F_{\times 2})^2\Big)+x_{1,i}x_{2,i}\Big((F_{+1}F_{\times 3}-F_{+3}F_{\times 1})(F_{+2}F_{\times 3}-F_{+3}F_{\times 2})\Big)\\ &+x_{1,i}x_{3,i}\Big(-(F_{+1}F_{\times 2}-F_{+2}F_{\times 1})(F_{+2}F_{\times 3}-F_{+3}F_{\times 2})\Big)+x_{2,i}x_{3,i}\Big((F_{+1}F_{\times 2}-F_{+2}F_{\times 1})(F_{+1}F_{\times 3}-F_{+3}F_{\times 1})\Big)\Bigg]\end{aligned}$$

Expansion of β and rearranging yields

$$\begin{aligned}\beta &= (F_{\times 1}^2+F_{\times 2}^2+F_{\times 3}^2)(F_{+1}^2+F_{+2}^2+F_{+3}^2)-(F_{+1}F_{\times 1}+F_{+2}F_{\times 2}+F_{+3}F_{\times 3})^2 &\text{(F29)}\\ &= (F_{+1}F_{\times 2}-F_{\times 1}F_{+2})^2+(F_{+1}F_{\times 3}-F_{\times 1}F_{+3})^2+(F_{+2}F_{\times 3}-F_{\times 2}F_{+3})^2 &\text{(F30)}\end{aligned}$$

Thus the result for the likelihood ratio statistic for three detectors may be written as

$$\ln(\Lambda)=\sum_{i=1}^{N}\Big[\kappa_{11}x_{1,i}^2+\kappa_{22}x_{2,i}^2+\kappa_{33}x_{3,i}^2+\kappa_{12}x_{1,i}x_{2,i}+\kappa_{13}x_{1,i}x_{3,i}+\kappa_{23}x_{2,i}x_{3,i}\Big] \qquad \text{(F31)}$$

where

$$\begin{aligned}\kappa_{11} &= \frac{1}{2\beta}\Big(f_{12}^2+f_{13}^2\Big), &\text{(F32)}\\ \kappa_{22} &= \frac{1}{2\beta}\Big(f_{12}^2+f_{23}^2\Big), &\text{(F33)}\\ \kappa_{33} &= \frac{1}{2\beta}\Big(f_{13}^2+f_{23}^2\Big), &\text{(F34)}\\ \kappa_{12} &= \frac{1}{\beta}f_{13}f_{23}, &\text{(F35)}\\ \kappa_{13} &= -\frac{1}{\beta}f_{12}f_{23}, \qquad \text{and} &\text{(F36)}\\ \kappa_{23} &= \frac{1}{\beta}f_{12}f_{13} &\text{(F37)}\end{aligned}$$

using the definitions

$$\begin{aligned}f_{pq} &= F_{+p}F_{\times q}-F_{+q}F_{\times p} \qquad \text{and} &\text{(F38)}\\ \beta &= f_{12}^2+f_{13}^2+f_{23}^2. &\text{(F39)}\end{aligned}$$

Note that $\kappa_{pp}>0$, that $\kappa_{11}+\kappa_{22}+\kappa_{33}=1$, and that κ_{pq} for p not equal to q may be positive, negative, or zero.

3. Deriving the likelihood ratio statistic for n detectors

The general likelihood ratio test statistic for n detectors is

$$\Lambda(\overline{x}|\overline{h})=\max_{\overline{h}}\frac{P_1(\overline{x}_1,\overline{x}_2,...,\overline{x}_n|\overline{h})}{P_0(\overline{x}_1,\overline{x}_2,...,\overline{x}_n)}. \qquad \text{(F40)}$$

Individual samples are uncorrelated, so these probabilities are

$$\begin{aligned}P_1 &= \prod_{i=1}^{N}\prod_{j=1}^{n}\exp\Big(-\frac{(x_{j,i}-h_{j,i})^2}{2}\Big) &\text{(F41)}\\ P_0 &= \prod_{i=1}^{N}\prod_{j=1}^{n}\exp\Big(-\frac{x_{j,i}^2}{2}\Big), &\text{(F42)}\end{aligned}$$

For detector j, the signal is

$$h_{j,i}=F_{+j}h_{+,j}+F_{\times j}h_{\times,j} \qquad \text{(F43)}$$

The log of the likelihood ratio statistic is

$$\begin{aligned}\ln(\Lambda) &= \frac{1}{2}\sum_{i=1}^{N}\sum_{j=1}^{n}\Big[-(x_{j,i}-h_{j,i})^2+x_{j,i}^2\Big] &\text{(F44)}\\ &= \sum_{i=1}^{N}\sum_{j=1}^{n}\Big[x_{j,i}h_{j,i}-\frac{1}{2}h_{j,i}^2\Big] &\text{(F45)}\\ &= \sum_{i=1}^{N}\Bigg[h_{+,i}\sum_{j=1}^{n}F_{+j}x_{j,i}+h_{\times,i}\sum_{j=1}^{n}F_{\times j}x_{j,i}\\ &\quad -\frac{1}{2}h_{+,i}^2\sum_{j=1}^{n}F_{+j}^2-\frac{1}{2}h_{\times,i}^2\sum_{j=1}^{n}F_{\times j}^2\\ &\quad -h_{+,i}h_{\times,i}\sum_{j=1}^{n}F_{+j}F_{\times j}\Bigg] &\text{(F46)}\end{aligned}$$

To maximize Λ requires

$$\frac{\partial}{\partial h_{+,i}}\ln\Lambda=0 \quad \text{and} \quad \frac{\partial}{\partial h_{\times,i}}\ln\Lambda=0 \qquad \text{(F47)}$$

which gives

$$\sum_{j=1}^{n} F_{+j}x_{j,i} - \left(\sum_{j=1}^{n} F_{+j}^2\right)h_{+,i} - \left(\sum_{j=1}^{n} F_{+j}F_{\times j}\right)h_{\times,j} = 0 \tag{F48}$$

and

$$\sum_{j=1}^{n} F_{\times j}x_{j,i} - \left(\sum_{j=1}^{n} F_{\times j}^2\right)h_{\times,i} - \left(\sum_{j=1}^{n} F_{+j}F_{\times j}\right)h_{+,j} = 0 \tag{F49}$$

These can be expressed as in the previous case in matrix form:

$$\begin{bmatrix} h_{+,i} \\ h_{\times,i} \end{bmatrix} = \frac{1}{\beta}\begin{bmatrix} a_1 & -b_1 \\ -b_1 & a_2 \end{bmatrix}\begin{bmatrix} \gamma_1 \\ \gamma_2 \end{bmatrix} \tag{F50}$$

simply using new definitions for these variables:

$$a_1 = \sum_{j=1}^{n} F_{\times j}^2, \qquad a_2 = \sum_{j=1}^{n} F_{+j}^2, \qquad \sum_{j=1}^{n} b_1 = F_{+j}F_{\times j},$$

$$\gamma_1 = \sum_{j=1}^{n} F_{+j}x_{j,i}, \qquad \text{and} \qquad \gamma_2 = \sum_{j=1}^{n} F_{\times j}x_{j,i}. \tag{F51}$$

The solution proceeds the same as before, then we substitute for these variables,

$$\begin{aligned}
\ln(\Lambda) &= \frac{1}{\beta}\sum_{i=1}^{N}\left[a_1\left(\frac{1}{2}\sum_{j=1}^{n} F_{+j}^2x_{j,i}^2 + \sum_{j,k,j<k}^{n} F_{+j}F_{+k}x_{j,i}x_{k,i}\right) + a_2\left(\frac{1}{2}\sum_{j=1}^{n} F_{\times j}^2x_{j,i}^2 + \sum_{j,k,j<k}^{n} F_{\times j}F_{\times k}x_{j,i}x_{k,i}\right)\right. \\
&\quad \left. + b_1\left(\sum_{j=1}^{n} F_{+j}F_{\times j}x_{j,i}^2 + \sum_{j,k,j<k}^{n}(F_{+j}F_{\times k} + F_{+k}F_{\times j})x_{j,i}x_{k,i}\right)\right] \\
&= \frac{1}{\beta}\sum_{i=1}^{N}\left[\frac{1}{2}\sum_{j=1}^{n} x_{j,i}^2(a_1F_{+j}^2 + a_2F_{\times j}^2 - 2b_1F_{+j}F_{\times j})\right. \\
&\quad \left. + \sum_{j,k,j<k}^{n} x_{j,i}x_{k,i}\left(a_1F_{+j}F_{+k} + a_2F_{\times j}F_{\times k} - b_1(F_{+j}F_{\times k} + F_{+k}F_{\times j})\right)\right] \\
&= \frac{1}{\beta}\sum_{i=1}^{N}\left[\frac{1}{2}\sum_{j=1}^{n} x_{j,i}^2\left(F_{+j}^2\sum_{p=1}^{n} F_{\times p}^2 + F_{\times j}^2\sum_{p=1}^{n} F_{+p}^2 - 2F_{+j}F_{\times j}\sum_{p=1}^{n} F_{+p}F_{\times p}\right)\right. \\
&\quad \left. + \sum_{j,k,j<k}^{n} x_{j,i}x_{k,i}\left(F_{+j}F_{+k}\sum_{p=1}^{n} F_{\times p}^2 + F_{\times j}F_{\times k}\sum_{p=1}^{n} F_{+p}^2 - (F_{+j}F_{\times k} + F_{+k}F_{\times j})\sum_{p=1}^{n} F_{+p}F_{\times p}\right)\right]
\end{aligned} \tag{F52}$$

Expanding and gathering terms, this can be expressed as

$$\ln(\Lambda) = \sum_{i=1}^{N}\left[\sum_{j=1}^{n}\kappa_{jj}x_{j,i}^2 + \sum_{j=1}^{n}\sum_{k=1}^{j-1}\kappa_{jk}x_{j,i}x_{k,i}\right] \tag{F53}$$

where

$$\kappa_{jj} = \frac{1}{2\beta}\sum_{k\neq j}^{n} f_{jk}^2 \tag{F54}$$

$$\kappa_{jk} = \frac{1}{\beta}\sum_{p\neq j,k}^{n} f_{jp}f_{kp} \tag{F55}$$

$$\beta = \sum_{j=1}^{n}\sum_{k=1}^{j-1} f_{jk}^2 \qquad \text{and} \tag{F56}$$

$$f_{pq} = F_{+p}F_{\times q} - F_{+q}F_{\times p} \tag{F57}$$

APPENDIX G: LR STATISTIC DERIVATION FOR UNKNOWN POLARIZATION ANGLE

The response functions of an IFO may be written

$$F_+(t) = \sin\xi[a(t)\cos 2\psi + b(t)\sin 2\psi] \tag{G1}$$

$$F_\times(t) = \sin\xi[b(t)\cos 2\psi - a(t)\sin 2\psi] \tag{G2}$$

where

$$\begin{aligned} a(t) &= \frac{1}{16}\sin 2\gamma(3-\cos 2\lambda)(3-\cos 2\delta)\cos[2(\alpha-\phi')] \\ &\quad -\frac{1}{4}\cos 2\gamma \sin\lambda(3-\cos 2\delta) sin[2(\alpha-\phi')] \\ &\quad +\frac{1}{4}\sin 2\gamma \sin 2\lambda \sin 2\delta \cos(\alpha-\phi') \\ &\quad -\frac{1}{2}\cos 2\gamma \cos\lambda \sin 2\delta \sin(\alpha-\phi') \\ &\quad +\frac{3}{4}\sin 2\gamma \cos^2\lambda \cos^2\delta \qquad \text{(G3)} \\ b(t) &= \cos 2\gamma \sin\lambda \sin\delta \cos[2(\alpha-\phi')] \\ &\quad +\frac{1}{4}\sin 2\gamma(3-\cos 2\lambda)\sin\delta \sin[2(\alpha-\phi')] \\ &\quad +\cos 2\gamma \cos\lambda \cos\delta \cos(\alpha-\phi') \\ &\quad +\frac{1}{2}\sin 2\gamma \sin 2\lambda \cos\delta \sin(\alpha-\phi') \qquad \text{(G4)} \end{aligned}$$

For a given detector. The response functions may be rewritten as

$$\begin{aligned} F_{+j} &= Q_j \cos 2\psi + R_j \sin 2\psi \qquad \text{(G5)} \\ F_{\times j} &= R_j \cos 2\psi - Q_j \sin 2\psi \qquad \text{(G6)} \end{aligned}$$

where the dependence on polarization angle ψ is separated from all other dependences on source direction, detector orientation and location, and time; these dependencies are contained in Q_j and R_j:

$$Q_j = a_j(t)\sin\xi \qquad \text{and} \qquad R_j = b_j(t)\sin\xi \qquad \text{(G7)}$$

Thus the signal in detector j is

$$h_{j,i} = Q_j \cos 2\psi + R_j \sin 2\psi + R_j \cos 2\psi - Q_j \sin 2\psi \qquad \text{(G8)}$$

which can be substituted in the previous results for $\ln(\Lambda)$:

$$\ln(\Lambda) = \sum_{i=1}^{N}\left[\sum_{j=1}^{n}\left(x_{j,i}h_{j,i} - \frac{1}{2}h_{j,i}^2\right)\right] \qquad \text{(G9)}$$

Substituting and collecting terms yields

$$\begin{aligned} \ln(\Lambda) &= \sum_{i=1}^{N}\Bigg[(h_{+i}\cos 2\psi - h_{\times i}\sin 2\psi)\left(\sum_{j=1}^{n} Q_j x_{j,i}\right) + (h_{+i}\sin 2\psi + h_{\times i}\cos 2\psi)\left(\sum_{j=1}^{n} R_j x_{j,i}\right) \\ &\quad +(-\frac{1}{2}h_{+i}^2\cos^2 2\psi - \frac{1}{2}h_{\times i}^2\sin^2 2\psi + h_{+i}h_{\times i}\sin 2\psi\cos 2\psi)\left(\sum_{j=1}^{n} Q_j\right) \\ &\quad +(-\frac{1}{2}h_{+i}^2\sin^2 2\psi - \frac{1}{2}h_{\times i}^2\cos^2 2\psi - h_{+i}h_{\times i}\sin 2\psi\cos 2\psi)\left(\sum_{j=1}^{n} R_j\right) \\ &\quad +(-h_{+i}^2\sin 2\psi\cos 2\psi - h_{+i}h_{\times i}\cos^2 2\psi)\left(\sum_{j=1}^{n} Q_j R_j\right) + (h_{+i}h_{\times i}\sin^2 2\psi + h_{\times i}^2\sin 2\psi\cos 2\psi)\left(\sum_{j=1}^{n} Q_j R_j\right)\Bigg] \end{aligned}$$

Defining the following variables,

$$a_1 = \sum_{j=1}^{n} Q_j^2, \qquad a_2 = \sum_{j=1}^{n} R_j^2, \qquad b_1 = \sum_{j=1}^{n} Q_j R_j, \gamma_1 = \sum_{j=1}^{n} Q_j x_{j,i}, \qquad \text{and} \qquad \gamma_2 = \sum_{j=1}^{n} R_j x_{j,i}.$$

allows expression of the statistic as

$$\begin{aligned} \ln(\Lambda) &= \sum_{i=1}^{N}\Bigg[h_{+i}(\gamma_1\cos 2\psi + \gamma_2\sin 2\psi) + h_{\times i}(\gamma_2\cos 2\psi - \gamma_1\sin 2\psi) - \frac{1}{2}h_{+i}^2(a_1\cos^2 2\psi + a_2\sin^2 2\psi + b_1\sin 4\psi) \\ &\quad -\frac{1}{2}h_{\times i}^2(a_2\cos^2 2\psi + a_1\sin^2 2\psi - b_1\sin 4\psi) + h_{+i}h_{\times i}\left(\frac{1}{2}(a_1-a_2)\sin 4\psi - b_1\cos 4\psi\right)\Bigg] \qquad \text{(G10)} \end{aligned}$$

We then take derivatives with respect to h_{+i}, $h_{\times i}$, and ψ_1 (most generally treating ψ as variable with time):

$$\begin{aligned}
\frac{\partial}{\partial h_{+i}}\ln\Lambda = 0 &= \gamma_1\cos 2\psi + \gamma_2 \sin 2\psi - h_{+i}(a_1\cos^2 2\psi + a_2\sin^2 2\psi + b_1\sin 4\psi) \\
&\quad + h_{\times i}\left(\frac{1}{2}(a_1-a_2)\sin 4\psi - b_1\cos 4\psi\right) \\
\frac{\partial}{\partial h_{\times i}}\ln\Lambda = 0 &= \gamma_2\cos 2\psi - \gamma_1\sin 2\psi \\
&\quad - h_{\times i}(a_2\cos^2 2\psi + a_1\sin^2 2\psi - b_1\sin 4\psi) + h_{+i}\left(\frac{1}{2}(a_1-a_2)\sin 4\psi - b_1\cos 4\psi\right) \\
\frac{\partial}{\partial h_{\times i}}\ln\Lambda = 0 &= -2(\gamma_1 h_{+i} + \gamma_2 h_{\times i})\sin 2\psi + (\gamma_2 h_{+i} - \gamma_1 h_{\times i})\cos 2\psi \\
&\quad + h_{+i}^2(a_1\sin 4\psi - a_2\sin 4\psi + 2b_1\cos 4\psi) + h_{\times i}^2(a_2\sin 4\psi - a_1\sin 4\psi - 2b_1\cos 4\psi) \\
&\quad + 2h_{+i}h_{\times i}\left((a_1-a_2)\cos 4\psi + 2b_1\sin 4\psi\right) \qquad \text{(G11)}
\end{aligned}$$

Whereas in previous cases we obtained a set of coupled linear equations, here we obtain non-linear equations involving h_{+i}, $h_{\times i}$, and ψ_i. However, the substitutions $X = \cos 2\psi$ and $Y = \sin 2\psi$ reduce the equations to a set of quadratic equations. If ψ is assumed constant, the equations become

$$\begin{aligned}
0 &= \gamma_1 X + \gamma_2 Y - a_1 X^2 h_{+i} - a_2 Y^2 h_{+i} \\
&\quad -2b_1 XY h_{+i} + (a_1-a_2)XY h_{\times i} - b_1(X^2-Y^2)h_{\times i} \\
0 &= \gamma_2 X + \gamma_1 Y - a_2 X^2 h_{\times i} - a_1 Y^2 h_{\times i} \\
&\quad -2b_1 XY h_{\times i} + (a_1-a_2)XY h_{+i} - b_1(X^2-Y^2)h_{+i} \\
0 &= -\gamma_1 Y h_{+i} + \gamma_2 X h_{+i} - \gamma_2 Y h_{\times i} - \gamma_1 X h_{\times i} \\
&\quad +(h_{+i}^2 - h_{\times i}^2)[(a_1-a_2)XY + b_1(X^2-Y^2)] \\
&\quad +h_{+i}h_{\times i}[(a_1-a_2)(X^2-Y^2) + 4b_1 XY] \\
0 &= X^2 + Y^2 - 1 \qquad \text{(G12)}
\end{aligned}$$

where

$$a_1 = \sum_{j=1}^{d} Q_j^2,\ a_2 = \sum_{j=1}^{d} R_j^2,\ b_1 = \sum_{j=1}^{d} Q_j R_j,$$

$$\gamma_1 = \sum_{j=1}^{d} Q_j x_{j,i},\ \text{and}\ \gamma_2 = \sum_{j=1}^{d} R_j x_{j,i} \qquad \text{(G13)}$$

For a polarization angle varying over time, X and Y would become X_i and Y_i.

APPENDIX H: SKY MAPS

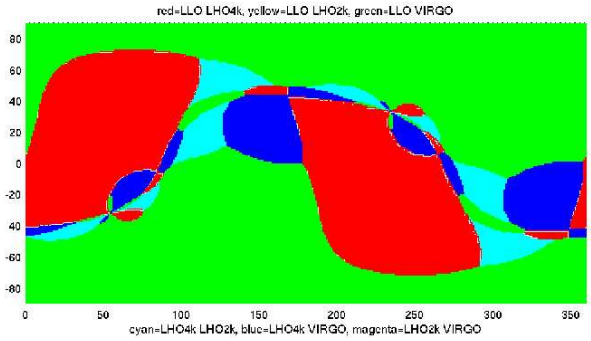

FIG. 22: Sky map of greatest CC contribution, 4 detectors, case 1: Detectors: LLO, LHO-4k, LHO-2k, VIRGO.

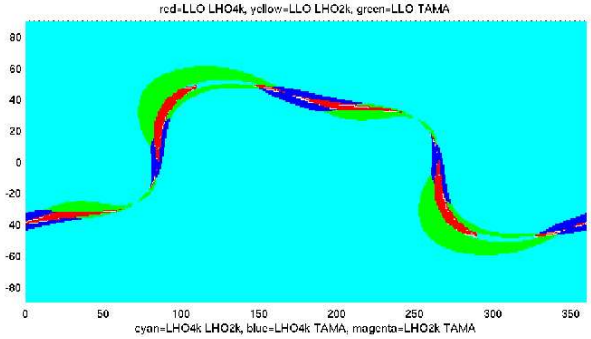

FIG. 23: Sky map of greatest CC contribution, 4 detectors, case 2: Detectors: LLO, LHO-4k, LHO-2k, TAMA.

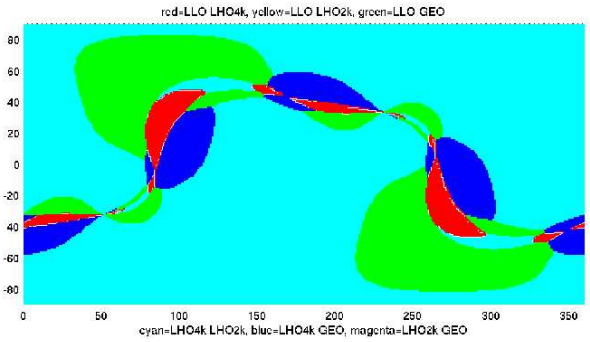

FIG. 24: Sky map of greatest CC contribution, 4 detectors, case 3: Detectors: LLO, LHO-4k, LHO-2k, GEO.

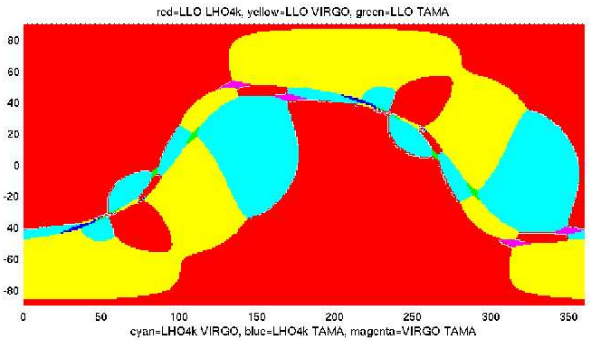

FIG. 25: Sky map of greatest CC contribution, 4 detectors, case 4: Detectors: LLO, LHO-4k, VIRGO, TAMA.

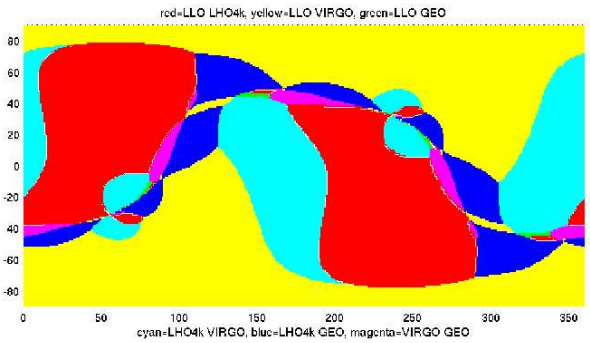

FIG. 26: Sky map of greatest CC contribution, 4 detectors, case 5: Detectors: LLO, LHO-4k, VIRGO, GEO.

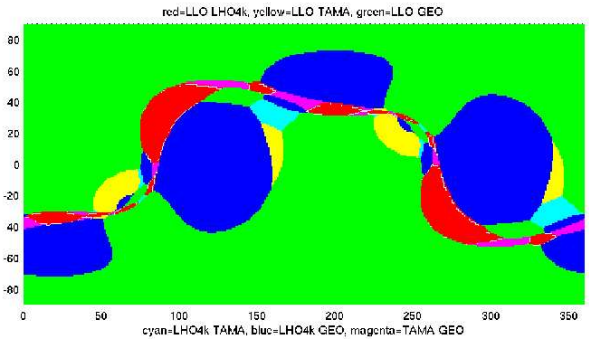

FIG. 27: Sky map of greatest CC contribution, 4 detectors, case 6: Detectors: LLO, LHO-4k, TAMA, GEO.

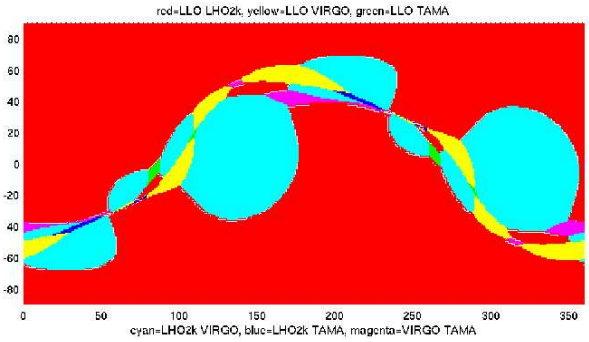

FIG. 28: Sky map of greatest CC contribution, 4 detectors, case 7: Detectors: LLO, LHO-2k, VIRGO, TAMA.

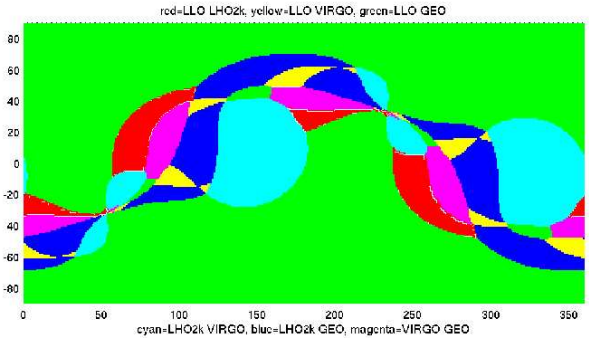

FIG. 29: Sky map of greatest CC contribution, 4 detectors, case 8: Detectors: LLO, LHO-2k, VIRGO, GEO.

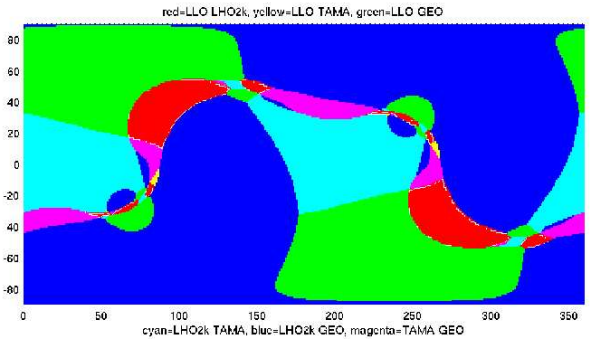

FIG. 30: Sky map of greatest CC contribution, 4 detectors, case 9: Detectors: LLO, LHO-2k, TAMA, GEO.

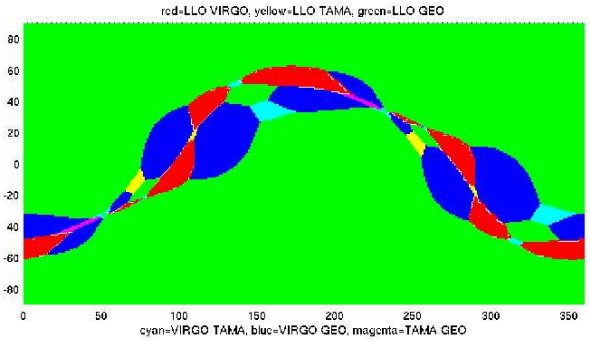

FIG. 31: Sky map of greatest CC contribution, 4 detectors, case 10: Detectors: LLO, VIRGO, TAMA, GEO.

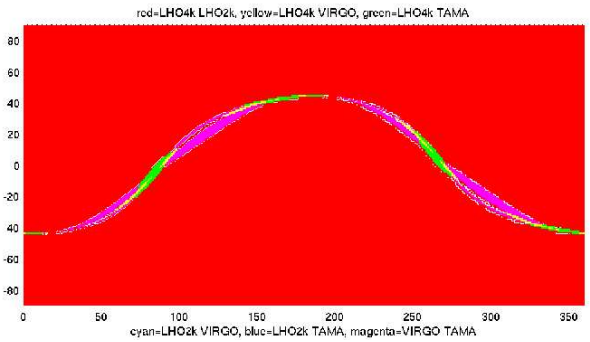

FIG. 32: Sky map of greatest CC contribution, 4 detectors, case 11: Detectors: LHO-4k, LHO-2k, VIRGO, TAMA.

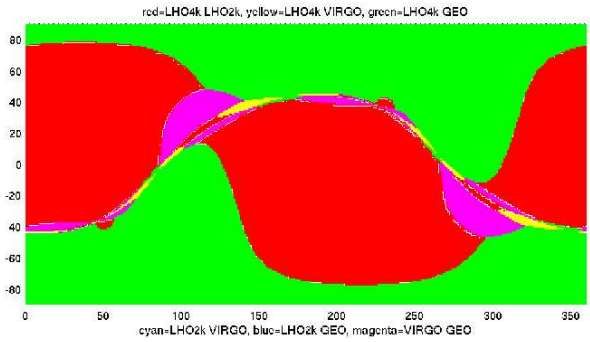

FIG. 33: Sky map of greatest CC contribution, 4 detectors, case 12: Detectors: LHO-4k, LHO-2k, VIRGO, GEO.

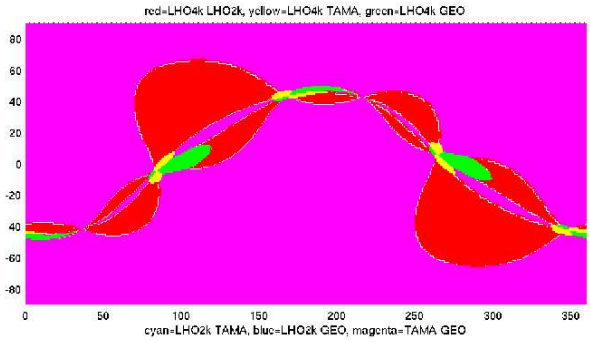

FIG. 34: Sky map of greatest CC contribution, 4 detectors, case 13: Detectors: LHO-4k, LHO-2k, TAMA, GEO.

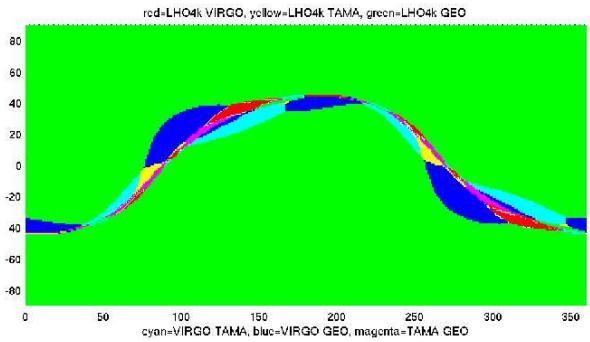

FIG. 35: Sky map of greatest CC contribution, 4 detectors, case 14: Detectors: LHO-4k, VIRGO, TAMA, GEO.

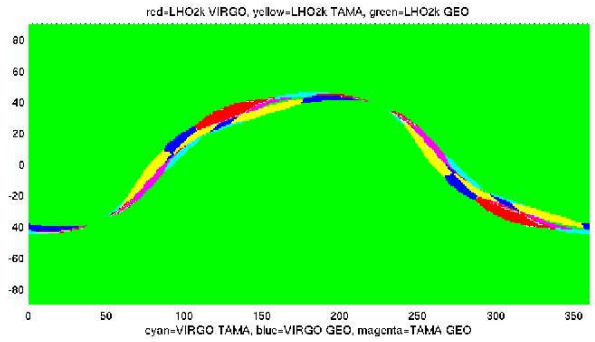

FIG. 36: Sky map of greatest CC contribution, 4 detectors, case 15: Detectors: LHO-2k, VIRGO, TAMA, GEO.

APPENDIX I: CODE FOR MONTE CARLO SIMULATIONS

The following code is written in Matlab [53].

```
% roc-combined1
%
% combined plot simulated/theoretical detector
% efficiency

clear
nsamp = 1024;
% nsamp = number of samples

deltm = 1;
% deltm = time interval

hwide = 0.1;
% hwide = for Gaussian signal pulse, time to
% drop from max to half max

freq = 0;
% freq = frequency for sinusoidal component
% of Gaussian signal pulse
% freq = 0 for no sinusoidal component

maxtr = 10000;
% maxtr = maximum number of trials

% thres = threshold for cc

snr = 2;
% snr = signal to noise ratio

% set legend

semilogx(0,0,'black','LineStyle','-');
hold on;
semilogx(0,0,'black','LineStyle','--');
semilogx(0,0,'red','LineStyle','-');
semilogx(0,0,'blue','LineStyle','-');
semilogx(0,0,'green','LineStyle','-');
legend('simulated','analytic','CC test',
     'LR test','var sum',2)

SNline='-';

% create signal

durk = hwide*hwide/log(2);
for c=1:nsamp
   x=deltm*(c/nsamp-0.5);
   H(c)=1/exp(x*x/durk);
   H(c)=H(c)*cos(x*freq*2*pi);
end    % c
snrp = sqrt(sum(H.*H));
H = H*snr/snrp;

chsum = sum(H.*H);

% conduct monte carlo trials

for trial=1:maxtr

% cross-correlation test

   N1=randn(1,nsamp);
   N2=randn(1,nsamp);

   S1=randn(1,nsamp)+H;
   S2=randn(1,nsamp)+H;

   cc(trial,1) = sum(N1.*N2);
   cc(trial,2) = sum(S1.*S2);

% likelihood ratio test

   N1=randn(1,nsamp);
   N2=randn(1,nsamp);

   S1=randn(1,nsamp)+H;
   S2=randn(1,nsamp)+H;

   cv(trial,1) = sum(N1.*N1)/4 + sum(N2.*N2)/4 ...
    + sum(N1.*N2)/2;
   cv(trial,2) = sum(S1.*S1)/4 + sum(S2.*S2)/4 ...
    + sum(S1.*S2)/2;

% sum of variances test

   N1=randn(1,nsamp);
   N2=randn(1,nsamp);

   S1=randn(1,nsamp)+H;
   S2=randn(1,nsamp)+H;

   cd(trial,1) = sum(N1.*N1)+sum(N2.*N2);
```

```
   cd(trial,2) = sum(S1.*S1)+sum(S2.*S2);

end      % trial

% compile data for roc curves

cc=sort(cc);
cv=sort(cv);
cd=sort(cd);

% cross-correlation test

for c2=1:maxtr
   thres=cc(c2,1);
   c3=1;
   for c4=1:maxtr
      if (cc(c4,2)>thres)
         c3=c3+1;
      end;     % if
   end      % c4

   Xc(c2)=1-c2/maxtr;
   Yc(c2)=c3/maxtr;
end         % c2

% likelihood ratio test

for c2=1:maxtr
   thres=cv(c2,1);
   c3=1;
   for c4=1:maxtr
      if (cv(c4,2)>thres)
         c3=c3+1;
      end;     % if
   end      % c4

   Xv(c2)=1-c2/maxtr;
   Yv(c2)=c3/maxtr;
end         % c2

% sum of variances test

for c2=1:maxtr
   thres=cd(c2,1);
   c3=1;
   for c4=1:maxtr
      if (cd(c4,2)>thres)
         c3=c3+1;
      end;     % if
   end      % c4

   Xd(c2)=1-c2/maxtr;
   Yd(c2)=c3/maxtr;
end         % c2

% plot results

semilogx(Xc,Yc,'red','LineStyle',SNline);
semilogx(Xv,Yv,'blue','LineStyle',SNline);
semilogx(Xd,Yd,'green','LineStyle',SNline);


% theoretical results

for tc = 1:10000
  valt = tc/10000;

% likelihood ratio

  meanno = nsamp/2;
  meansg = chsum + nsamp/2;
  varno = nsamp/2;
  varsg = nsamp/2 + 2*chsum;
  Xv(tc) = valt;
thres=meanno+sqrt(2*varno)*erfinv(1-2*valt);
Yv(tc)=0.5-0.5*erf((thres-meansg)/sqrt(2*varsg));

% variance sum

  meanno = nsamp*2;
  meansg = chsum*2 + nsamp*2;
  varno = nsamp*4;
  varsg = nsamp*4 + 8*chsum;
  Xd(tc) = valt;
thres=meanno+sqrt(2*varno)*erfinv(1-2*valt);
Yd(tc)=0.5-0.5*erf((thres-meansg)/sqrt(2*varsg));

% cross-correlation

  meanno = 0;
  meansg = chsum;
  varno = nsamp;
  varsg = nsamp + 2*chsum;
  Xc(tc) = valt;
thres=meanno+sqrt(2*varno)*erfinv(1-2*valt);
Yc(tc)=0.5-0.5*erf((thres-meansg)/sqrt(2*varsg));

end


% plot results

semilogx(Xv,Yv,'blue','LineStyle','--');
semilogx(Xd,Yd,'green','LineStyle','--');
semilogx(Xc,Yc,'red','LineStyle','--');



axis([0.0001 1 0 1]);
xlabel('false alarm probability');
ylabel('detection probability');
A=['Signal G ',num2str(hwide),' S ',
     num2str(freq)];
title([A,'  (SNR 2 and 7)']);
%title([A,':  LR test (blue), CC test (red),
%       variance sum (green)']);
```

```
% done
```

APPENDIX J: CODE FOR LR COEFFICIENTS IN DETECTOR CORRELATIONS

The following code is written in Matlab [53].

```
% newant5.m

clear

% 1=LLO
% 2=LHO 4k
% 3=LHO 2k
% 4=VIRGO
% 5=TAMA
% 6=GEO
% 7=AIGO (postulated values)

det(1).name = 'LLO';
det(2).name = 'LHO4k';
det(3).name = 'LHO2k';
det(4).name = 'VIRGO';
det(5).name = 'TAMA';
det(6).name = 'GEO';
det(7).name = 'AIGO';

% D = vector list of network detectors by
%  detector number from above
D = [1 2 3 4];
ND = length(D);

% detector latitudes, degrees E
LAT=[30.56 46.45 46.45 43.63 35.68 52.25 -31.4];
% detector longitudes, degrees N
LON=[90.77 119.41 119.41 -10.5 -139.54 -9.81 -115.7];
% detector azimuths, degrees from E to arm
%  bisector
AZI=[243.0 171.8 171.8 116.5 225.0 68.775 315];
% detectors, angle between arms
ARM=[90 90 90 90 90 94.33 90];
% detectors relative sensitivity, illustrative
%  values
COF=[1 1 0.5 0.75 0.17 0.5 0.17];
%COF=[1 1 1 1 1 1 1];

dtr = 45/atan(1);

LAT = LAT/dtr;
LON = LON/dtr;
AZI = AZI/dtr;
ARM = sin(ARM/dtr);

phi = 45/dtr;

mmax=100;
nmax=50;

% loop over celestial ra, dec

for m=1:mmax+1;
   ra=(m-1)*2*pi/mmax;
   era = ra;

   for n=1:nmax+1;
      dec=(n-1)*pi/nmax-pi/2;
%     decvec(n)=dec;

      f(7,7) = 0;
      cof(7,7) = 0;

      for detnum=1:ND
        k=D(detnum);
```

```
     A(k) = (1/16)*sin(2*AZI(k))*(3-cos(2*LAT(k))) ...
              *(3-cos(2*dec))*cos(2*era) ...
      -(1/4)*cos(2*AZI(k))*sin(LAT(k))*(3-cos(2*dec))*sin(2*era) ...
      +(1/4)*sin(2*AZI(k))*sin(2*LAT(k))*sin(2*dec)*cos(era) ...
      -(1/2)*cos(2*AZI(k))*cos(LAT(k))*sin(2*dec)*sin(era) ...
      +(3/4)*sin(2*AZI(k))*cos(LAT(k))*cos(LAT(k))*cos(dec)*cos(dec);

     B(k)=cos(2*AZI(k))*sin(LAT(k))*sin(dec)*cos(2*era) ...
      +(1/4)*sin(2*AZI(k))*(3-cos(2*LAT(k)))*sin(dec)*sin(2*era) ...
      +cos(2*AZI(k))*cos(LAT(k))*cos(dec)*cos(era) ...
      +(1/2)*sin(2*AZI(k))*sin(2*LAT(k))*cos(dec)*sin(era);

        P(detnum) = ARM(k)*(A(k)*cos(2*phi)+B(k)*sin(2*phi));
        C(detnum) = ARM(k)*(B(k)*cos(2*phi)-A(k)*sin(2*phi));
        G(detnum) = COF(k);
```

```
      end     % detnum

      be = 0;
      f(:,:) = 0;
      for det1=1:ND-1
        for det2=det1+1:ND
          f(det1,det2)= (P(det1)*C(det2) ...
            - P(det2)*C(det1))*G(det1)*G(det2);
          f(det2,det1)= (P(det2)*C(det1) ...
            - P(det1)*C(det2))*G(det1)*G(det2);
          be = be + f(det1,det2)*f(det1,det2);
        end      % det2
      end       % det1

      cof(:,:)=0;
      for det1=1:ND
        for det2=det1:ND
          for det3=1:ND
            if ((det3~=det2) & (det3~=det1))
              cof(det1,det2)=cof(det1,det2) ...
                + f(det1,det3)*f(det2,det3)/be;
            end   % if
          end     % det3
          if (det1==det2)
            cof(det1,det2) = cof(det1,det2)/2;
          end     % if
        end       % det2
      end         % det1

% store data for skymap plot


      nc=0;
      for det1=1:ND
       for det2=det1:ND
        map(m,n,det1,det2) = abs(cof(det1,det2));
          if (det1~=det2)
            nc=nc+1;
            cvec(nc) = map(m,n,det1,det2);
          end    % if
        end      % det2
      end        % det1

      [mxcof,mxn] = max(cvec);
      map2(m,n,1) = mxn;

      map2(m,n,2) = era*dtr;
      map2(m,n,3) = dec*dtr;

    end       % n
  end         % m

% plot results

figure
  caxis([5 10]);
  surf(map2(:,:,2),map2(:,:,3),map2(:,:,1),
          'EdgeColor','none');
   view(2)
    xlim([0 360])
    ylim([-90 90])
    axis equal
    ylim([-90 90])
    specialcolor
  caxis([1 6])
    title(['red=',det(D(1)).name,'-',
        det(D(2)).name,', yellow=',
        det(D(1)).name,'-',det(D(3)).name,
        ', green=',det(D(1)).name,'-',
        det(D(4)).name])
    xlabel(['cyan=',det(D(2)).name,'-',
        det(D(3)).name,', blue=',
        det(D(2)).name,'-',det(D(4)).name,
        ', magenta=',det(D(3)).name,'-',
        det(D(4)).name])
```